

Structural performance of steel-concrete composite floor systems utilising reused concrete slabs

A numerical study into the application and influence of a demountable concrete deck-to-deck connection

K.J.M. Brouwer

Delft University of Technology

Structural performance of steel-concrete composite floor systems utilising reused concrete slabs

A numerical study into the application and influence of a
demountable concrete deck-to-deck connection

by

K.J.M. Brouwer

to obtain the degree **Master of Science** in Civil Engineering
at the Delft University of Technology
to be defended publicly on February 5th, 2025 at 09:00.

Faculty: Civil Engineering and Geosciences
Track: Structural Engineering
Section: Steel, timber and composite structures

Student number: 4719638
Project duration: January 2024 – February 2025

Thesis committee: Prof. Dr. M. Veljkovic, TU Delft, Chair
Dr. F. Kavoura, TU Delft, Supervisor
MSc. Y. Zhang, TU Delft, Supervisor
Prof. Dr. Ir. L.J. Sluys, TU Delft, Supervisor
MSc. M. Hahury, Van Rossum B.V., Supervisor

Cover: Beresford's in-situ concrete specialists [1]

An electronic version of this thesis is available at <https://repository.tudelft.nl/>.



Acknowledgements

This thesis constitutes the final part to obtain the Master's degree in Civil Engineering at Delft University of Technology. My interest in buildings and structures led me to the research of reuse practices and repurposing structural components for sustainable development in the construction sector. Over the past few months, I have been fully committed to completing this study. I believe that the research performed can make a small but valuable contribution to the subject.

I would like to express my gratitude to my graduation committee members who guided me throughout this thesis. First of all, I would like to thank Milan Veljkovic for offering me the opportunity to work on the subject of reusing structural components and his guidance during my thesis. The discussions were always substantive and provided me new insights, which improved the quality of my work. Secondly, I would like to thank my daily supervisors, Florentia Kavoura and Yufei Zhang, for their supervision, discussions and help whenever needed, especially regarding the complexities I encountered during the finite element modelling. Thirdly, I want to thank Bert Sluys for being part of the committee and providing valuable insights on the subject. Lastly, I would like to express my gratitude to Milco Hahury and Van Rossum Raadgevend Ingenieurs. They gave me the incredible opportunity to work collaboratively, and I am thankful for their guidance and willingness to share their knowledge whenever I needed it during my thesis.

Last but not least, I would like to thank my family, roommate and all friends, who surrounded me throughout this journey. I am grateful for all their support, which motivated me to finish this thesis.

*K.J.M. Brouwer
Delft, January 2025*

Abstract

In light of the growing impact of the production of construction materials, the imperative for sustainable design is considered a necessity. Newly developed design strategies and design for deconstruction offer great potential and perspective to achieve the sustainability goals that are set in the European Commission's "Green Deal" towards net zero greenhouse gas emissions by 2050. Demountable and reusable steel-concrete composite structures allow for the opportunity to contribute to these sustainability goals. Demountability in steel-concrete composites is generally offered through the application of demountable shear connectors. Multiple studies have investigated the performance of various shear bolt connectors. Shear connectors generally showed inferior structural performance compared to that of conventional welded shear studs. Throughout the years, there has been significant advancement in the practice of reusing structural steel elements in the construction industry. Conversely, the exploration of re-purposing concrete from existing structures for structural use has not been extensively investigated. In response to this growing emphasis, reusing concrete slabs appears to be a sophisticated and innovative strategy. To enable deconstruction and reuse practices in such steel-concrete composite structures, bolted connections are considered a key characteristic in establishing the incentive. To maintain the strength characteristics of conventional shear studs in composite beams, demountability of a steel-concrete floor system can be offered through a concrete deck-to-deck connection between the composite beam and concrete slab. However, there exists a scarcity of solutions for connecting concrete slabs through demountable shear connectors, limiting comprehension on the structural behaviour and performance on true floor level.

This thesis presents two numerical finite element models, the first of which is a simplified deck-to-deck connection subjected to tensile loading conditions to determine basic characteristics and behaviour. The knowledge gained from the first model is implemented in the secondary finite element model, comprising a demountable floor system which is compared with a traditional conventional floor system. A subsequent parametric study focused on altering bolt spacing, edge distance and span width to allow for a broader perspective on the performance of the proposed demountable floor system. The numerical results showed that the demountable beam model is able to replicate the behaviour of the conventional beam system, where local plastic deformation of the connecting elements was hardly observed. The numerical results demonstrated that the serviceability loading capacity of the demountable floor system was 3% lower, and the discrepancy in ultimate loading resistance was magnified further. The parametric study indicated that modifications to the distance of the bolts from the edge of the slab and bolt spacing did not show a shift in the ultimate loading resistance and ductility. Increasing the span width of the demountable slab model indicated a gradual reduction of approximately 24% in load carrying capacity, where the ductility was not affected. While future research into the reliability and validity of the numerical results is considered necessary, the proposed solution for connecting concrete slabs has shown significant potential in terms of replicating the structural behaviour of conventional floor systems, without compromising the structural integrity. The solution demonstrated the ability to develop a demountable and reusable floor system, thus contributing to an enhanced sustainable and circular built environment.

Keywords:

Sustainable structural design, Reusable floor system, Demountable shear connectors, Deck-to-deck connection, Numerical modelling

Contents

Acknowledgments	i
Abstract	ii
Nomenclature	v
1 Introduction	1
1.1 Background	1
1.2 Context and problem statement	2
1.3 Objectives and research questions	2
1.3.1 Objectives	2
1.3.2 Research questions	3
1.4 Methodology	3
1.5 Document structure	4
2 State of the art	5
2.1 Sustainable development	5
2.1.1 Design for deconstruction	5
2.1.2 Reuse of structural elements	5
2.2 Hybrid- and composite construction	6
2.2.1 Composite action	6
2.2.2 Applications of steel-concrete composite systems	7
2.3 Shear connectors	8
2.3.1 Design principles for welded shear connectors according to Eurocode 4	8
2.3.2 Welded-headed stud shear connectors	9
2.3.3 Bolted shear connectors	10
2.3.4 Other demountable shear connectors	12
2.3.5 Comparison of experimentally tested shear connectors	14
2.4 Improving composite interaction for larger tolerances	16
2.4.1 Preloaded bolted connections	16
2.4.2 Injected bolted connections	17
2.5 Demountable reinforced concrete slabs using dry connections	18
2.5.1 Concrete half-joints and Gerber beams	18
2.5.2 Experimental research on concrete dry connections	20
2.6 Bolt applications for newly cast/precast concrete construction	21
2.6.1 Mechanical & chemical concrete anchors	22
2.6.2 Applications - HILTI	23
2.7 Design of composite floor systems according to Eurocode 4	24
2.7.1 Ultimate limit state (ULS)	24
2.7.2 Serviceability limit state (SLS)	25
2.8 Demountable continuous composite floor system	25
2.8.1 Concept and application	25
2.8.2 Application in precast concrete: High-strength friction-grip bolt	27
3 Preliminary analytical analysis	30
3.1 Floor systems	30
3.1.1 Structural behaviour	31
3.1.2 Sensitivity study	32
3.2 Theoretical framework for FEA	34
3.2.1 Optimised design	34
3.2.2 Theoretical predictions	35

3.3	Recapitulative conclusion	37
4	Finite element model	38
4.1	General and geometry	38
4.2	Material models	39
4.2.1	Steel material constitution	39
4.2.2	Concrete material constitution	41
4.3	Element type and meshing	43
4.4	Interaction and contact conditions	45
4.5	Boundary and loading conditions	47
4.6	Computational solver	49
5	Numerical model validation	50
5.1	Failure mode	50
5.1.1	Failure mechanism analysis - HSFGB shear connector	52
5.1.2	Failure mechanism analysis - Concrete block	53
5.2	Load-slip curve	55
5.2.1	Critical stages in load-slip curve	55
5.2.2	Evaluation of load-slip curve	57
5.2.3	Influence of concrete block height	57
5.2.4	Pretensioned vs. non-pretensioned bolts	58
5.3	Convergence study	59
5.3.1	Element order and mesh size	59
5.3.2	Output	61
6	Application of shear connector connection in beam model	64
6.1	Numerical model	64
6.1.1	Geometry	65
6.1.2	Material models	67
6.1.3	Element type and meshing	67
6.1.4	Interaction and contact conditions	68
6.1.5	Boundary and loading conditions	69
6.1.6	Computational solver	70
6.2	Numerical results and discussion	71
6.2.1	Validation and evaluation of global beam behaviour	71
6.2.2	Precast vs. reused slabs	76
6.2.3	Local connection behaviour	77
6.3	Parametric study	77
6.3.1	Design variations, material models	77
6.3.2	Evaluation	78
6.3.3	Results and discussion	79
7	Discussion	84
7.1	Simplifications in numerical model	84
7.2	Limitations	85
8	Conclusions and perspectives for future work	86
8.1	Conclusions	86
8.2	Perspectives for future work	87
	References	89
A	Push-out test - Experimental programme EN 1994-1-1	96
A.1	Testing procedure	96
A.2	Loading protocol and load-slip curve	96
B	Failure mechanism validation FE block-model	98
B.1	Failure mechanism analysis - concrete block	98
B.2	Allocation and overlapping of distinct damage regions	100
C	Parametric study - Load-deflection & initial flexural stiffness diagrams	101

Nomenclature

Acronyms

BB1	Blind bolt 1 (Hollow bolt)
BB2	Blind bolt 2 (Ajax bolt)
BSC-EN	Bolted shear connector with embedded nut
BSC-WEN	Bolted shear connector without embedded nut
BSC-CS	Bolted shear connector with coupler system
CDP	Concrete damage plasticity
DfD	Design for deconstruction
DSC	Demountable shear connector
EC2	Eurocode 2
EC4	Eurocode 4
FBSC	Friction-based shear connector
FE	Finite Element
FEA	Finite Element Analysis
HCS	Hollow core slab
HSFGB	High-strength friction-grip bolt
IBC	Injection bolted connections
LB-DSC	Lockbolt demountable shear connector
LNSC	Locking nut shear connector
LVDT	Linear Variable Differential Transformer
PRECS	Piecewise Reuse of Extracted Concrete in New Structures
SCC	Steel concrete composite
SLS	Serviceability limit state
UHPC	Ultra-high performance concrete
ULS	Ultimate limit state
YP	Yielding pocket
YPDSC	Yielding pocket demountable shear connector

Symbols

Latin alphabet

A_s	Gross cross-sectional area of bolt	mm ²
A_{sc}	Effective cross-sectional area of bolt	mm ²
b_e	Effective width for steel-concrete composite T-sections	mm
D_δ	Displacement ductility	-
d	Diameter of shank	mm
d_c	Damage compression parameter	-
d_t	Damage tension parameter	-
E_{cm}	Modulus of elasticity of concrete	N/mm ²
E_s	Modulus of elasticity of steel	N/mm ²
e	Edge distance	mm
$F_{b,Rd,resin}$	Nominal bearing strength of resin	kN
$F_{p,C}$	Preload force in a single bolt	kN
$F_{s,Rd}$	Design slip resistance	[kN]
f_{ck}	Characteristic cylinder concrete compressive strength	N/mm ²
f_{cm}	Mean cylinder compressive strength	N/mm ²
f_{ctm}	Mean tensile strength	N/mm ²
f_u	Ultimate tensile strength	N/mm ²
f_{ub}	Nominal ultimate tensile strength	N/mm ²
f_y	Yield strength	N/mm ²
f_{yd}	Design yield strength	N/mm ²
h_{sc}	Nominal shear connector height above flange	mm
K_c	Ratio of second stress invariant	-
k_f	Flexural stiffness	kN/mm
k_t	Loading duration factor in limit state	-
k_s	Increased hole clearance factor	-
k_{sc}	Initial stiffness	kN/mm
L_e	Distance between point of zero - maximum bending moment	mm
$M_{Rd,p}$	Plastic bending moment design resistance	kNm
n	Number of shear planes	-
P	Pretension load	kN
P_{Rd}	Design resistance of stud	kN
P_{Rk}	Characteristic cylinder strength of concrete	kN
P_u	Ultimate load capacity	kN
P_μ	Friction resistance	kN
R	Ductility condition	-
s	Bolt spacing	mm
$t_{b,resin}$	Thickness of resin layer	mm
$V_{pl,Rd}$	Plastic shear design resistance	kN
$V_{pl,a,Rd}$	Plastic shear design resistance of steel I-section	kN
V_y	Yield slip	mm
$V_{y,est}$	Estimated yield slip	mm

Greek alphabet

α	Aspect ratio factor in EC4	-
β	Factor for effect of plate thickness	-
γ_{M3}	Partial safety factor	-
γ_{M4}	Partial safety factor	-
γ_v	Partial safety factor	-
δ_{el}	Slip at load of $0.7P_{Rk}$	mm
δ_u	Ultimate slip	mm

δ_y	Yield slip	mm
ϵ	Eccentricity	-
ϵ_c^{in}	Inelastic compressive strain	-
ϵ_{cu1}	Nominal ultimate strain	-
ϵ_t^{ck}	Cracking tensile strain	-
ϵ_{true}	True limit strain	-
ϵ_{pl}	Plastic strain	-
ϵ_u	Ultimate limit strain	-
ϵ_y	Yield strain	-
μ_s	Degree of shear interaction	-
μ	Viscosity coefficient	-
ν	Poisson ration	-
ρ	Density	kg/m ³
σ_{bo}/σ_{co}	Ratio of initial biaxial to uniaxial compressive stress	-
σ_{true}	True stress	MPa
σ_y	Yield stress	MPa
ψ	Dilation angle	°

1

Introduction

1.1. Background

In the transition towards a sustainable construction industry it is crucial to mitigate environmental impacts and meeting the requirements set in the European Commission's 'Green Deal' [2]. The imperative for sustainable design in the construction sector today is of great importance. The circular economy model in the construction industry aims to maintain the value of materials and mitigate waste production [3], as the production of construction materials has a significant impact on the environment [4, 5]. A sustainable built environment is achieved, with an emphasis on structural design that allows for deconstruction and reuse of structural elements at end-of-life of a structure.

Challenge with the incitements arise within the application of composite floor systems. Composite floor systems, as defined in this study, are engineered using a concrete floor element and supplementary supporting steel beam that are connected through mechanical shear connectors. The traditional type of shear connector deployed in composite floor systems regards a permanent connection through welded shear studs (see Figure 1.1a). Composite action is achieved by welding the studs on the top flange of the steel beam. The welded studs are embedded in either concrete or grout, depending on the application. However, this conventional shear connector does not allow for reuse of structural elements due to the permanent connection between steel beam and concrete floor component. A transition towards sustainable construction can be achieved through the development of a reusable and demountable floor system utilising demountable connectors. The concept is depicted in Figure 1.1b.

A lot of research has been performed on the mechanical performance of various demountable shear connectors through push-out tests, drawing comparisons with conventional welded shear studs. Jakovljevic et al. [7] and Pimentel et al. [8] conducted a comparative analysis of demountable shear connectors explored in literature. The overarching conclusion that is drawn from the state of the art reviews indicate that demountable connectors do not exhibit equivalent performance compared to welded shear studs. Research performed by Kavoura et al. [9] extended the research on a broader scale to determine

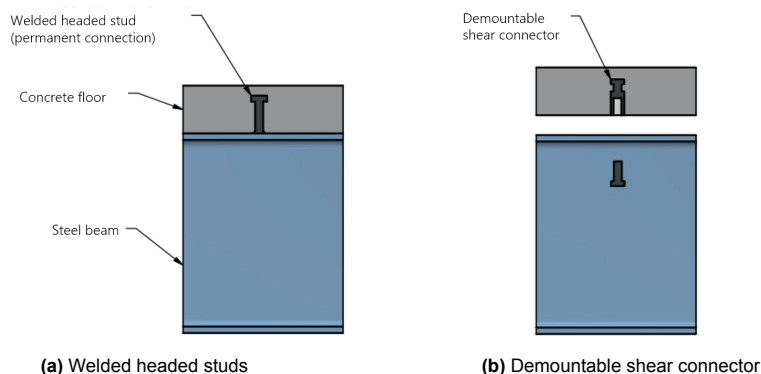


Figure 1.1: Steel-concrete composite floor system deploying a permanent and demountable connection by Nijgh [6]

the effect of demountable shear connectors in steel-concrete hybrid floor systems under monotonic and cyclic loading. Identical challenges, as were identified in push-out tests, were observed for floor systems deploying demountable shear connectors. A review of the literature reveals that push-out tests have consistently demonstrated that composite floor systems utilising demountable shear connectors exhibit deficient performance in terms of strength and stiffness when compared to traditional welded shear studs [7, 8].

1.2. Context and problem statement

Steel-concrete composite floor systems are frequently constructed on-site, with the concrete typically intended for a single life-cycle. In response to the growing emphasis on sustainability in the construction industry, reusing concrete appears to be a sophisticated and feasible strategy. Integrating concrete slabs that are cut from existing structures for reuse presents a practical and innovative solution, which concomitantly provides the opportunity for a demountable connection in the floor system.

To promote the reuse of concrete slabs that are extracted from existing structures, a floor system could be designed using continuous composite beams and reused concrete slab components as suggested by Kavoura and Veljkovic [10]. This involves the utilisation of a non-demountable composite beam, comprising welded shear studs. Demountability is offered through the concrete deck-to-deck connection between the composite beam and existing concrete slabs that are cut for reuse purposes such as depicted in Figure 1.2. This approach offers the potential to maintain the strength characteristics of welded shear studs in composite beams while ensuring the floor system remains demountable and available for reuse. The implementation of an innovative concrete deck-to-deck connection, allows for the incorporation of reusable concrete slabs contributing to a further reduction in carbon emissions.

Although prior studies have thoroughly examined the mechanical characteristics of demountable shear connectors in steel-concrete composite applications, there exists a scarcity of solutions for demountable shear bolt connections specifically designed for connecting concrete slabs. Additional research is required to understand the mechanical behaviour of a demountable connection between concrete elements and assess the structural performance of a steel-concrete composite floor system incorporating recycled concrete slabs and composite beams.

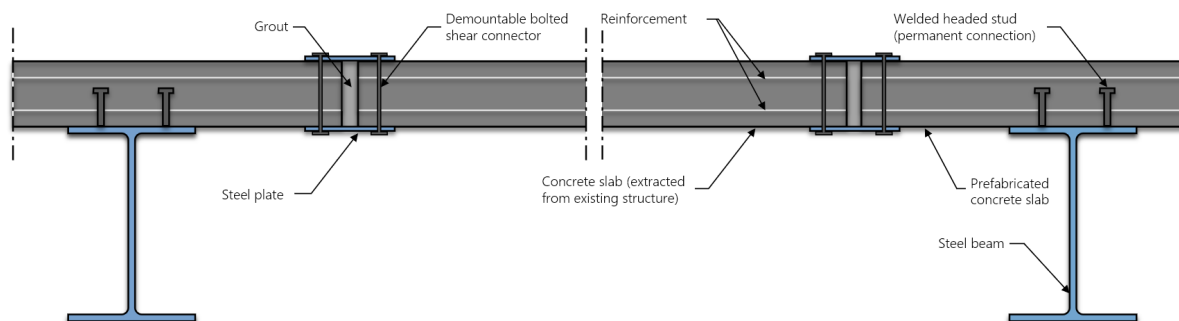


Figure 1.2: Demountable steel-concrete composite floor system utilising concrete deck-to-deck connections (not in scale)

1.3. Objectives and research questions

1.3.1. Objectives

The overarching objective of this work is to provide research and gain insight into the demountability and reusability of steel-concrete composite floor systems. This study aims to develop a demountable connection, thus improving sustainability within the construction industry and mitigating carbon emissions during production. To this extent, numerical prediction models of a demountable shear connector of a concrete deck-to-deck connection will be developed to determine its mechanical behaviour and to determine the performance of the steel-concrete composite floor system. Thereby, the numerical models are evaluated on a small scale model and examined on a large scale model by integrating the developed connector in a simplified beam system. The overarching objective is determined through the following (sub)objectives:

- Establish the mechanical behaviour of (bolted) demountable shear connectors based on experimental/numerical tests available in the literature through state-of-the-art review.
- Propose and develop a numerical model of a demountable concrete deck-to-deck connector through FEA and determine its mechanical behaviour and performance, validated through experimental data available in literature;
- Develop a numerical model through FEA that utilises a demountable deck-to-deck connection in coherence with external concrete slabs and determine the performance of the floor system through its load-deflection information.

The study within the research is primarily focused on the mechanical behaviour and application of a demountable deck-to-deck connector. Moreover, the performance of the demountable connector is evaluated through the application of steel-concrete composite floor systems only. I.e. the numerical models are modelled using steel-concrete configurations. Numerical and parametric studies are conducted to provide answers to the research questions. The study is limited by validation of the mechanical behaviour of the deck-to-deck connector. The results from the numerical model related to the deck-to-deck connector cannot be compared with the experimental test results. Validation is only possible through comparison with experimental test results from other studies available in the literature. Furthermore, the numerical models developed use a degree of simplification with respect to full-scale steel-concrete composite floor systems in regards to the computational effort needed to run an analysis. Moreover, this research primarily focuses on the behaviour of the concrete deck-to-deck connector and the application of this connection. The behaviour of the concrete and the reinforcing steel is only established on macro scale. The components of the numerical model are incorporated into a simplistic theoretical model, following assumptions stated in corresponding sections.

1.3.2. Research questions

In accordance with the research objectives, this thesis will address the following primary research question. During the course of the work, complementary sub-questions will be addressed to aid in answering the main question stated.

How does the structural performance of steel-concrete composite floor systems utilising demountable composite beams and reused slabs connected through a novel concrete deck-to-deck connector compare to conventional steel-concrete composite floor systems?

1. What are the details and the mechanical behaviour of a demountable concrete deck-to-deck shear connector in steel-concrete floor systems with reused concrete deck?
2. What parameters affect the mechanical behaviour of the deck-to-deck shear connector, and how do they impact its behaviour?
3. What is the structural performance of the floor system with deck-to-deck shear connectors?

1.4. Methodology

In order to answer the sub-questions and the main research question, the following structure is used in this thesis (see Figure 1.3). Firstly, a review of the state of the art is carried out to establish the importance of the research and determine the application and behaviour of different shear connectors. In addition, the application of demountable concrete slabs is considered, which allows a demountable model to be proposed and used for numerical analysis. The review is followed by the development of a numerical model to determine the behaviour of a deck-to-deck shear connector in demountable composite floor systems. As well as providing insight into the mechanical behaviour at the connection level, the model can also be used as a verification tool. This provides results for the behaviour of the system and answers the first sub-question. The verification model is based on the reliability of the results and a convergence study. The input from the verification model is then incorporated into the finite element model to assess the performance of steel-concrete floor system that incorporates a demountable shear connector on a global scale. The results of the numerical studies allow to answer the sub-questions, from which the main research question is answered.

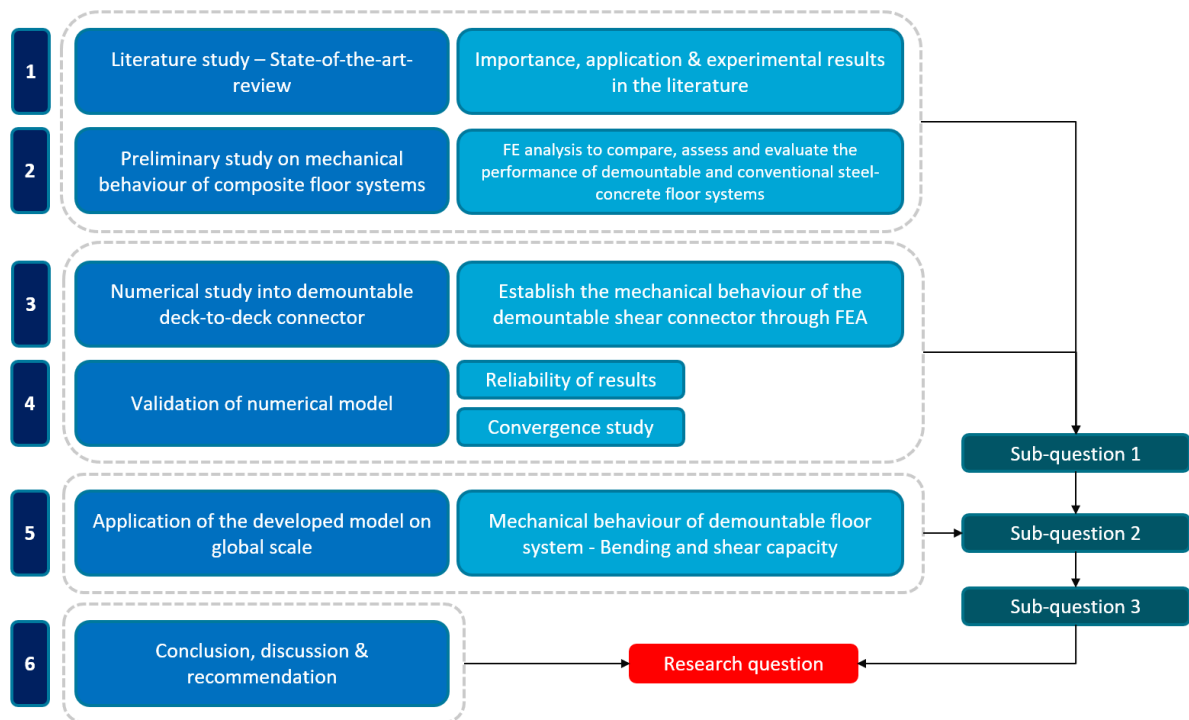


Figure 1.3: Methodology - Approach

1.5. Document structure

This thesis is comprised of five chapters, which collectively present the main content of the study. The first chapter provides a literature review, the second presents a preliminary analytical analysis, the third details the finite element model of the connection, the fourth validates the finite element model, and the fifth applies the developed FE model in a beam system. Chapter 2 presents a review of the state of the art, including developments in the design and concept of composite structures, the types and performance of variant shear connectors, and potential applications. Chapter 3 presents a preliminary study on the performance of a simplified conventional and demountable floor system, with a view to providing insight into its behaviour, including a theoretical framework. The thesis continues in Chapter 4, where a numerical model of a simplified block model is developed. The findings of the numerical model developed are presented in Chapter 5, which also includes a validation of the results. Chapter 6 demonstrates the application of the developed connection to the beam model. This chapter presents the results of a parametric study on geometrical variations in the beam model. Finally, a discussion and conclusion including perspectives for future work are given in Chapters 7 and 8, respectively.

2

State of the art

2.1. Sustainable development

In light of the growing impact of the contribution of the construction sector to the environment, progress should be made toward sustainable policies. The objective is to move from a linear economy model to a circular one, fostering the reuse of construction materials and reduce the production of greenhouse gas emissions. The transition from a linear to a circular economy model is achieved by closing the loop between the stages of collection and disposal of (construction) materials. Design for demounting and reuse of structural components is the preferred strategy. According to Brambilla et al. [5], designing for deconstruction is expected to make a significant contribution to sustainable construction.

2.1.1. Design for deconstruction

To promote sustainable development in the construction sector it is encouraged to reuse and repurpose structural elements from existing structures. However, to reuse materials that are extracted from existing structures requires for the development of a methodology for reusing structural components. A strategy that is gradually being implemented in the construction industry relates to design for deconstruction (DfD). Deconstruction is defined as the process of demolishing a structure, while restoring demolished materials for reuse. This method follows a design that not only facilitates the adaption and renovation of the structure, but also allows for the reuse of structural materials and elements [11]. Although the concept of DfD is considered a promising strategy, success of the incentives has not been achieved due to the impracticality of design standards and regulations [12]. DfD is an essential strategy for closing the loop on the circular economy model. The environmental benefits of closing the loop include extended raw material life, lower material costs and reduced carbon emissions from the construction industry [13]. Denseley Tingely and Davidson [14] looked into the barriers for reuse. One of the barriers related to composite construction. Although the barrier stated, various studies in the literature have demonstrated that demountable composite structures can be achieved [15, 16].

2.1.2. Reuse of structural elements

Reusing structural elements is a concept that is dependent on the ability of a structure to be deconstructed without demolishing the components. The main idea of reusing elements is to reduce material consumption and reduce greenhouse gas emissions. Throughout the years, there has been significant advancement in the practice of reusing structural steel elements in construction [10]. Several methods have explored the reusability of steel and steel-dominating hybrid structures leading to the development of the NTA 8713 (Reutilisation of structural steel) [17]. Steel-dominating structures consists mainly of structural steel elements that can be reused provided that bolted connections are applied. Such structures offer the opportunity to reuse a vast amount of steel elements for other purposes. Although the reuse of structural steel requires considerable effort and testing for updating standards and regulations, the construction sector can significantly mitigate its contribution to carbon emissions by embracing reuse practices [18]. The exploration of re-purposing concrete slabs from existing structures for structural use has not been extensively investigated in comparison to the reuse of steel elements. Currently, the primary focus of concrete reuse is focused around utilising prefabricated concrete slabs [19]. Ex-

tracting concrete components from existing structures and reusing them is a sustainable strategy that is not often considered [20]. Nevertheless, this strategy avoids the process of crushing and demolishing concrete mitigating the need for cement production. Initial investigations on the piecewise reuse of extracted concrete in new structures (PRECS) demonstrated to reduce raw material consumption and greenhouse gas emissions [21, 22]. However, the application of PRECS requires further investigation and development into the design of connection details [23].

2.2. Hybrid- and composite construction

Hybrid- and composite construction are terms that are used interchangeably in the literature. Both hybrid- and composite construction involve combining different materials across various sections in a building. Combining materials enables to improve the structural performance, efficiency and functionality. A hybrid structure comprises a structure in which two or more materials are not bonded, but connected through mechanical devices. Hybrid construction offers solutions where weaknesses of a specific material are compensated for by the other material(s). Common hybrid structures comprise of steel-timber configurations. Hybrid solutions in construction are also applied by combining materials to create a single component. The single structural component disposes enhanced properties due the interaction between the materials, such as improved tensile- and compressive strength. This interaction refers to composite construction. Typical applied composite structures include steel-concrete systems. This thesis exclusively explores the performance of (reused) steel-concrete floor systems utilising demountable shear connectors. Therefore, the terminology employed throughout this study pertains specifically to composite construction.

2.2.1. Composite action

Composite floor systems exhibit eminent performance in terms of stiffness and strength. The materials complement each other based on individual characteristics. A composite floor system is engineered using a floor element and supporting beam that are connected through shear connectors. The shear connectors transfer the longitudinal shear stresses and account for continuity of curvature at the interface between the steel beam and concrete slab [24]. The strength of composite beams is determined by the ability of the system to prevent the occurrence of slip. Slip is defined as the change in position in longitudinal direction in between the interface of the elements. Figure 2.1 depicts the behaviour of a steel-concrete non-composite- and composite beam.

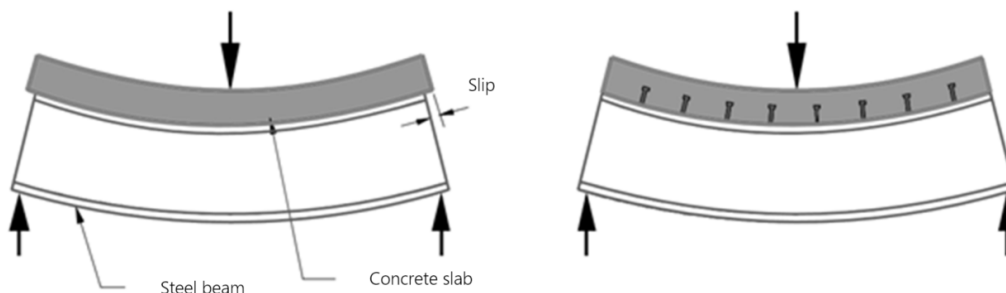


Figure 2.1: Non-composite beam vs. composite beam [25]

The degree of composite interaction between beam and floor elements can be described based on the strain (ϵ) diagram in the composite system [26]. In non-composite behaviour the steel beam and floor bend separately from one another. The elements act as individual sections, if frictional forces at the interface are neglected. As a consequence, there is no shear force that can be transferred from the floor to the supporting beam. The slip (δ) here is defined as the difference in strain. In case of full composite interaction the difference in strain is equal to zero. The connection provides sufficient strength which implies that the strength of the composite system is either governed by the steel girder or the concrete deck. As a result full flexural capacity of the composite section is achieved. The system acts as a monolithic unit where deformation is negligible [26]. A schematic overview of strain distributions

for composite interactions is provided in Figure 2.2. It should be noted that the real behaviour of a composite beam is often in between the extremes of composite behaviour, following partially-composite interaction [27]. In a partially composite beam the flexural strength is determined by the strength of the shear connectors. I.e. the connectors are considered the weakest part of the system.

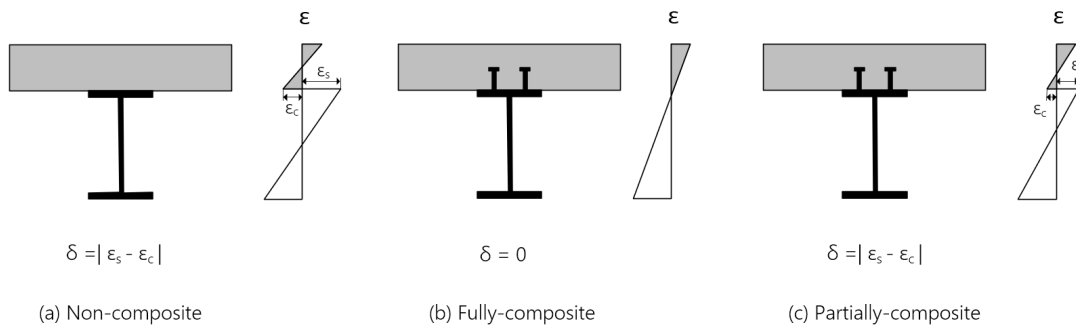


Figure 2.2: Strain distributions for steel-concrete composite beam interaction

2.2.2. Applications of steel-concrete composite systems

Composite construction in steel-concrete floor systems comprise different applications. The steel element typically regards an I-profiled beam, whereas the concrete floor differs in application. The traditional application of steel-concrete composites uses in-situ poured concrete. The combination of steel and concrete in composite floor systems allow for a sufficient coherence between the materials, in which the steel accounts for tension and concrete for compression. The most common applied system regards the slab with profiled metal decking, in which the steel beam is connected to the metal deck using welded shear studs on top of the steel beam. The metal deck acts as formwork for the in-situ poured concrete during construction. After concrete hardening the deck functions as a tensile reinforcement for the concrete slab allowing for full composite interaction. Figure 2.3a depicts the application of in situ concrete with and without metal deck.

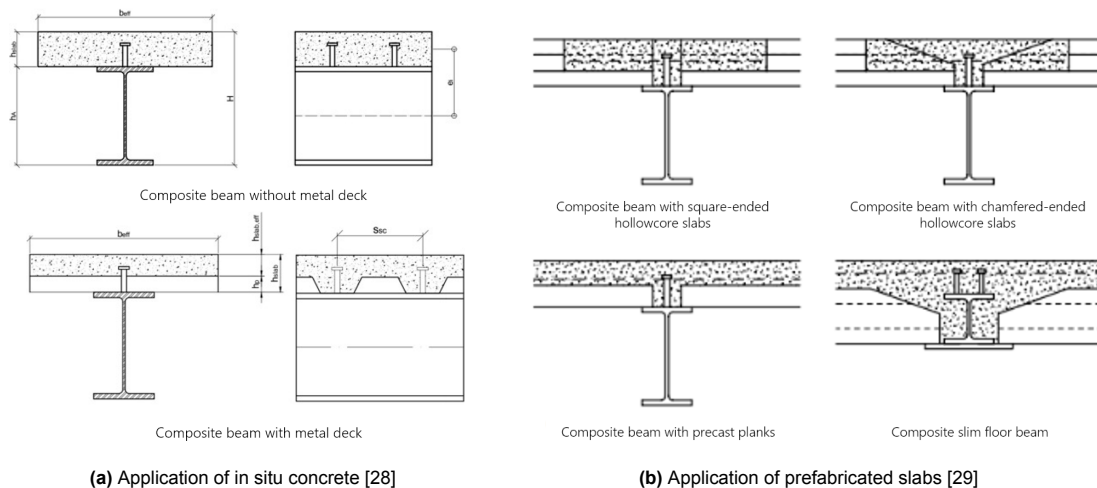


Figure 2.3: Steel-concrete composite floor systems

In pursuit of sustainability practices, prefabricated slabs have gradually been implemented in composite construction [19]. Prefabricated concrete slabs reduces waste disposal and leads to more efficient production. Moreover, precast concrete components can be reused and recycled. The components can be rearranged or disassembled preventing land-fill of materials such as fly ash, blast furnace slag and silica fume [30]. For that reason the application of solid slabs and concrete hollow core slabs are considered a sustainable alternative for steel-concrete composite floor systems. The engineered systems that use precast concrete slabs can differ through design. The steel beam can either be en-

gineered below or integrated and aligned within two concrete slabs. The application of precast solid- and hollow core slabs in composite floor systems is depicted in Figure 2.3b.

Solid slabs are monolithic concrete slabs that have a uniform thickness over full length and width. Solid slabs have a larger spanning capacity than hollow core units. Hollow core slabs consist of hollow canals in longitudinal direction, which lead to a significant reduction of self-weight. The canals within the slab allow for both thermal and acoustic insulation. Hollow core slabs have fast and cost-effective installation which contributes to the process in construction. The application of steel-concrete hollow core slabs composites has been investigated through the connection by Lam et al. [31]. The near ends of two hollow core slabs rest on top of a steel I-section, in which composite action is activated through the welded shear studs on top of the steel beam. Transverse reinforcement is placed in between the milled slots, and filled with in situ concrete. The research by Lam et al. [31] concluded that the design exhibits considerable results regarding reliability and cost-effectiveness.

2.3. Shear connectors

2.3.1. Design principles for welded shear connectors according to Eurocode 4

Eurocode 4 [32] provides detailed design rules for welded shear studs. The behaviour of welded shear connectors is generally defined by means of a push-out test. The experimental programme for push-out tests defined by EN 1994-1-1 is provided in annex A. The parameters that characterise the shear behaviour of welded studs, relate to the ultimate capacity (P_u), initial stiffness (k_{sc}) and the ultimate slip capacity (δ_u). The design resistance of welded shear connectors embedded in concrete is obtained as the minimum of two values determined through Eq. 2.1 (failure of the concrete) and 2.2 (shear failure of stud):

$$P_{Rd} = \frac{0.29\alpha d^2 \sqrt{(f_{ck} E_{cm})}}{\gamma_v} \quad (2.1)$$

$$P_{Rd} = \frac{0.8 f_u A_s}{\gamma_v} \quad (2.2)$$

with

$$\alpha = \begin{cases} 0.2 \left(\frac{h_{sc}}{d} + 1 \right) & \text{for } 3 \leq h_{sc}/d \leq 4 \\ 1 & \text{for } h_{sc}/d > 4 \end{cases} \quad (2.3)$$

where

P_{Rd}	Design resistance of stud
A_s	Area of the shank of stud
d	Diameter of the shank of stud
h_{sc}	Nominal height of stud
f_u	Ultimate tensile strength of stud
f_{ck}	Characteristic cylinder strength of concrete
E_{cm}	Modulus of elasticity of concrete
γ_v	Partial safety factor (1.25 according to EN 1994-1-1)

The (initial) stiffness of the shear connector is determined through Equation 2.4 (see Figure 2.4a):

$$k_{sc} = \frac{0.7 P_{Rk}}{\delta_{el}} \quad (2.4)$$

where

k_{sc}	Stiffness of shear connector
P_{Rk}	Characteristic resistance of shear connector
δ_{el}	Slip at a load of $0.7 P_{Rk}$

According to En 1994-1-1, a shear connector is considered to have a ductile behaviour if the connector has sufficient deformation capacity to assume an ideal plastic behaviour, such as depicted in Figure 2.4b. A ductile classification is defined if the connector has a slip capacity of 6 mm. A slip capacity of 6 mm or higher facilitates composite beams to redistribute shear forces inelastically. The diameter of the stud is limited to a range of 16 mm to 25 mm. The maximum diameter limit of 25 mm is established due to welding challenges encountered with larger diameters. The standard states that shear connectors should deform sufficiently for the inelastic shear distribution that is assumed in the design. In addition, the connectors should satisfy the ductility condition from Equation 2.5:

$$R = \frac{\delta_u - 1}{1} \geq 5 \quad (2.5)$$

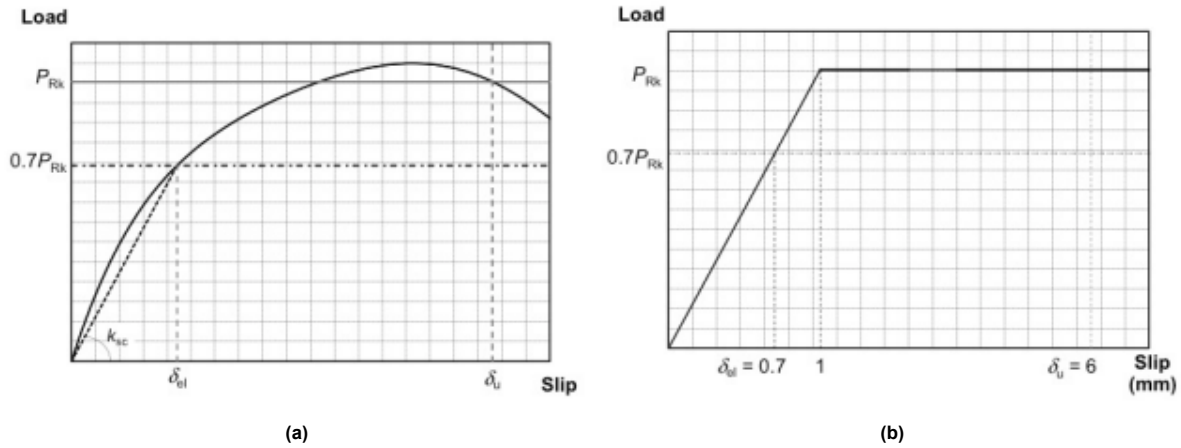


Figure 2.4: (a) Characteristic load-slip curve from EN1994-1-1 [32] and (b) idealised load-slip curve for welded shear studs

EN 1994-1-1 defines a minimum degree of shear connection for welded shear studs, that are considered ductile. The degree of shear connection μ_s is defined as the ratio between the actual number of shear connectors and required number of shear connectors for full shear interaction over a specified length L_e . This length relates to the distance between the points of zero and maximum bending moment. The minimum degree is obtained through Equation 2.6:

$$\mu_s = \begin{cases} \text{For } L_e \leq 25 \text{ m: } \mu \geq 1 - \left(\frac{355}{f_y}\right)(0.75 - 0.03L_e) \text{ and } \mu \geq 0.4 \\ \text{For } L_e > 25 \text{ m: } \mu \geq 1 \end{cases} \quad (2.6)$$

2.3.2. Welded-headed stud shear connectors

In practice, welded-headed stud shear connectors are the most used shear connectors in steel-concrete composite floor systems. Using welded studs offers different advantages. Stud welding is rapid, and the studs securely anchor into concrete. Additionally, the reinforcement can be easily embedded within the concrete slab and the stud head enables the connector to withstand uplift forces on the slab [33]. A lot of studies looked into the mechanical behaviour of welded studs through push-out tests. The first study that looked into the behaviour of welded-headed studs by performing push-out tests was executed by Viest [34] in 1956. A relation between the load and deflection of the connectors was obtained including governing failure modes (concrete crushing and shear failure). Further investigation into the static and cyclic behaviour of welded-headed studs was pursued, followed by subsequent research endeavours. Pallarés and Hajjar [35] provided a state of the art review on 391 existing experimental results for welded-headed studs in the period 1956-2005. The behaviour of the studs were compared through different design codes. Based on the ratios obtained the research concluded that the design rules from Eurocode 4 give conservative estimates for the welded-headed studs. A comparison between the different experimental programs indicated that an increase in the diameter of the stud results in higher initial stiffness. The ultimate load capacity and slip capacity are correlated to the concrete slab strength. Higher concrete compressive strength yields higher capacities. [35].

2.3.3. Bolted shear connectors

Welded headed studs do not provide the ability to be demounted as a result of the permanent connection. The application of steel-concrete composite floor systems treated in 2.2.2 all use non-demountable shear connectors that are welded on the top flange of the steel I-section. The transition towards a sustainable construction industry requires a demountable shear connector to enable deconstruction without demolishing structural components. A lot of research has been performed on demountable bolted connectors that should allow for an easy deconstruction process and reuse of structural elements. To establish the performance of these demountable connectors a study on the mechanical behaviour is executed. Figure 2.5 depicts an overview of the bolted shear connectors taken for analysis.

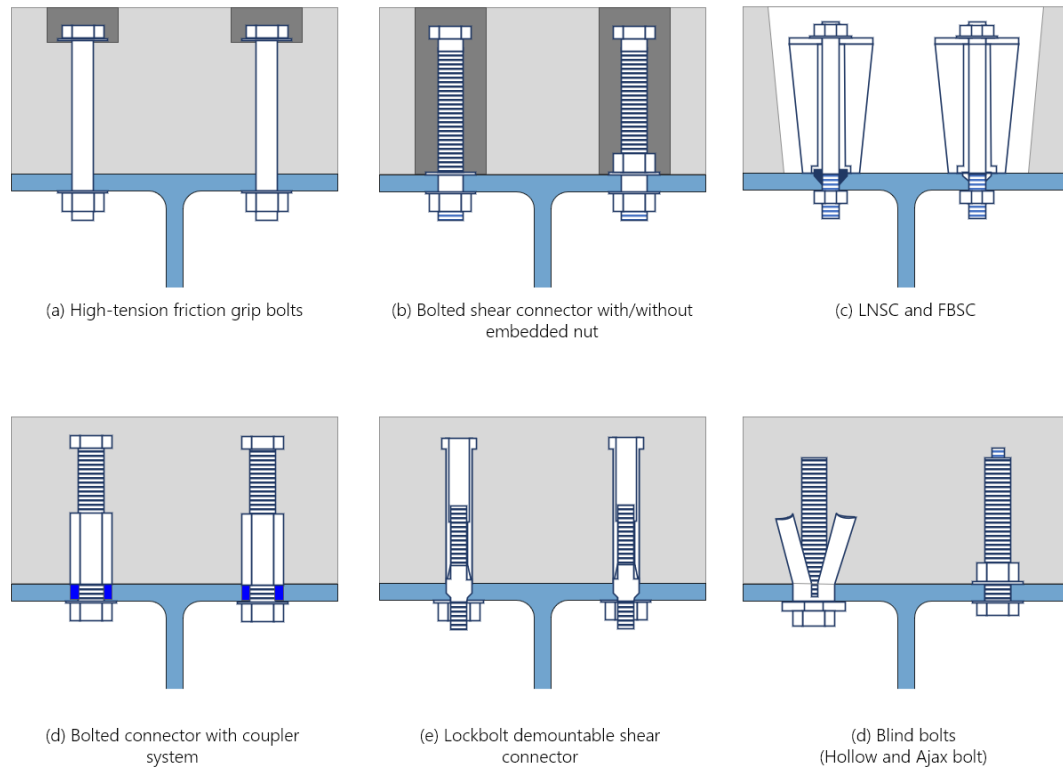


Figure 2.5: Bolted shear connectors for steel-concrete composite systems analysed in the literature (a) [36–42], (b) [43–49], (c) [50–52], (d) [40, 53, 54], (e) [55], (f) [56–59]

To replace welded shear studs, advancement was made with the introduction of demountable high-tension friction grip bolts (HSFGB) depicted in Figure 2.5a. The mechanical behaviour has been evaluated in different studies [36–42]. The bolts are preloaded which causes transfer of the shear force through friction. Kwon et al. [36] investigated the behaviour of post-installed HSFGB under static and fatigue loading. Post-installed shear connectors installed in beam specimens indicated to have an increasing strength and stiffness of approximately 50% when compared to non-composite beams. A very high ultimate slip capacity was observed from the tests. To decrease maximum slip Chen et al. [37] introduced through-bolts in steel-precast concrete composite bridges, using PVC pipes to create the bolt holes. Subsequent research by Kozma et al. [40] improved the idea of through-bolts by using cast-in steel cylinders. The solution of cast-in steel cylinders prevents the (possible) loss of prestress due to the effects of creep and shrinkage. The application of through-bolts indicated that the HSFGB have comparable ductility and peak load level to welded shear studs. The results from the experiments using through-bolts showed that initial slip and ultimate load capacity increased with an increase in the bolt diameter and/or pretension force. A parametric study performed by Ataei [42] complemented the results found in [40] showing that the bolt size, bolt grade and the concrete compressive strength have high influence on the ultimate load capacity of the connector. Failure modes observed in the experimental tests included shear fracture of the bolt, concrete crushing and steel beam flange deformation around oversized holes.

The application of bolted shear connectors is a common method to achieve demountability shown in Figure 2.5b. Bolted shear connectors without embedded nuts (BSC-WEN), also threaded-headed studs, do not require pretension. Studies performed by Rehman et al. [43] and J. Yang et al. [44] focused on the application of threaded-headed studs in metal decking composite slabs. The studies concluded that the demountable connectors have high shear resistance and ductility when compared to equivalent welded shear studs. Moreover, an increase in concrete strength leads to an increase of the shear capacity, but a decrease in ductility. Wang et al. [45] determined the effect of ultra-high performance concrete (UHPC) in composite construction. The experimental results indicated that an identical UHPC-slab with increasing stud diameter leads to higher ultimate shear capacities. The initial stiffness of the connectors in coherence with the UHPC increased with an increased shank diameter.

To increase the stiffness of the bolted shear connector, it was proposed to use a bolted shear connector with an embedded nut (BSC-EN) in the concrete (see Figure 2.5b). This solution expects to control the bolt rotation and slip deformation. Experimental research by Pavlović et al. [46] indicated that single embedded nut reached to almost identical shear resistance (95%) for static loading compared to welded-headed studs. However, the stiffness reduced to 50% for the bolts. Dai et al. [47] investigated the influence of continuous, partially discontinuous and separate slabs with metal decking, concluding that high-strength bolts with embedded nuts can function as demountable shear connector. The response to monotonic and cyclic loading in precast concrete panels has been studied by Ataei et al. [48]. The monotonic tests indicated that the size of the bolted shear connectors has a great impact on the composite behaviour. Increasing the size and strength of the connectors resulted in a higher initial stiffness when subjected to cyclic loading. Identical results were obtained in a study on BSC-EN in cold-formed SCC beams with metal deck application by Ataei et al. [49].

In order to control initial slip that is caused by bolt-hole clearance Suwaed and Karavasilis [50, 51] presented a locking nut shear connector (LNSC) and friction-based shear connector (FBSC) depicted in Figure 2.5c. The locking nut shear connector transfers the load through bearing of the nut. The LNSC system is designed using a high-strength bolts which has a small threaded length. The connector consists of three nuts from one of which a conical nut at the countersunk seat. This conical nut prevents slip of the bolt in the bolt hole. An inclination angle of 5° in the pockets of a prefabricated slab is applied to accommodate the shear connectors. The clearance in between the pocket and connector is later filled with grout. Tightening of the top nut is performed before grout hardening. From the push-out test conducted a high shear resistance and stiffness were observed. The almost identical connector comprise the friction based shear connector which transfers the load through friction. The FBSC differs in geometry and mechanism from the LNSC through a retaining washer instead of a conical nut. The FBSC is pretensioned by tightening one of the two nuts. The FBSC offers a high shear resistance, stiffness and slip capacity as well. The connectors proposed are considered a great alternative when compared to welded and other bolted shear connectors due their mechanical performance [52]. However, by grouting the clearances in both connectors the installation process in second life cycles may be obstructed. Therefore, the application of the LNSC and FBSC cause reuse impairment, as the components need to be mechanically separated.

The bolted shear connector with a coupler system, also a novel bolted shear connector, is proposed to facilitate the dismantling process (see Figure 2.5d). The bolt consists of two bolts and a coupler. A long bolt is embedded in the concrete slab, a short removable bolt is installed from below the steel flange and the coupler connects the two bolts. The bolted shear connector proposed is analysed through static push-out tests using different bolt configurations by F. Yang et al. [53]. The shear bearing capacity of bolted connectors was almost equal to conventional welded shear studs with similar diameters. The peak slip of the bolted connectors increases with an increasing bolt diameter. The authors concluded that the shear stiffness of the bolted connectors was influenced by the bolt-hole clearance in the steel flange. Kozma et al. [40] looked into shear connectors with a coupler system that may prevent deflection in the execution stage caused by bolt slip. Therefore, two types of coupler systems were taken for analysis. This included a coupler system with pre-tensioned bolts and a coupler system with epoxy resin-injected bolts. The couplers are welded to a L-shaped profile to enhance edge protection and augment friction resistance between the beam and slab. The coupler system with pre-tensioned bolts indicated a lower initial stiffness compared to the epoxy resin-injected bolts. The epoxy resin prevents the decrease in stiffness and load-bearing capacity. The coupler system with injection bolts appeared to have a lower slip capacity which is probably a result of no pretension applied to the bolts. Bolt shear failure appeared as the generic mode of failure, which was also found in the push-test in F. Yang et

al. [53]. Nijgh [6] conducted a thorough investigation into the performance of a connector with injected epoxy resin, including significantly oversized holes, which aids in the assembly and disassembly of bolts. The experimental results demonstrated that the use of injection bolts enhances the slip capacity and initial stiffness of the shear connector. Demountability of the coupler system was proved by the successful removal of the bolts. The systems developed appeared to be suitable for reuse. Similar observations were noted by Nijgh et al. [54] who demonstrated the ability to demount and reuse elements from a composite flooring system with the application of resin-injected bolts.

He et al. [55] came up with the idea on the design of the lockbolt (LB-DSC) to exclude sudden occurrence of slip (see Figure 2.5e). The LB-DSC includes a grout-filled steel tube that is embedded within the concrete. The tube is fastened to a compatible thread-bolt that is connected through bolts with the flange of the steel I-section. The occurrence of slip is prevented by the conical seat lug. This lug is located inside a predrilled hole in the flange of the steel section. Epoxy resin is used to fill the gap in between the bolt holes. Deconstruction of the LB-DSC is achieved by simply loosening the nut or tube from the system. This allows for an easy detachment in which the components are adequate for reusable SCC flooring systems. Experimental and numerical results indicated that the LB-DSC has very high shear resistance and initial stiffness. The slip capacity of the connector exceeds the required 6 mm required by EN 1994. The parametric study showed that the shear resistance and stiffness of the LB-DSC significantly can be improved by increasing the bolts diameter. Increasing the tube thickness and compressive strength of the slab has moderate improvement on the bolts stiffness and resistance.

The application of blind bolts should benefit the process of faster and easy bolt mounting. Two types of blind bolts are distinguished and taken for analyses in different experiments, see figure 2.5f. This comprises the BB1 (hollow) bolt and BB2 (ajax) bolt. Blind bolt marked BB1 can be easily installed as the bolt does not require assembly, but tightening only. The bolt consists of a collar that spreads open when put into place. Blind bolt BB2 requires a specialised tool for bolt installation. The reliability of the bolts is higher than that of welded shear studs since the quality is assessed through non-destructive methods. In order to establish whether blind bolts have the ability to achieve composite interaction push-out tests have been carried out by Pathirana et al. [56]. From the push-test results it was observed that both blind bolts had a varied slip response compared to welded shear studs. According to Patirana et al. [56] this type of slip response is attributed by deformation of the connector during loading and the presence of bolt hole clearance. Moreover, the welded stud and blind bolt BB1 showed a higher stiffness compared with BB2 connector. However, both bolted connectors demonstrated a higher shear capacity than the welded studs. In general all demountable connectors can be used to rehabilitate and strengthen existing structures. However, blind bolts allow to be installed from below the flange, which makes this type more suitable for rehabilitation when compared to other connectors. Henderson et al. [59] and Pathirana et al. [57] performed push-out tests on BB1 and BB2 and compared the results to conventional welded shear studs. From the load-slip curves it was observed that the ultimate shear strength of the blind bolts was much higher than the welded shear studs. Furthermore, the BB1 connector had a larger initial stiffness value than the BB2 connector, though the BB1 connector had a lower ductility and ultimate load capacity when compared to BB2. To determine the deconstructability of the connectors, research by Pathirana et al. [58] demonstrated demountability of a steel-concrete composite beam that contained BB1 connectors. After reassembly no considerable change in the load-deflection behaviour was observed which indicated the ability of the system to be reused without degradation of the beams characteristics.

2.3.4. Other demountable shear connectors

Several other types of shear connectors for steel-concrete composites have been developed during the last couple of years, for the replacement of welded shear studs. Recent studies by Wang et al. [60] and Feidaki et al. [61] looked into other types of demountable shear connectors through push-out tests. These relate to the clamping connector and yielding pocket demountable shear connector (YPDSC) (see Figure 2.6a and 2.6b). The connectors both use precast concrete slabs in application. Although the 'unconventional' shear connectors presented are designed differently from the bolted connectors, they have shown great potential in steel-concrete composite floor systems.

Wang et al. [60] introduced the clamping connector as a means of eliminating the need for bolt holes in the flange of the steel girder. Additionally, deconstructable clamping connectors provide the opportunity the utilise precast concrete planks in a demountable composite floor systems. To provide for flexibility during assembly, T-bolts are placed into cast-in channels. High-strength bolts are pre-

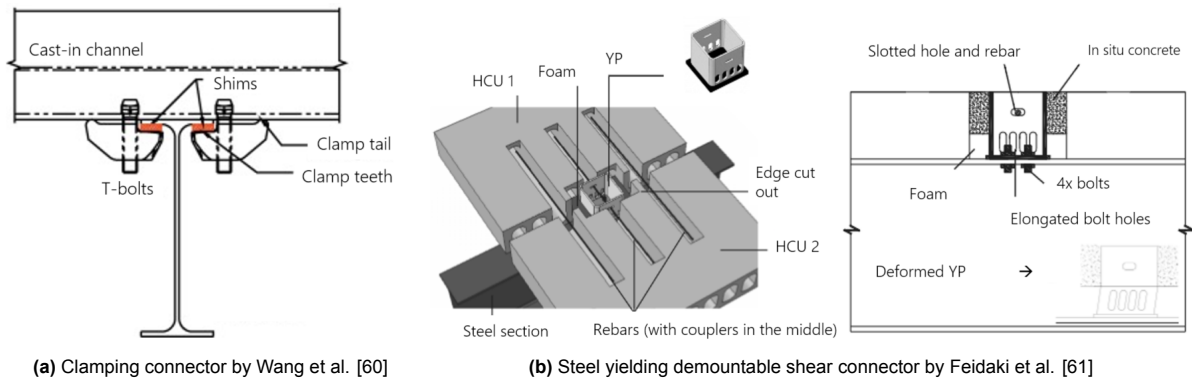


Figure 2.6: Other types of demountable shear connectors

tensioned, creating friction to achieve composite action. The authors of [60] carried out experimental tests under monotonic and cyclic loading conditions. The specimens indicated have high initial stiffness and very high ductility and slip capacity. Similarly to welded-headed studs, the clamping connector exhibit a strength reduction when subjected to cyclic loading. The concrete planks and steel I-section can be easily separated by loosening the bolts and rods.

To promote the reuse of precast concrete hollow core slabs, Feidaki et al. [61] investigated the application of a yielding pocket (YP) in steel-concrete composite floor systems. The connector consists of a steel square hollow yielding pocket that is welded on a steel plate. The steel plate is connected with the steel section's top flange through four high strength bolted connectors. Experimental results indicated that the yielding pocket can provide high strength, high initial stiffness and high slip capacity as well. The specimens that were designed to fail in a ductile mode had slip capacities in excess of 30 mm slip. The main failure modes of the connector relate to yielding of the yielding pocket and shear failure of the hollow core units. Successful deconstruction of the yielding pocket was demonstrated by reusing the steel I-sections and hollow core units from different specimens.

Research into the application of a novel demountable bolted shear connector for hollow core slabs has been performed by Wintermans [62]. The research investigated the sustainability index and the demountability aspect of the shear connector, which incorporates greater tolerances between the HCS and the steel frame section to achieve a demountable and reusable connection. The connection presented in Figure 2.7 consists of steel squared hollow sections in which a shear bolt connects the HCS to the steel flange of the I-section. The squared hollow sections are positioned at the near ends of hollow core sleeves. Strength verification and stiffness analysis of the joint were carried out, but no experimental push-out tests were carried out. The study concluded that the use of square hollow sections with bolted shear connectors has great demountability potential with greater design tolerances while meeting structural requirements.

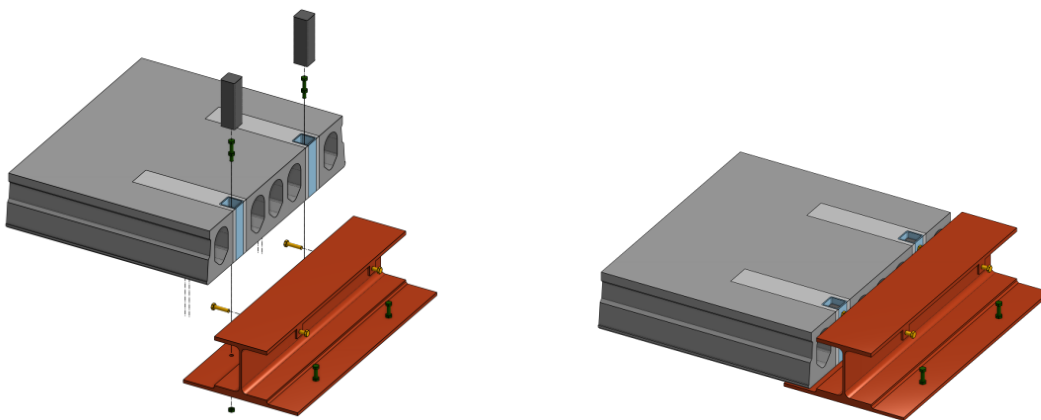


Figure 2.7: Application of demountable bolted shear connector in hollow core slabs, integrated with the steel I-section [62]

2.3.5. Comparison of experimentally tested shear connectors

Demountable shear connectors have been introduced to replace welded shear studs, while maintaining the same function and characteristics. The performance of the demountable shear connectors in literature is assessed through comparison of the mechanical behaviour and additional parameters that affect this behaviour. Therefore, to establish this behaviour of the connectors proposed in the literature, a comparison to conventional welded shear studs is performed. The mechanical behaviour of various push-out tests on welded shear studs and demountable shear connectors are depicted in Figure 2.8-2.10 [7]. From the load slip curves in the figure it is observed that the welded shear studs exhibit higher initial stiffness compared to the demountable connector. In addition, the welded studs have higher ultimate load capacities while retaining ductile behaviour.

The bolted shear connectors without embedded nuts appear to have poor performance when compared to other bolted shear connectors. From the load-slip curves depicted in Figure 2.8a it is observed that the bolts with embedded nuts have an increased stiffness compared to bolted connectors without embedded nuts (threaded studs). However, a very low slip rate at failure is observed for the bolts with embedded nuts which indicates a (brittle) bolt failure. The mechanical behaviour of blind bolts type I (hollow bolt) and type II (ajax bolt) are compared to conventional welded shear studs in Figure 2.8b. BB1 connector shows a higher initial stiffness compared to the BB2 connector. However, a considerable smaller ductility and load capacity before failure is observed as well. The slip capacity of the BB1 connector is problematic compared to other connectors since does not fulfil the minimum slip requirement.

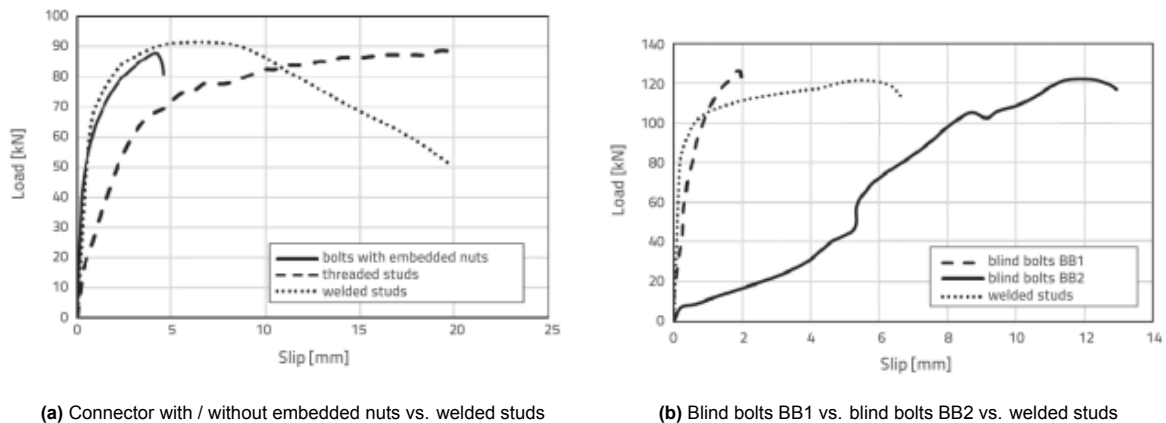


Figure 2.8: Comparison of bolted shear connector behaviour from existing experiments [7]

Figure 2.9a presents the load-slip curves for friction grip bolts and the coupler system with and without the application of epoxy resin. The initial stiffness of all connectors in the load-slip curve from the figure are comparable. However, the ductility of the connectors is considered problematic with respect to the low slip capacity. All connectors exhibit a load capacity that is comparable to the welded studs. The LNSC and FBSC connector are compared to friction grip bolts and bolts with embedded nuts in Figure 2.9b. A very high initial stiffness is observed from the load-slip curves for the LNSC and FBSC. Moreover, the ultimate strength and slip capacity appear high as well. The connector with embedded nuts behaves inferior in terms of strength and stiffness capacities, but shows a ductile behaviour. The friction grip bolt has a reasonable stiffness but low slip capacity.

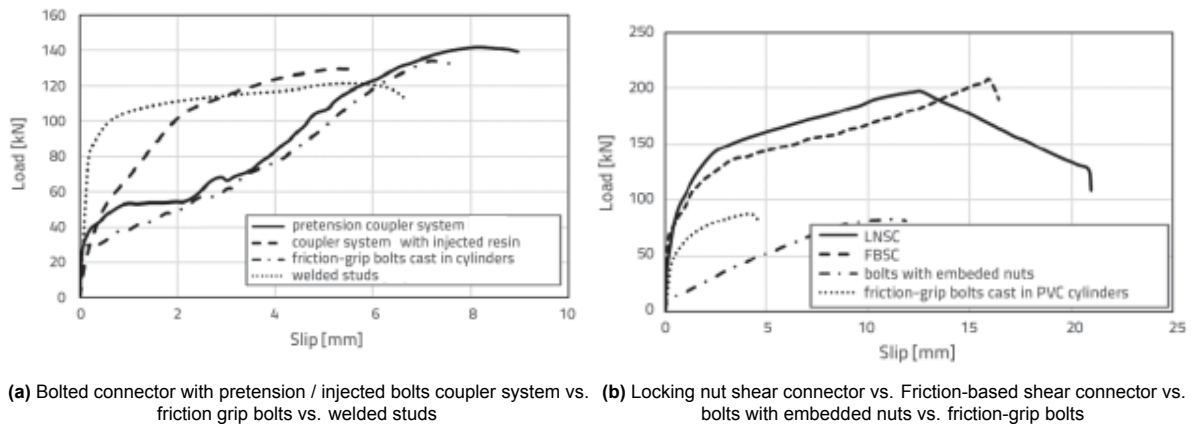


Figure 2.9: Comparison of bolted shear connector behaviour from existing experiments [7]

The push-out experiment conducted by Wang et al. [60] showed that the clamping connector has a high initial stiffness and very high ductility (see Figure 2.10a). The figure compares the load-slip behaviour of the clamping connector to shear connectors with embedded nuts and high-tension friction grip bolts. The ultimate strength of the clamping connector appear to have a lower strength at 10 mm slip compared to the other connectors. According to Jakovljevic [7] this is attributed by bolt rotation and bolt head fracture. The load-slip curve of the yielding pocket from Feidaki et al. [61] is presented in Figure 2.10b. The mechanical behaviour is compared to welded studs that were applied in hollow core units as well in a study performed by Lam et al. [31]. The figure shows that the mechanical performance of the yielding pocket exceeds that of the conventional shear studs. A very high shear capacity and slip capacity are observed from the curve. However, as highlighted by Jakovljevic et al. [7] it is important to consider that the connector proposed entails substantial material usage.

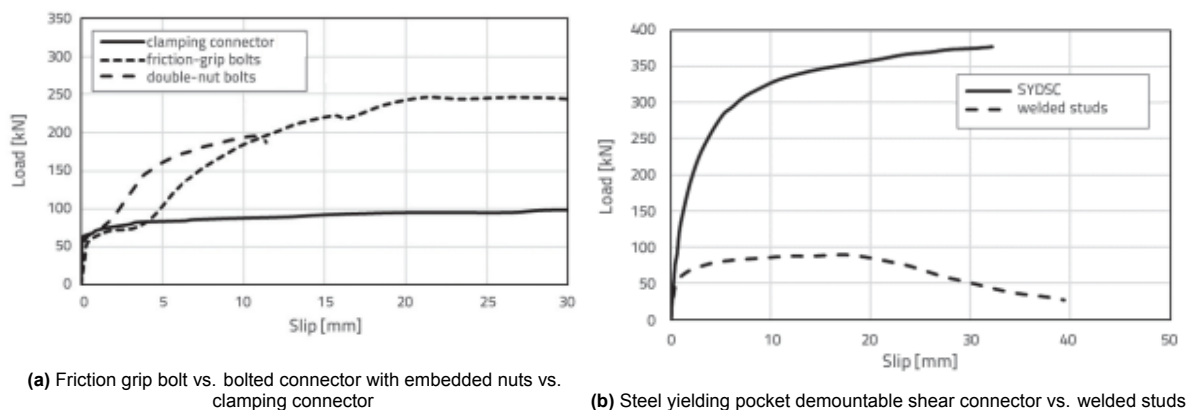


Figure 2.10: Comparison of other types of shear connector behaviour from existing experiments [7]

The analysis of literature on various connectors suggests that the ultimate resistance, stiffness, and ductility of demountable shear connectors are crucial requirements for the performance of steel-concrete composite structures. To achieve these properties, a sufficient number of shear connectors can be provided in the composite beam, which can relatively easily increase the ultimate resistance. However, increasing the stiffness and ductility of shear connectors is more challenging. These properties significantly affect the behaviour of composite beams. Shear connectors with low stiffness and high flexibility cannot provide sufficient interaction between materials to achieve composite action. Ductile behaviour of the shear connectors is a key characteristic as it determines whether a connector has sufficient deformation capacity to redistribute shear stresses. The ductility of the shear connectors varies with composition and design.

2.4. Improving composite interaction for larger tolerances

The utilisation of oversized holes serves to facilitate the assembly and disassembly of a demountable composite floor system. Nevertheless, the application of oversized holes is incompatible with the necessity of maintaining tight tolerances between the bolt and steel flange, which is essential to generate composite interaction between the concrete and steel element. Consequently, two generic solutions are available to provide composite interaction with oversized holes: (I) preloaded and (II) injected bolted connections.

2.4.1. Preloaded bolted connections

Preloaded bolted connections or pretensioned bolts refer to a connection where an axial force is applied within the bolt-section. Preloading a bolt in composite structures allows the shear force to be transferred by friction at the steel-concrete interface. The frictional force generated by bolt preloading increases the resistance of the joint to bolt slippage. When the applied preload force exceeds the frictional resistance, slip is induced and the bolt is subjected to its bearing resistance. Figure 2.11 presents the load transmission mechanism through friction in a shear connection.

Bolts that transfer a load through friction are also known as high-strength friction-grip bolts (HSFGB). HSFGB connections are generally applied for their relatively high stiffness capacity, and ability to endure alternating forces. Moreover, various research papers ([36]) have shown that the behaviour of HSFGB under fatigue loading is more enhanced compared to bearing bolted connections. The preload force in a single bolt is determined through Eq. 2.7, where f_{ub} represents the nominal ultimate stress and A_s the tensile stress area of the bolt.

$$F_{p,C} = 0.7f_{ub}A_s \quad (2.7)$$

The preloading force within the bolt pertains to the vertical force vector that compresses the plates. The reaction force is translated into a friction force, which is activated at the shear planes of the plates. The design slip resistance, $F_{s,Rd}$, is determined through Eq. 2.8 following the principle prescribed by EN1993-1-8 [63]:

$$F_{s,Rd} = \frac{k_s n \mu}{\gamma_{M3}} F_{p,C} \quad (2.8)$$

where k_s presents the factor for bolthole clearance, n the number of shear planes and μ the friction coefficient at the interface of the plates. The factor k_s depends on the clearance of the bolt hole, with a distinction being made between normal, oversized and slotted holes. The friction coefficient accounts for the relation between the normal and friction force. A higher friction coefficient induces a higher slip resistance.

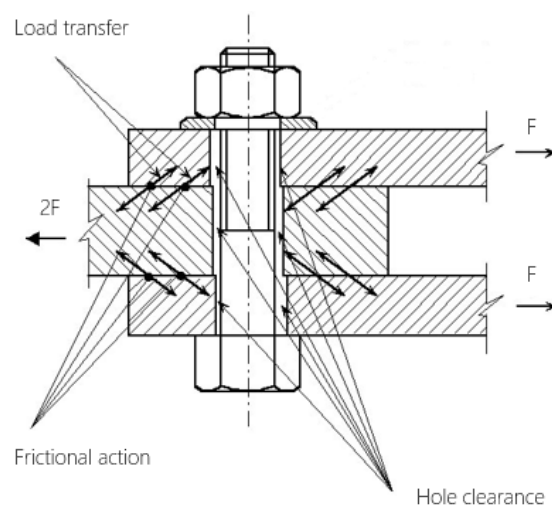


Figure 2.11: Load transmission in shear connection through friction

2.4.2. Injected bolted connections

Another solution involves the injection of epoxy resin within the bolt hole cavity to transfer the load through bearing. Nijgh et al. demonstrated the viability of a multi-storey car park structure constructed using resin-injected demountable shear connectors in a demountable steel-concrete composite floor system (see Figure 2.12). This system allows for the utilisation of oversized holes in the steel flange. Injection bolts in composite systems permit greater tolerances between the bolt and steel flange, while also increasing shear interaction within the joint. The experiment demonstrated that the application of resin-injection bolts that function as shear connectors resulted in an immediate composite interaction between the concrete slab and steel beam, preventing any sudden slip at increased load levels.

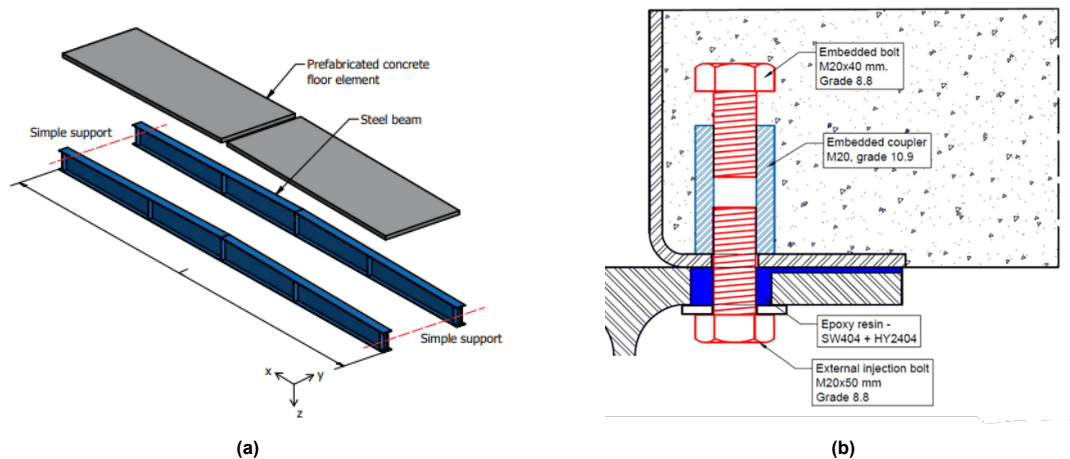


Figure 2.12: (a) Global overview of composite car park system and (b) cross-section of demountable shear connector with coupler system and injected epoxy resin in bolt hole [64]

The implementation of epoxy resin in bolted demountable shear connectors originate from the application of injected bolted connections (IBC). IBC relate to joints in which the clearance around the bolt hole is filled with a specific resin after assembly. A hole in the head of the bolt allows the resin to be injected. Figure 2.13 shows the application of an injected bolted connection. Injecting resin into the bolt hole cavity increases slip resistance. No sudden slipping can occur due to the hardened injectant which prevents movement of the bolt in its bolt hole [65]. Slip resisting connections are essential in applications where the connection is subjected to cyclic shear loading. Moreover, the application of injection bolts allows for protection against corrosion. The bolt hole cavity is concealed which prevents the infiltration of water. Although the performance of injected bolted joints is inferior to that of fitted bolts, the use of this type of bolt provides a more practical solution when compared to fitted bolts as greater clearances allow the opportunity to reuse structural elements in composite structures [66].

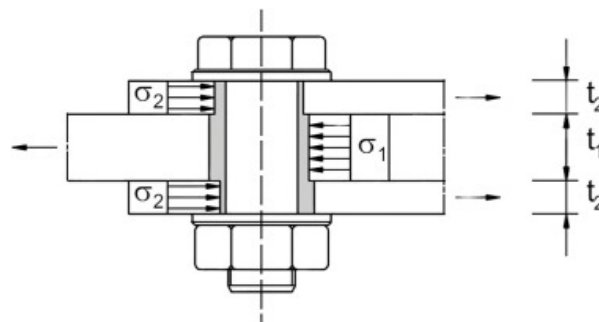


Figure 2.13: Double lap steel-to-steel injected bolted shear connection according to EN 1993-1-8 [63]

For injected bolted joints, two-component epoxy resins may be used if they meet the requirements of EN 1090-2 [67]. The conditions relate to the viscosity, thixotropic behaviour and pot time of the epoxy resin. The thixotropic behaviour is described by the ability of the resin to prevent a decrease in viscosity when the injection pressure is removed. The pot time ensures workability after a minimum

of 15 minutes. Various studies have looked into the behaviour of different epoxy resins [66, 68, 69]. However, the most widely used (certified) two-component epoxy resin relates to RenGel SW 404 + HY 2404/5159 [68]. The resistance of the resin injected bolt is determined through Eq. 2.9. The nominal bearing strength of the resin ($f_{b,resin}$) is defined by EN 1090-2 [67]. The standard describe the strength as the nominal bearing stress that leads to 0.30 mm slip after 50 years.

$$F_{b,Rd,resin} = k_t k_s \beta \frac{d t_{b,resin} f_{b,resin}}{\gamma_{M4}} \quad (2.9)$$

Within the formulae d represents the diameter of the bolt, the factor k_t relates to the loading duration in the limit state (1.0 in SLS and 1.2 in ULS) and k_s accounts for the increased hole clearances. The effect of the plate thicknesses is described by the magnitudes of β and $t_{b,resin}$ (see Table 2.1). The thickness of double-lapped joints (L) cannot exceed three times the bolt diameter ($3d$), due to a non-uniform stress distribution in the epoxy resin. The resistance to bearing is determined through a specific height that depends on the thickness [63].

t_1/t_2	β	$t_{b,resin}$
≥ 2.0	1.0	$2t_2 \leq 1.5d$
$1.0 < t_1/t_2 < 2.0$	$1.66 - 0.33(t_1/t_2)$	$t_1 \leq 1.5d$
≥ 1.0	1.33	$t_1 \leq 1.5d$

Table 2.1: Determination of β and $t_{b,resin}$ per plate thickness ratio according to EN1993-1-8 [63]

2.5. Demountable reinforced concrete slabs using dry connections

Concrete structures can be disassembled and reassembled if the connection follows the principle of so-called "dry connections". Dry connections are achieved by using dowels, anchor rods, threaded bolts, steel plates and/or steel angles. The use of dry joints is considered to be an efficient DfD strategy, where the demolition of structural elements should be such that the concrete elements can be reused.

2.5.1. Concrete half-joints and Gerber beams

Dry connections can be applied in the form of a concrete half-joint (shear key). Concrete half-joints consists of dapped-end beams which are supported on the nibs of abutments and form suspended spans. Concrete half-joints are used to improve strength, maintain integrity and increase the resistance to sliding. This connection type is commonly applied in reinforced concrete spans to simplify buildability.

A simply supported static scheme allows for an easy determination of the stress distribution, where internal actions do not develop because of settlements and/or thermal variations. However, the (sagging) bending moment at mid-span is greater than that of continuous supported beams where the bending moments are redistributed at the supports (hogging). The scheme of the simply supported continuous beam tends towards the diagram of a beam fixed at both ends. Hence, it is established that continuous beams have better distribution of bending moments, but this comes at the cost of developing additional internal stresses.

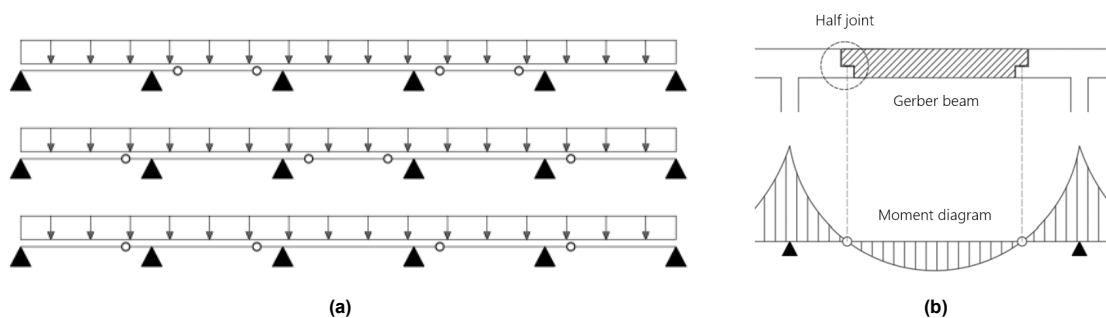


Figure 2.14: (a) Positioning of joints in simply supported continuous beam and (b) static scheme for optimisation model of suspended span and half-joint

A sophisticated solution is provided by the application of Gerber beams. The principle of Gerber beams allows for the incorporation of an optimised bending moment distribution, while minimising the development of additional stresses. The positioning of joints at points of zero bending moment, leads to a simply supported static scheme with the moment distribution of a continuous beam (see Figure 2.14a). Consequently, half-joints and Gerber beams have frequently been employed due to their ease of prefabrication and the optimisation of stress distribution. Figure 2.14b depicts an optimised static scheme for simply supported continuous beams, with the application of a Gerber beam.

The performance of concrete half-joints is highly dependent on the reinforcement configuration in the Gerber beam and nib-section. The reinforcement configuration and design of such prefabricated joints is nowadays performed through the strut-and-tie model. This method relies on the principles that external loads and the internal stress distribution must be in equilibrium, and the internal stress may not exceed the plastic stress of any element [70]. The design of reinforced concrete half-joints is performed by dividing the half-joint in B- and D-regions such as depicted in Figure 2.15. The B-regions follow the hypothesis of Bernoulli using beam theory, where the D-regions follow the design principles of the strut-and-tie model. The struts in the model account for the compressive forces, and the ties the members in tension.

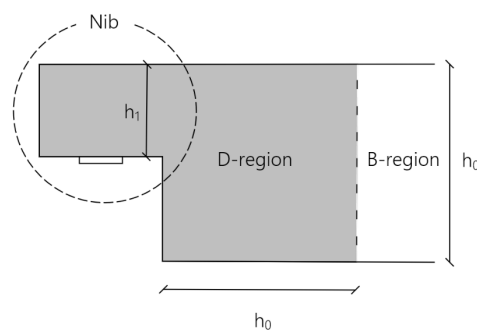


Figure 2.15: Geometry of a half-joint, including D- and B-region

Desnerck et al. [71] performed experimental research into strut-and-tie modelling of reinforced concrete half-joints, and proposed different reinforcement configurations within the half-joint. The potential failure modes in half-joint connections are nib shear failure, inclined shear failure in the nib, crack initiation failure in the corner and shear failure in the beam [72]. Half-joints are considered brittle, which is why very limited deformations occur before failure. From the test campaign performed by Desnerck et al. [73] the following reinforcement details within the configuration affect the crack pattern at ULS:

- Rebars that present in diagonal, horizontal and vertical directions in the nib-section and nearby area, a critical crack develops within the nib in coherence with secondary cracks in the beam;
- In case the reinforcement configuration includes only inclined and vertical reinforcing bars, the critical crack causes a vertical cut in the nib;
- In case the reinforcement configuration includes only horizontal and vertical reinforcing bars, then failure occurs with limited deformation.

Half-joints with a given geometry can be designed following numerous strut-and-tie models. The strut-and-tie models only require equilibrium and that the strain criteria is met. The most common strut-and-tie designs relate to diagonal and orthogonal models, or a combination of the two. Figure 2.16 depicts potential strut-and-tie models. The model that is selected for the half-joint should be such that the ties line up to the best of one's ability with the reinforcement. Eurocode 2 [74] reports no minimum value for the angle between the struts and ties, but stipulates that higher concrete stresses (10%) are allowed where angles are greater than 55°.

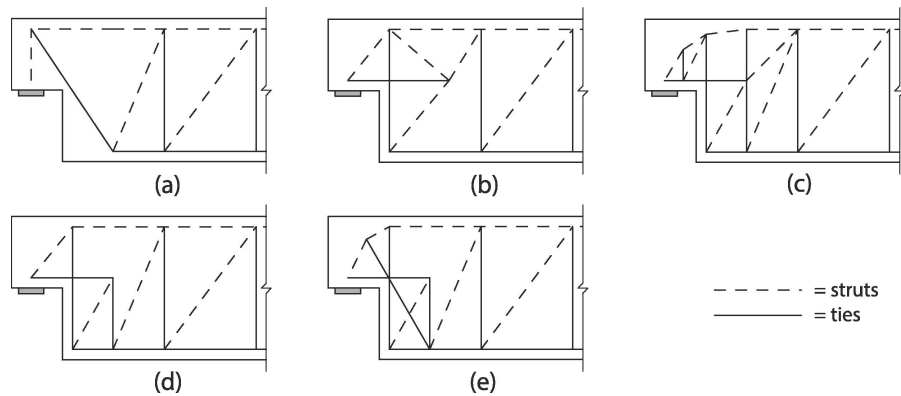


Figure 2.16: Feasible strut-and-tie models for prefabricated reinforced half-joints: (a) diagonal, (b) orthogonal I, (c) orthogonal II, (d) orthogonal III and (e) combination [71]

2.5.2. Experimental research on concrete dry connections

The application of demountable concrete slabs has not been extensively investigated in the literature. The research performed by Figueira et al. [75] presents a state-of-the-art review on dry connections between precast reinforced concrete components including beam/beam-, beam/column- and slab/slab joints. The review indicated that there exists a scarcity on experimental investigations available into these concrete connections in the literature.

In order to investigate the potential of design for deconstruction (DfD), Xiao et al. [76] conducted a study on a proposed moment-resisting concrete beam/beam connection. In beam/beam- and beam/column connections, the flexural stress should be transferred between the connected structural elements. The proposed design incorporates reinforcing steel and concrete half-joints such as visualised in Figure 2.17. The main reinforcement at the upper and lower extremities of the beam is welded to the principal reinforcement on the protruding beam of the precast column section. Cast-in-situ concrete is placed within the concrete section to embed the reinforcement. The concrete serves to transfer compression stresses and to protect the reinforcement against corrosion. The experimental programme employed a total of five distinct specimens, which were subjected to both static and cyclic loading tests. The concrete specimens were constructed using either natural aggregate concrete or recycled aggregate concrete. The specimens were tested through to a cantilever beam test, with a point load applied at the critical extreme.

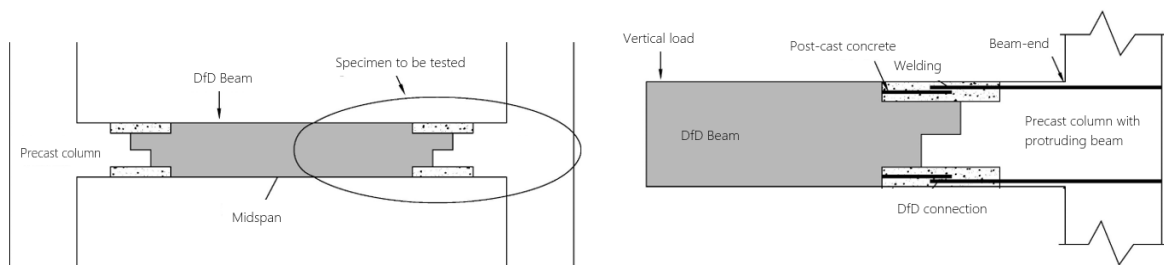


Figure 2.17: Prototype of DfD concrete structure and details of proposed DfD beam/beam connection [76]

The results of the experiment demonstrated that the proposed moment-resisting concrete connection was capable of providing sufficient moment resistance. In both static and cyclic loading conditions, the specimens exhibited ductile behaviour. As anticipated, the concrete specimens that utilised recycled aggregate exhibited more cracks, with a particular concentration observed in the connection area. Nevertheless, the utilisation of recycled aggregate concrete is deemed a viable proposition based on the outcomes observed. Furthermore, the structural behaviour was markedly enhanced as a consequence of welding the longitudinal reinforcement. Furthermore, the DfD specimens exhibited comparable cracking patterns, energy dissipation, moment capacity, and ductility ratio to those observed in the reference models.

A new configuration of connecting precast concrete slabs was proposed by the authors of [77] in which the slabs are connected through top and bottom steel plates. The plates are attached to the slabs using threaded bolts. Almahmood et al. [78] carried out the first experimental investigation of solutions for this demountable precast concrete slab/slab connection. The slab/slab joint was for each specimen positioned at mid-span. The specimens for the experimental investigation were designed to be assembled using the steel plates at the top and bottom of the concrete slabs connected by high strength bolts. The bolts connect a bottom steel plate to the concrete slabs, where the plates carry the tensile stress at the bottom of the slab. Compressive stresses at the top of the slab can be transferred by either bearing or by adding an identical steel plate at the top of the slab. The bolts were held in position by embedding steel channels in the slabs.

The specimens differed in design by the use of shear keys (half joints) and embedded steel blocks. The embedded steel plates are welded to the ties at the bottom of the slabs. The application of the embedded plates should benefit the transfer of tensile stresses within the connection. However, according to Figueira et al. [75] the slab section may be weakened due a reduction in concrete cross-sectional area as a result of the steel plates and through bolts. The specimens were tested through a 4-point flexural test with the connection located at mid-span for each specimen. The specimen with and without the application of a shear key and an embedded block is depicted in Figure 2.18.

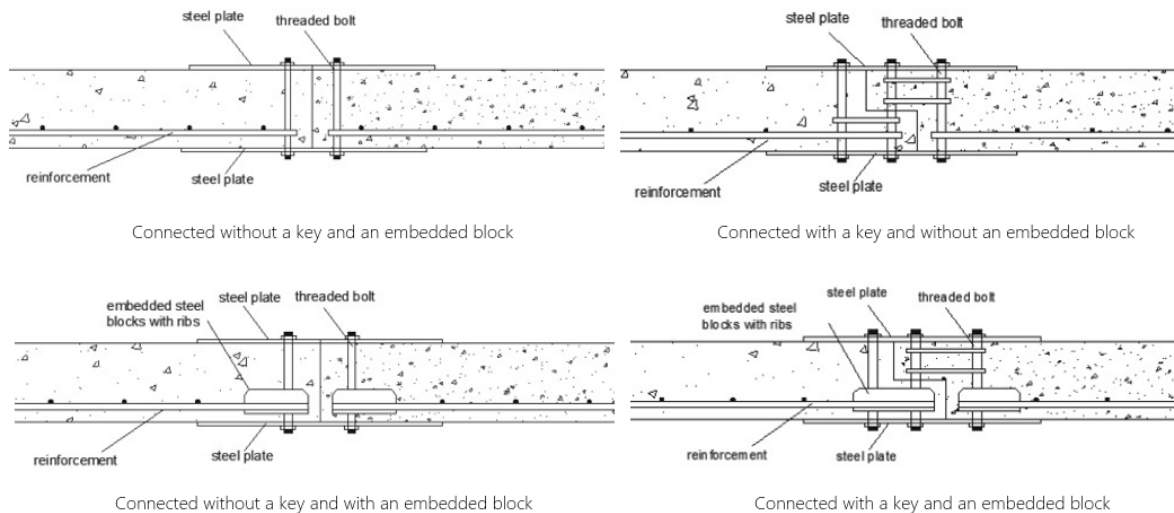


Figure 2.18: Specimen design alternatives with/without a shear key (half joint) and an embedded block [78]

The results from the experiments by Almahmood et al. [78] indicated that slabs without embedded steel block, failed as result of cracks that extended along the bolt line due to high stress concentrations and a reduction on the concrete's cross-section due to the bolt holes. The specimens that consist of embedded steel blocks led to premature failure as these exhibited wide cracks at the steel block edge. The slabs with a dry connection that consist of a shear key demonstrated to have largest load-capacity and flexural stiffness. In addition, these specimens exhibited the least deflection and crack width. Lastly, the slabs that consist of a dry connection and embedded steel blocks demonstrated to fail prematurely as a result of a high stress concentrations at the block edge and reduction of the concrete's cross-section.

2.6. Bolt applications for newly cast/precast concrete construction

The reuse of concrete slabs in newly constructed buildings may present certain design challenges. Although the concept of connecting concrete slabs is relatively novel in the construction industry, it can be implemented using a variety of bolt applications, which include mechanical and chemical concrete anchors. The applications available are offered by multiple providers that specialise in (de)mounting precast concrete materials. The different applications suitable for precast concrete components offered by HILTI company [79] are elaborated within this section.

2.6.1. Mechanical & chemical concrete anchors

Mechanical and chemical concrete anchors provide the opportunity to be assembled in precast concrete components. The mechanism of mechanical concrete anchors occurs through mechanical adhesion, where there is resistance of the plug to the embedded material. The anchors are secured by either screwing or wedging into the concrete (or any other material) at the tip. Mechanical anchors are suitable for both uncracked and cracked concrete in the range of C20/25 to C50/60. As a result of the high strength expansion and shear sleeves, the anchors have a high shear performance. Moreover, the anchors can be easily removed for temporary and machine fastening applications.

A chemical concrete anchor is an anchor that is formed through a chemical reaction between the injected substances. After hardening a high-strength connection between the anchor and its surroundings exists. Although chemical anchors require a hole to be drilled as opposed to mechanical anchors, chemical anchors have specific advantages over mechanical anchors (see Figure 2.19 and Table 2.2). Chemical anchors allow for more flexibility at construction site with respect to alternating the maximum load bearing capacity. The load capacity is relatively easily increased by increasing either the length of the drilling depth or the drill diameter. Moreover, no stress is exerted on the substrate around the borehole since the chemical anchor does not expand as it hardens. Additionally, the load is distributed over the entire surface of the borehole, resulting in an exceptionally strong bond. This allows for secure fastening close to the edge without causing the concrete to crack. The risk of corrosion or weakening due to moisture or chemical substances is prevented as the anchor is airtight and waterproof. A drawback of chemical anchors is that they are difficult to remove and therefore reuse, as the chemicals are bonded to the concrete, which makes it very likely that the concrete will break or tear off if the anchor is removed.

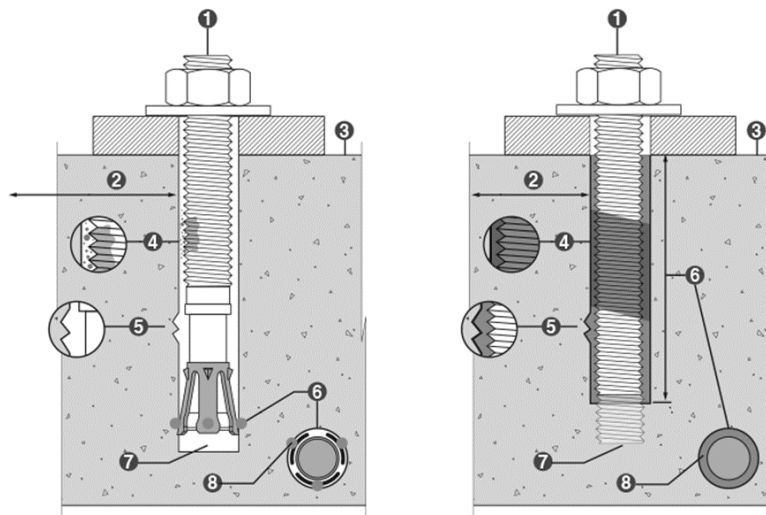


Figure 2.19: Mechanical and chemical concrete anchor [80]

Mechanical type anchors	Chemical type anchors
1 Limited to stock sizes, length, diameter & steel grades	Large range of sizes and high-grade steel available
2 Larger edge distances are required	Can be installed close to the edge
3 Not suitable for softer base materials	Suitable for many base materials
4 Prone to water ingress leading to corrosion	Protects the anchor from corrosion
5 Not ideal for imperfect drilled holes	Chemical injection can fill imperfect & oversized drilled holes
6 Load is concentrated at limited points	Load is applied to embedment length
7 Hole depth, diameter & installation torque are critical	Unlimited setting depths can be specified
8 Stress is imparted directly into base material	A molecular bond occurs with even distribution of stress

Table 2.2: Mechanical and chemical type anchors; Application, workability and characteristics [80]

2.6.2. Applications - HILTI

Hilti company [79] offers various amount of mechanical and chemical anchors for concrete components. The mechanical and chemical anchors considered applicable to concrete floor systems are reported accordingly within this subsection. The anchors developed by HILTI follow the anchor design prescribed in EN 1992-4 [74] for concrete applications. The mechanical anchors in Table 2.3 comprise the HST4-R- and HSL4 expansion anchor. The HST4-R anchor is considered a high-performance expansion anchor that is suitable for uncracked and cracked concrete class C20/25 to C50/60. The anchor has the ability to be applied in concrete members with a reduced thickness, limited edge distance and a small spacing. The HST4-R anchor is appropriate in structural design for static/quasi-static and seismic load conditions.

The HSL4 expansion anchor is considered appropriate for ultimate performance where heavy loads are subjected to the anchor. Similarly to the HST4-R anchor, the base material for the anchor comprises uncracked and cracked concrete class C20/25 to C50/60. The anchor is suitable especially to provide a high shear resistance as a result of the high strength expansion and shear sleeves. Moreover, the HST4-R anchor is suitable for static/quasi-static, seismic and fatigue loading conditions and loads that are induced by shocks and fire.



Mechanical anchors - HILTI					
Type	Applicability	Base material	Load conditions	Design life	
HST4-R	M8-M20	Cracked/uncracked concrete, Dry concrete	Static/quasi-static, Seismic-C1/C2, Fire-resistance	50 years	
HSL4	M8-M24	Cracked/uncracked concrete, Dry concrete	Static/quasi-static, Seismic-C1/C2, Fire-resistance, Fatigue-ETA, Shock	50 years	

Table 2.3: Mechanical type anchors offered by HILTI [79]

The chemical concrete anchors that are considered applicable relate to the three types reported in Table 2.4. The HIT-HY 200-A V3 injection mortar anchor is suitable for uncracked and cracked concrete class C20/25 to C50/60 in both dry and wet concrete conditions. The injection mortar provides after hardening and a well established contact a high corrosion resistance. The application of injection mortar allows for small edge distance and anchor spacing. The injection anchor is approved for seismic loading conditions within category C1 and C2.




Chemical anchors - HILTI					
Type	Applicability	Base material	Load conditions	Design life	
HIT-HY-200-A-V3 Injection mortar	M8-M30	Cracked/uncracked concrete, Dry/wet concrete	Static/quasi-static, Seismic-(C1-C2), Fire-resistance, Fatigue-ETA	100 years	
HIT-RE-500-V4 Epoxy mortar	M8-M39	Cracked/uncracked concrete, Dry/wet concrete	Static/quasi-static, Seismic-(C1-C2)	100 years	
HIT-HY-170 Injec- tion mortar	M8-M24	Cracked/uncracked concrete, Dry/wet concrete	Static/quasi-static, Seismic-(C2)	50 years	

Table 2.4: Chemical type anchors offered by HILTI [79]

The HIT-RE 500 V4 anchor bolt has similar technical characteristics, but uses epoxy as the filler material. The anchor type is also suitable for identical strength classes both uncracked and cracked concrete in dry and wet conditions. Unlike the HIT-HY 200-A V3 anchor, only static/quasi-static and seismic loading conditions are applicable. The anchor is considered to have a high load capacity and allows for small edge distances.

Lastly, the HIT-HY 170 injection mortar anchor is considered a suitable chemical concrete anchor. This type of anchor shares lot of similarities with the first two types of chemical anchors, but is limited in its resistance. The anchor is only suitable for static/quasi-static and seismic category C2 loading conditions. In addition, the design life for this application is guaranteed to be 50 years rather than 100 years.

2.7. Design of composite floor systems according to Eurocode 4

Eurocode 4 [32] covers the design of steel-concrete composite structures. To evaluate the performance of a demountable composite floor system that use reused concrete decks, it is pivotal to consider the design verification for ultimate limit state and serviceability limit state.

2.7.1. Ultimate limit state (ULS)

The resistance of composite beams to critical cross-section forces, lateral-torsional buckling, shear buckling and longitudinal shear should be verified through design standard provided in EN 1994 [32]. Composite T-beams provide an efficient structural member that can be used for a variety of structural applications. The non-uniform cross section of the T-beam could cause the phenomenon known as shear lag, as the stresses are non-uniformly distributed. Following bending theory, shear lag can result in an inaccurate estimation of stresses and displacements at extreme fibers of the composite T-section [81, 82]. To account for the reduction in capacity of the flange, the effective width (b_e) of the flange is introduced. The concept of the effective width assumes a constant stress distribution over that particular width. The result is an equal sum of stresses. Figure 2.20 depicts the theoretical and assumed constant stress over the effective width that is prescribed by Eurocode 4 [32]. The standard uses the effective width for cross-section verifications, accounting for shear lag effects. The performance of a composite beam system is verified through either an elastic or plastic analysis, both of which are presented and elaborated on in the following subsections.

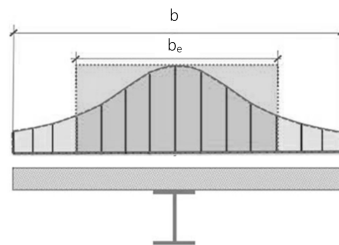


Figure 2.20: Effective width for steel-concrete composite T-sections [83]

Plastic analysis

The plastic bending moment of a steel-concrete cross-section is determined based on the assumptions that the elements work as one solid element assuming a fully rigid connection. The structural steel is assumed to be stressed to its design yield strength (f_{yd}) over its full cross-sectional area. In addition, the reinforcement is assumed to be stressed to its design yield strength (f_{sd}) as well. The effective concrete area in compression assumes to have a constant stress of $0.85 \cdot f_{cd}$ over its height between the plastic neutral axis and the most stressed fibre of the concrete. The plastic bending moment $M_{Rd,p}$ is obtained using the (plastic) stress distribution of the composite cross-section. To account for the resistance of axial forces and enable shear force transfer, a sufficient number of shear connectors should be present in the composite beam. The shear connectors are required to be ductile, which is considered adequate in case of a minimum characteristic slip capacity of 6 mm as defined in EN 1994-1-1 [32]. As per the standard, the spacing of longitudinal shear connectors should not exceed 6 times the thickness of the slab or 800 mm. The degree of shear connection is defined by the ratio of the applied number of connectors over the number of connectors that are required for a full shear

connection ($\eta = \frac{n}{n_f}$). The ratio for a partial shear connection should satisfy the condition of $\eta \geq 0.4$. The plastic shear force resistance $V_{pl,Rd}$ of a composite beam is supposed to equal the plastic resistance of the structural steel's I-section $V_{pl,a,Rd}$, unless the resistance of reinforced concrete of the beam is established. The design value is determined in accordance with EN 1993-1-1 section 6.2.6 [63].

Elastic analysis

The bending resistance of composite beams is assumed to be elastic, with the assumption that cross-sections remain plane during bending. The elastic bending resistance is designed according to the theory of elasticity, taking into account the effective flange width of the concrete. Furthermore, the elastic bending moment resistance, which is determined by the effective cross-section, is limited by stresses for concrete compressive strength, reinforcement strength, and steel yield strength. The stresses that originate from loads on the steel only should be added to the stresses that result from loads on the steel-concrete element [32]. The shear connectors should be spaced following the same requirements as for plastic design.

2.7.2. Serviceability limit state (SLS)

The design verification for serviceability limit state in Eurocode 4 [32] includes stresses, deformations and concrete cracking. Verification for stresses in composite beams are not considered since fatigue verification is not required in ULS. In addition, the behaviour of concrete is outside the scope of this work, which is why concrete cracking verification is not discussed further. Therefore, the requirements related to deformation verifications are elaborated on only. Deformation of composite beams that are only burdened by loads active on the steel components should be verified in accordance with EN 1993-1-1 [63]. If deformations occur as result of loads active on both steel-concrete element, than the deformation is determined following the elastic calculation verification in EN 1994-1-1 section 5. The deformation of a composite beam can follow the approach of a rigid joint if the following conditions are satisfied:

1. The design of the shear connection is in accordance with ULS (section 6.6 in EN 1994-1-1);
2. Either at least half of the number of shear connectors that are required for a fully shear-resistant connection is used, or the forces that result from elastic behaviour in SLS cannot exceed P_{Rd} ;
3. In case of a ribbed plate perpendicular to the beam, the ribs cannot exceed a height of 80 mm.

2.8. Demountable continuous composite floor system

Steel-concrete composite beams are as a result of efficiency in material use and performance intensively used within the construction industry. Various research papers ([16, 84]) have experimentally and/or numerically demonstrated the concept. This section elaborates on the introduced concept and application of continuous floor systems in line with this work.

2.8.1. Concept and application

To promote the reuse of steel- and concrete members from existing structures, the demountable composite floor system follows the design accordingly to the model that was proposed by Kavoura and Veljkovic in [10]. The floor system includes external concrete slabs that are connected by means of a concrete deck-to-deck connection. Within the research of [10] a simplified approach was conducted where the connections were modelled using spring elements to connect the structural concrete components. The spring elements were assigned shear and tensile mechanical properties of a bolt, where the bolts connect the concrete slabs at point of zero bending moment. The maximum deformations for vertical displacement and bending moment around the y-axis occur near the end supports, which is a result of the semi-rigid connection (spring elements) between the composite beams and concrete slabs.

The concept involves the utilisation of a non-demountable composite beam that incorporates welded shear studs. The composite beam is coupled through a demountable deck-to-deck connection employing external (reused/reusable) concrete slabs. The approach offers the potential to maintain the strength of welded shear studs in composite beams while ensuring the floor system remains demountable and available for reuse. Figure 2.21 presents the concept of the demountable steel-concrete

composite floor system utilising reused concrete slabs. The continuous system includes the composite beam, the (reused) concrete deck and the demountable slab/slab joint.

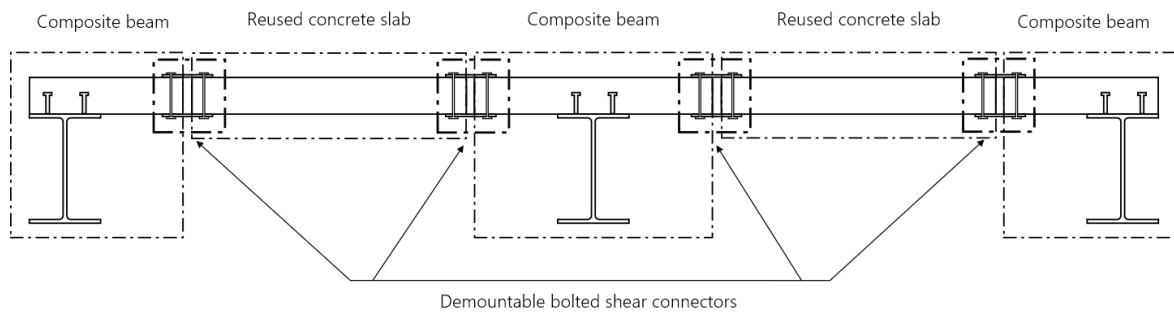


Figure 2.21: Concept of demountable steel-concrete composite floor system

Composite beam and reused concrete slab component

Although the idea of extracting slabs from existing structures offers a serious strategy in sustainable construction through reusing structural elements, the concept comes with limitations and challenges in terms of applicability and mechanical performance of the slab. Over the years, there have been significant advances and improvements in the performance of concrete and reinforcing steel due to the development of the material's strength properties [85]. As a result, today's structural element designs in construction require less material to meet the standards. However, structures built 50 years ago, which have reached their approximate expected end-of-life, used components with poorer mechanical characteristics. Reusing concrete from these structures presents practical challenges and potential issues. Due to the inferior properties of the material, structural elements are designed using greater dimensions to meet the necessary resistance. When incorporating existing slabs from end-of-life structures, it is important to consider a realistic model that accounts for the larger dimensions and poorer mechanical properties of the structural components. Therefore, concrete slabs extracted from existing structures limit their applicability. Furthermore, slabs that are cut from existing structures leads to a cut of both the concrete and internal reinforcement. Thereby, the concrete slab does not consist of any reinforcing anchoring. The strength development of the reinforcement is highly dependent on its bond with the surrounding concrete. This bond is affected by factors such as the circumference of the reinforced bars and the minimum anchorage length, which is determined based on the allowable bond stress between the concrete and steel. In practice, to enhance the effective anchorage length, reinforcements are bent at the ends into 90° or 180° hooks [86]. However, for the extracted slabs that do not include anchoring, a demountable shear connection between concrete components should be used to ensure shear force transfer in the absence of anchorage. This connection should include a steel plate, which serves both to connect the components and to transfer shear force.

Demountable deck-to-deck shear connector component

The shear connectors taken for comparative analysis are considered demountable connectors, but not all connectors are suitable for the application of a concrete deck-to-deck connection. Although the presented demountable connectors are designed to connect the steel beam to the concrete floor for composite action, the high-tension friction grip bolt appears to be the most significant and considerable shear connector in terms of application for use in a concrete deck-to-deck connection, as the connector can be applied in precast construction (see Figure 2.22).

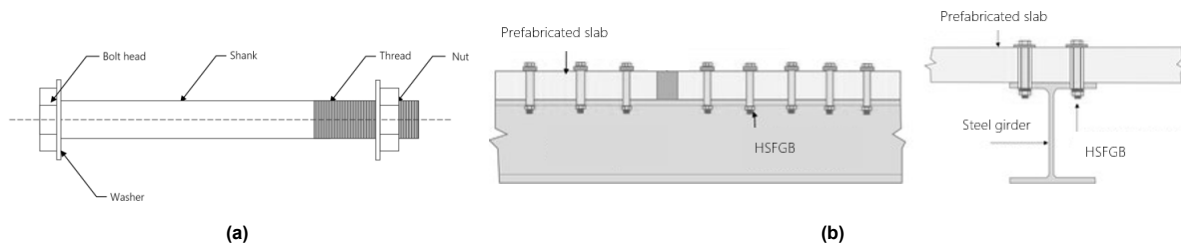


Figure 2.22: (a) HSFGB for concrete deck-to-deck connection and (b) application of HSFGB comprising precast concrete slab components

2.8.2. Application in precast concrete: High-strength friction-grip bolt

High-strength friction grip bolts are generally used to connect steel-to-steel connections in spliced joint to help prevent slippage. However, the application and performance indicate its ability to be implemented through a concrete slab/slab joint. Friction grip bolts transfer the shear force between the connected elements through friction that is induced by a preloaded clamping force. HSFGB have undergone push-out tests in various studies (section 2.3.3).

The experiments in studies have shown that the load-slip behaviour for the HSFGB in precast concrete can be divided into four distinct phases [41] (Figure 2.23a). The initial phase concerns the transfer of shear force through friction. The bolts are in the elastic stage, and the load is insufficient to overcome the friction at the steel-concrete interface. The external load that is generated by the push-test counterbalances the static friction force, resulting in no relative slip. The resistance to friction is determined by pretension of the bolts. The initial phase is followed by the slipping phase. Frictional resistance is overcome as the load increases, eventually causing slip at the interface between the steel and concrete. Within the third phase, the force is transmitted through the shank of the bolt, which comes into contact with the surface of the bolt holes in the concrete slab and steel flange, where the bolts are subjected to a combination of shear, tension, and bending forces such as depicted in Figure 2.23b. This phase is referred to as the bolt bearing phase. The fourth and final phase pertains to the failure of the HSFGB. Slip increases gradually with increasing load until the bolt fails.

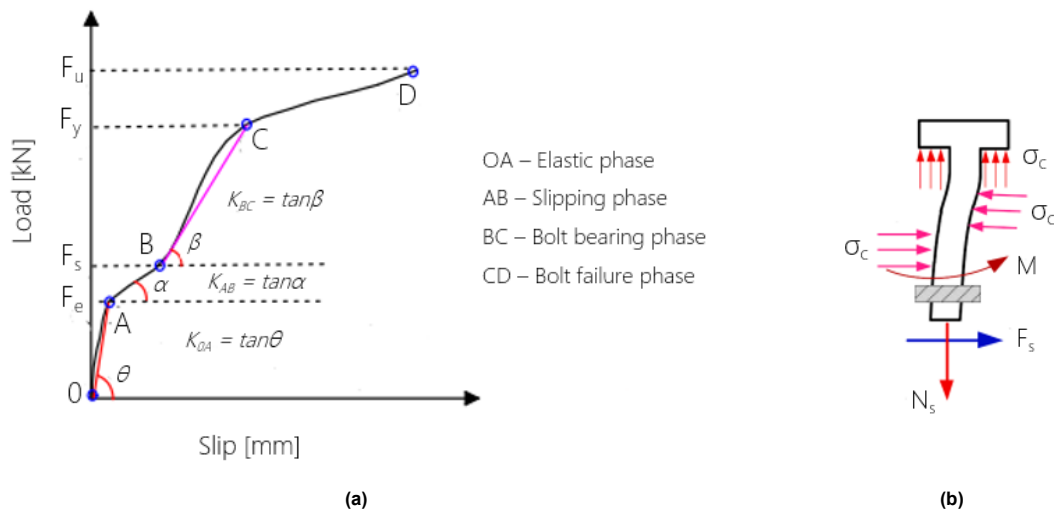


Figure 2.23: (a) Typical load-displacement behaviour for shear connectors and (b) loads active on the HSFGB in phase 3: Bolt bearing phase [87]

Although the phases described typically lead to failure of the bolt, it should be noted that failure possibly could also occur through the concrete. The failure mode that occurs is determined through the geometry and material properties of the elements. To achieve a better comprehension on the failure mode of high-strength friction-grip bolts, various studies performed parametric analyses. Modifying parameters allows to gain a greater insight into to structural behaviour of the bolt including the influence of a specific parts within the specimen. This involves parameters that comprise geometry and/or material properties. Parametric studies on HSFGB that use precast concrete slabs have been carried out by

Liu et al. [38], Chen et al. [39], Ataei [42], Fang et al. [88] and Xu et al. [87]. The conclusions drawn on the effect of specific parameters are presented in Table 2.5. From the studies that are performed it appears that the shear resistance, stiffness and ductility that typically describe the performance of a bolt are heavily dependent on the key variables of a demountable shear connection. This includes the diameter of the bolt, clearance of the bolthole and applied pretension force which are strongly correlated to one another [87].

Parameter	Effect
Bolt size	An increase of the bolt size leads to an increase of ultimate shear resistance and slip capacity. The initial stiffness is not affected by an increasing bolt size;
Bolt grade	The load-slip behaviour is highly dependent on the bolt tensile strength. The shear resistance and maximum slip increase with increasing bolt tensile strength. The initial stiffness and the maximum slip value during the slipping phase are not affected by the increase in bolt size;
Preloading force	Increasing the bolt preload leads to the maximum value of slip in the slip stage at a higher load. It can be concluded that the friction between the concrete slab and the steel beam has been increased, resulting in an increase in the force required to overcome the friction. The bolt pretension force does not have a significant effect on the maximum shear resistance and corresponding slip;
Bolt-hole clearance	Increasing the bolt clearance in the concrete slab and steel beam leads to an increase of the maximum slip capacity and ductility. Changing the hole clearance does not significantly affect the shear capacity of the shear connector. It has been observed that the maximum slip value is approximately equal to the sum of the clearances between the bolt and the hole in the steel flange and the bolt and the hole in the (precast) concrete slab;
Concrete compressive strength	Increasing the compressive strength of the concrete results in a slightly increased maximum shear capacity. However, this increase in the compressive strength of the concrete results in a much reduced maximum slip and ductility. According to Ataei [42] this reduction is probably attributed to a decrease in deformation of the bolt and limited damage of the concrete slab around the bolt hole.
Bolt length-to-diameter ratio*	The bolt length-to-diameter ratio that is greater than 4 demonstrated no increase in shear resistance. Ratios of the length-to-diameter below 4 showed to have an increasing shear resistance

*Bolt length-to-diameter ratio parameter is not applicable for the deck-to-deck shear connector

Table 2.5: Results from parametric studies on HSFGB [38, 39, 42, 87, 88]

Some of the studies that performed experimental and/or numerical analysis on high-tension friction grip bolts proposed formulas for the determination of the ultimate shear bearing capacity of high-tension friction grip bolts, and compared these to the design standards for conventional welded shear studs presented in EC4 [32] (see section 2.3.2). The equations were found based on the results obtained from the experimental and/or numerical tests and validated through FEA. The formulas discovered in the literature are presented in Table 2.6. The performance of the formulas found all appeared to give more accurate results as the standard of EC4 showed more conservative results for the shear resistance of the demountable connector.

Author(s)		Proposed Formula	
Kwon et al.	[36]	$P_u = 0.5A_{sc}f_u$	(2.10)
Liu et al.	[38]	$P_u = 0.66A_{sc}f_u$	(2.11)
Chen et al.	[39]	$P_u = 0.23d^{1.78} f_{cu}^{0.29} (0.0007f_s + 0.53)$	(2.12)
Zhang et al.	[41]	$P_u = 0.7A_{sc}\sqrt{f_{ck}E_c}$	(2.13)
		$P_u = 0.62A_{sc}f_u$	(2.14)
Ataei	[42]	$P_u = 0.6345A_{sc}f_u$	(2.15)

Table 2.6: Proposed formulas for shear capacity of HSFGB in push-out test

3

Preliminary analytical analysis

To determine the performance and establish design principles for the conventional/demountable floor system an analytical analysis is performed. A simplified model for both systems is taken for analysis to provide insight into the structural behaviour and effect of various parameters. The floor systems are assessed through finite element analysis, excluding the consideration of the performance of the demountable shear connector. A linear response is assumed in the FE calculation.

3.1. Floor systems

The simplified floor systems use the concept of a continuous concrete deck that is simply supported. The steel girders of the composite floor are modelled as line supports. A floor thickness of 200 mm is adopted in the model to ensure the applicability of reinforcement. The initial dimensions of the conventional and demountable floor systems are presented in Figure 3.1. Both floors comprise an area of 8.0 meters in width and 10.0 meters in length. The demountable floor system consists of three composite beams and two slabs which present the application of reused slabs. The composite beams at the end supports have a width that is half that of the central composite beam. The (reused) concrete decks span four meters in width. The conventional and demountable floor systems use a reinforcement structure that is automatically calculated and established through the software SCIA Engineer. A top and bottom reinforcement net is embedded in the concrete, which both use a $\varnothing 10$ diameter.

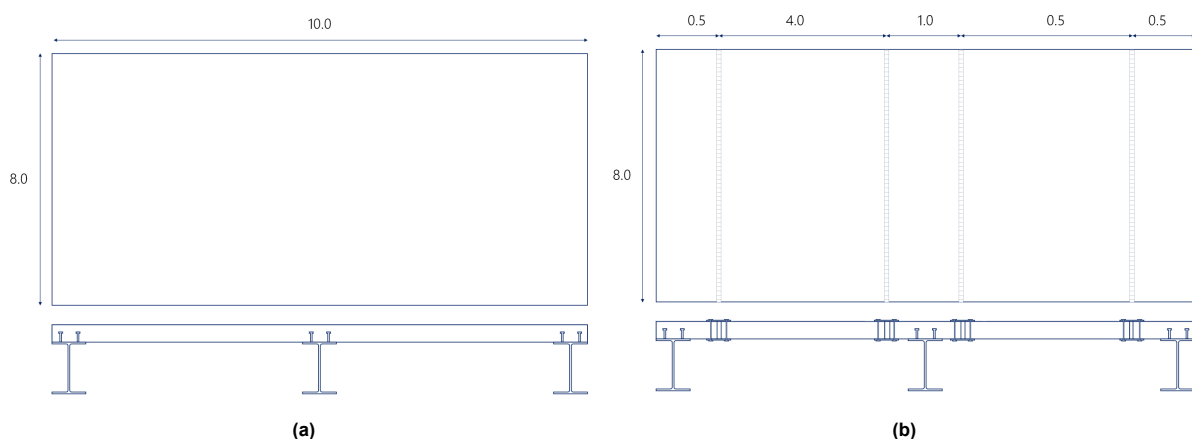


Figure 3.1: Dimensions for (a) conventional and (b) demountable floor system - not in scale (adapted from [10])

The systems are designed following the fundamentals for structural design and load protocol described by Eurocode. Theoretically, when concrete is poured, the strength of concrete increases over time. Where the hydration process through curing of the concrete slows down over time, the chemical reaction in concrete continuous for a long period of time, thus (slightly) increases the strength with time. I.e. the rate of strength gain is higher at the start of the process and reduces over time as the concrete

ages [89]. However, strength reduction in the concrete section may occur due to deterioration in the cross-section that is cut from an existing structure [90]. As discussed in section 2.8.1, to simulate this (potential) decreased strength of the concrete slabs that are extracted from existing structures, different strength and performance classes for both concrete and reinforcing steel are adopted in the reused slab configuration within the model's properties. The conventional floor system and composite beam elements of the demountable floor are engineered using contemporary strength classes for concrete and reinforcing steel which are in line with current (safe and economical) design decisions (see Table 3.1). The floor systems are designed according to the principles related to consequence class CC2. For the FE analysis permanent and variable loading conditions are considered. Table 3.2 presents these permanent and variable loads to which the floor system is subjected. Self-weight of the flooring system is considered only for permanent load. Variable load considers the loading principles for office buildings. The design loads are determined through the fundamental loading combinations for ULS and SLS.

Material properties			Floor loads			
New elements	Concrete	C30/37	Permanent	Self-weight	4.70	kN/m ²
	Reinforcing steel	B500B				
Reused elements	Concrete	C20/25	Variable	Office	2.50	kN/m ²
	Reinforcing steel	B400B				

Table 3.1: Material properties for new and reused elements

Table 3.2: Permanent and variable load

3.1.1. Structural behaviour

The structural behaviour of the systems is assessed through a simplified model in FE software SCIA Engineer [91], where the model does not implement the local performance of the connector. In order to incorporate a connection within a finite element (FE) model, the utilisation of spring elements is a viable option. These elements can be regarded as one-dimensional finite elements, characterised by two nodes to which a specific stiffness can be assigned. However, it should be noted that SCIA Engineer does not provide the functionality to implement spring elements into the model. In order to incorporate the effect of the demountable joint in the floor system, a hinged connection has been implemented along the slab length to represent the deck-to-deck joint that connects the concrete members. For a member to be hinged, a hinge must be incorporated into the member. It is imperative to define the degrees of freedom and positioning when adding hinges to the system. With respect to the hinges in between the slabs the degrees of freedom relate to rigid conditions for u_x , u_y and φ_y and free conditions for u_z , φ_x and φ_z (see Figure 3.2 for reference coordinate system).

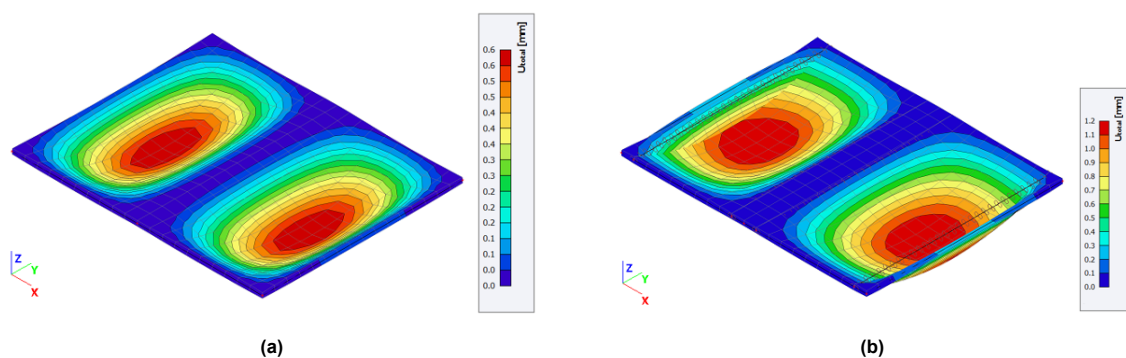


Figure 3.2: Deflection for (a) conventional and (b) demountable steel-concrete composite floor system design modelled in FEA SCIA Engineer [91].

The floor systems are modelled using line supports on all edges. Limitations on the model stem from the reinforcement configuration. Concrete slabs that are extracted from existing structures do not consist of anchorage as a result of cutting. Therefore, the FE model cannot incorporate the effect of missing anchorage. In addition, construction tolerances are not implemented in the system.

The simplified conventional and demountable floor system are modelled through a linear analysis comprising a mesh size of 0.2 meter. Figure 3.2 presents the deflections of the simply supported conventional and demountable floor system. The analysis suggests that the demountable floor system exhibits higher deflections, which aligns with the expected results. It is observed that the deflection is greater towards to the end supports, where there is a more pronounced deflection close to the hinge which represents the presence of the (demountable) connection. This behaviour is caused by the semi-rigid connection between the composite beam and concrete slab.

Although the floor systems are simply supported, the internal force distribution from the model for the demountable floor system obtained shows high values for m_x , m_y and m_{xy} at the corners of the end supports (see Table 3.3). The effect of singularities appears not to be the reason for the high moment concentrations. Increasing the number of elements through a smaller mesh size leads to smaller internal moments at the corners. I.e. the internal forces do not tend to infinity as mesh size tends to zero. The high moment concentrations can be explained through the application of the (uniform) distributed load on the concrete floor. As a result of the distributed load, the floor bends in both x- and y-direction. The supports in the corner restrain deformation of the floor which induces torsional moments in the corners. Therefore, m_x , m_y do not equal to zero

Floor	Deflection	Internal forces						
		u_z [mm]	m_x [kNm/m]		m_y [kNm/m]		m_{xy} [kNm/m]	
			Max.	Min.	Max.	Min.	Max.	Min.
Conventional floor system	0.6	7.5	-14.2	4.7	-2.8	4.2	-4.2	
Demountable floor system	1.2	18.2	-10.6	17.7	-10.3	15.3	-15.3	

Table 3.3: Results on FEA in SCIA Engineer including deflection and 2D internal forces

3.1.2. Sensitivity study

To establish a greater understanding on the behaviour of the demountable floor system, the effect of alternating element dimensions of the demountable floor system is taken for analysis. A small-scale sensitivity analysis is performed on the effect of the slab thickness, width of the reused slab and width of the composite beam on the maximum deflection of the floor system. Naturally, smaller thicknesses and/or larger spans of the concrete slabs are expected to result in greater critical internal forces and maximum deflections. Within this small-scale analysis, the original principles for the floor systems remain identical (original principles are indicated in red).

Effect of thickness

To account for the applicability of reinforcement in the concrete slabs, the thickness of the floors ranges between 100 to 200 mm. As aforementioned, for sake of simplicity the minimum reinforcement required is determined automatically through the FE software SCIA [91], where a top and bottom reinforcement net ($\varnothing 10$) is used. Alternation of the slab thickness results in different deflections for the conventional and demountable floor system. Table 3.4 demonstrates that decreasing the slab thickness leads to higher deflections for both floor systems, where the latter has approximately a 2 times (50%) higher maximum deflections. In relation to the SLS criterion, the maximum permissible deflection limit is required to satisfy the condition $L/250$. Based on the deflections in Table 3.4 it is evident that all variation models (conventional and demountable) satisfy this condition.

Thickness h [mm]	Deflection u_z [mm]	
	Conventional	Demountable
	100	2.4
120	1.7	3.3
140	1.3	2.4
160	1.0	1.9
180	0.8	1.5
200	0.6	1.2

Table 3.4: Effect of slab thickness on the maximum deflection of the floor system (slab width $w_{slab} = 4.0$ and beam width $w_{beam} = 1.0$ m are kept constant).

Effect of slab- and beam width

The non-demountable floor system does not incorporate reused slabs, but instead consists of continuous concrete slabs that span from support to support. In order to compare the deflection of the conventional floor system with the one of the demountable floor system, the width of the reused concrete slabs and the composite beam are incorporated into the width of the conventional decks. The effect of the slab width and beam width on the maximum deflection of the floor systems is presented in Table 3.5 and 3.6. The demountable floor system's deflection increases linearly with incremental increases in slab width. The effect of increasing the slab width in conjunction with a constant beam width (Table 3.5) shows a gradual increase in deflection for both the conventional and demountable floor system. The demountable system indicates a logarithmic growth in deflection that has an approximate increase starting from 50% to 80%.

Slab width w_{slab} [m]	Span l [m]	Deflection u_z [mm]		Beam width w_{beam} [m]	Span l [m]	Deflection u_z [mm]	
		Conventional	Demountable			Conventional	Demountable
4.0	5.0	0.6	1.2	1.00	5.00	0.6	1.2
5.0	6.0	1.1	1.9	1.25	5.25	0.7	1.4
6.0	7.0	1.8	2.7	1.50	5.50	0.9	1.6
7.0	8.0	2.6	3.6	1.75	5.75	1.0	1.8
8.0	9.0	3.4	4.5	2.00	6.00	1.1	2.0
9.0	10.0	4.2	5.5	2.25	6.25	1.3	2.2
10.0	11.0	5.1	6.3	2.50	6.50	1.4	2.4

Table 3.5: Effect of slab width on maximum deflection of the floor system (beam width $w_{beam} = 1.0$ m is kept constant).

Table 3.6: Effect of beam width on maximum deflection of the floor system (slab width $w_{slab} = 4.0$ m is kept constant).

The same behaviour is observed when the beam width is alternated. Furthermore, the results suggest that altering the beam width at an identical span results in slightly higher deflections compared to changing the slab width. The shift of the demountable slab/slab joint further away from the supports is attributed to this result. Increasing the beam width (Table 3.6) shows a gradual increase of 2 mm in deflection for the demountable floor system. The demountable floor system shows an averaged increased deflection of 55% with respect to the conventional floor system. In relation to the SLS criterion, for both the slab and beam width variations, all the deflections (Table 3.5 and 3.6) in the demountable models indicate that the L/250 criterion is met.

3.2. Theoretical framework for FEA

The performance of a demountable floor system can be determined through a theoretical analysis. In the analysis simplifications relating to the connecting elements, slab/slab joints, are made. A framework allows to determine the design for the floor system and establish its structural behaviour. This relates to an initial design of the model including predictive assessment.

3.2.1. Optimised design

The main idea of the demountable floor system is to incorporate reused concrete slabs that are connected through edge- and centralised composite beams. To overcome the distributed load that act on the floor system, the alignment of the demountable shear connectors is crucial. In an optimised design, it is favourable for the deck-to-deck connector to be located at positions of zero bending moment, leaving the connector to withstand a shear force only. A shift in the position of zero bending moment is influenced by the number of spans and the span width. For centralised composite beams alternation of the number of spans leads to a small shift of the position of zero bending moment. Figure 3.3 presents the shear force- and bending moment diagram for simply supported continuous floor system comprising two and three spans. The diagrams provide parametric variables that indicate how the location of zero bending moment shifts with span variation over the length. The location of zero bending moment (M_X and/or M_Y) equals to a distance X and/or Y from the support R_2 . At the position of zero bending moment the shear force equals to V_X and/or V_Y . The figure shows that increasing the number of spans leads to almost identical distributions for shear and bending moment, with slight variations in the critical forces. The number of spans not only affects the critical forces but also the location of the zero bending moment. Table 3.7 reports the position of zero bending moment and corresponding shear force expressed in length and distributed load for the different number of spans.

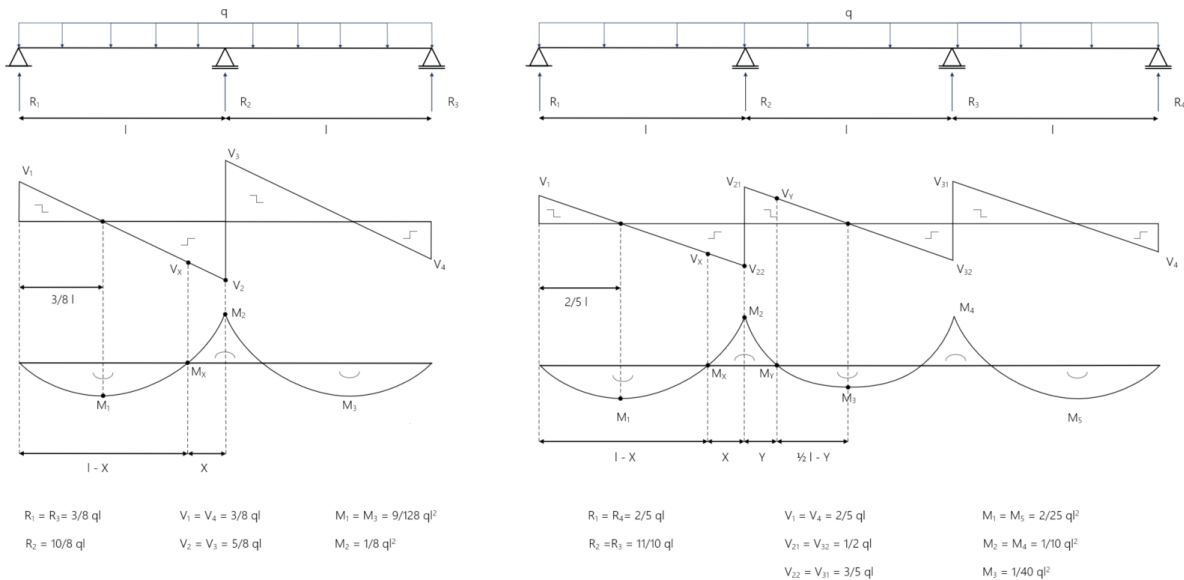


Figure 3.3: Bending moment and shear force diagram for simply supported continuous floor system comprising two and three spans demonstrating the effect of varying number of spans on point of zero bending moment.

Span(s)	Bending moment		Shear force	Zero bending moment point & corresponding shear			
	M_{Max} Sag.	Hog.		X	V_X	Y	V_Y
				$M_X = 0$		$M_Y = 0$	
1	$1/8 ql^2$		$1/2 ql$				
2	$9/128 ql^2$	$1/8 ql^2$	$5/8 ql$	$1/4 l$	$3/8 ql$		
3	$2/25 ql^2$	$1/10 ql^2$	$3/5 ql$	$1/5 l$	$2/5 ql$	$0.276 l$	$0.224 ql$

Table 3.7: Effect of number of spans on critical forces and point of zero bending moment in continuous slabs (Figure 3.3)

Alternating the span width causes a shift in the location of zero bending moment along the beam length. It should be noted that the positioning of the location of zero bending moment is dependent on the load-distribution to which the system is subjected. To ensure zero bending moment at the deck-to-deck connector while alternating the span width, the width of the composite beam is also affected. An increase in the span width leads to a linear increment of the beam- and slab width. Furthermore, the moment and shear distributions indicate that an increase in span leads to greater forces and deflections. For an optimal design it is beneficial to have the slab/slab joint located at the position of zero bending moment. However, the boundary conditions of the continuous floor system dictate that the location of zero bending moment is also positioned at the edge supports rather than within the field (see Figure 3.3). Therefore, following this principle, the demountable slab/slab joint should only be applied at point(s) of zero bending moment that are positioned within the field such as depicted in Figure 2.14a (section 2.5).

3.2.2. Theoretical predictions

Prediction of moment capacity (at midspan)

The flexural moment capacity of the conventional slab that does not consist of demountable connections can be predicted through the stress distribution for rectangular cross-sections that is provided by Eurocode 2 [74], which considers equilibrium of forces and strain compatibility. The distance from the top surface of the concrete to the neutral axis (concrete pressure zone x_u) is obtained through Eq. 3.2, which is obtained by setting the compressive force in the concrete N_c equal to the tensile force N_s in the reinforcing steel. The corresponding strain - and stress diagrams and equilibrium of forces according to EC2 for rectangular cross-sections is depicted in Figure 3.4.

$$N_s = N_c \quad (3.1)$$

$$x_u = \frac{A_s f_{yd}}{\alpha b f_{cd}} \quad (3.2)$$

Within the formula A_s and f_y relate to the area and yield strength of the longitudinal reinforcing bars and α equals to 3/4 for concrete classes \leq C50/60. The moment capacity of the slab can be determined through either the resultant of the compression force in the concrete or tensile force in the reinforcement. The latter approach reads the following:

$$M_{Rd} = A_s f_{yd} (d - \beta x_u) \quad (3.3)$$

where d is the effective slab depth. The effective depth of reinforced concrete slabs is the distance from the compression face to the centre of the tensile steel (longitudinal reinforcement) when the slab is subjected to bending moment. The factor β that is multiplied with the concrete's compressive zone height x_u is determined and assigned by EC2. For concrete classes \leq C50/60 β is equal to 7/18.

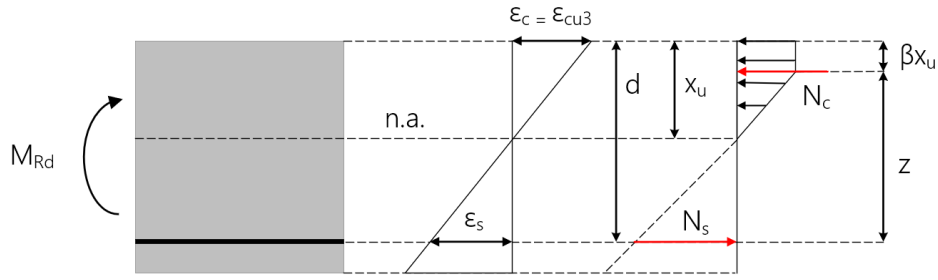


Figure 3.4: Strain - and stress distribution for rectangular concrete cross-sections following EC2 [74]

A prediction model of the theoretical load capacity for demountable slabs was proposed by Almahmood et al. [78]. The experimental research performed multiple 4-point bending tests for a slab/slab joint that is positioned at mid-span. However, the force transfer is identical for the demountable slabs where the connection is positioned where the bending moment is considered to be zero, which is why the prediction model is adopted to determine the flexural resistance of the demountable floor system. According to the authors, to predict the bending moment capacity of the systems that considers demountable slabs the effect of the difference in stress concentration and reduction of the concrete area as result of the positioning of the bolts should be accounted for. Assuming that there is an equilibrium of forces within the slab section, the compressive and tensile forces in the top and bottom steel plates should be equal. Figure 3.5a depicts the force transfer through the plates that is induced by the bending moment at mid-span. The compressive and tensile forces may be determined as follows:

$$F_t = F_c = \frac{M_{Rd}}{z} \quad (3.4)$$

where F_t and F_c are the forces that are active in the bottom and top steel plates, M_{Rd} is the moment at mid-span and z relates to the centre-to-centre distance between the top and bottom steel plates. The bending moment induces tensile and compressive forces in the bolts (see Figure 3.5b). The forces that are transferred through the bolts causes tensile stresses to occur in the concrete which can be calculated through Eq. 3.5, where $A_{net} = (b - nd_h)h$ is the reduced net cross-sectional area of the concrete, in which n and d_h represent the number of bolts and diameter of the bolt hole. The flexural moment capacity of the demountable concrete slab section may be determined through Eq. 3.6 where it is assumed that the tensile stresses (f_t) that are induced by the bolts approximate the concrete's tensile stress (f_{ts}).

$$f_t = \frac{F_t}{A_{net}} \quad (3.5)$$

$$M_{Rd} = f_{ts} A_{net} z \quad (3.6)$$

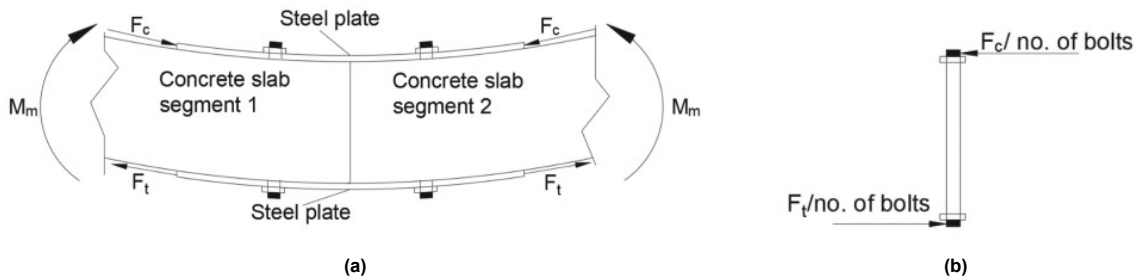


Figure 3.5: (a) Force transfer through steel plate and (b) force transfer through steel bolts where M_m represents the moment at mid-span [78]

In case of strategically positioning the connections at the zero bending moment location, the prediction proposed by Almahmood et al. [78] is considered not an executorial solution since the prediction

is based on the connection located at the midspan. When performing either a three-/four-point bending test with the connection not located at the midspan, the bending moment capacity is determined following equilibrium of forces. Figure 3.6 presents the moment distribution and application of a single/double point load on a simply supported and fixed beam. However, with respect to the effect of using a continuous simply supported beam/floor structure the application of an inclined beam is considered a feasible representation following the optimised design structure. From the moment distributions it is observed that the point of zero bending moment is located at a specified distance from the support which deviates through the application of either a single ($x = \frac{1}{4}l$) or double load ($x = \frac{2b^2+2b^3+3ab^2+2ab+a^2b}{3}$). This point is considered the optimal location regarding the connection.

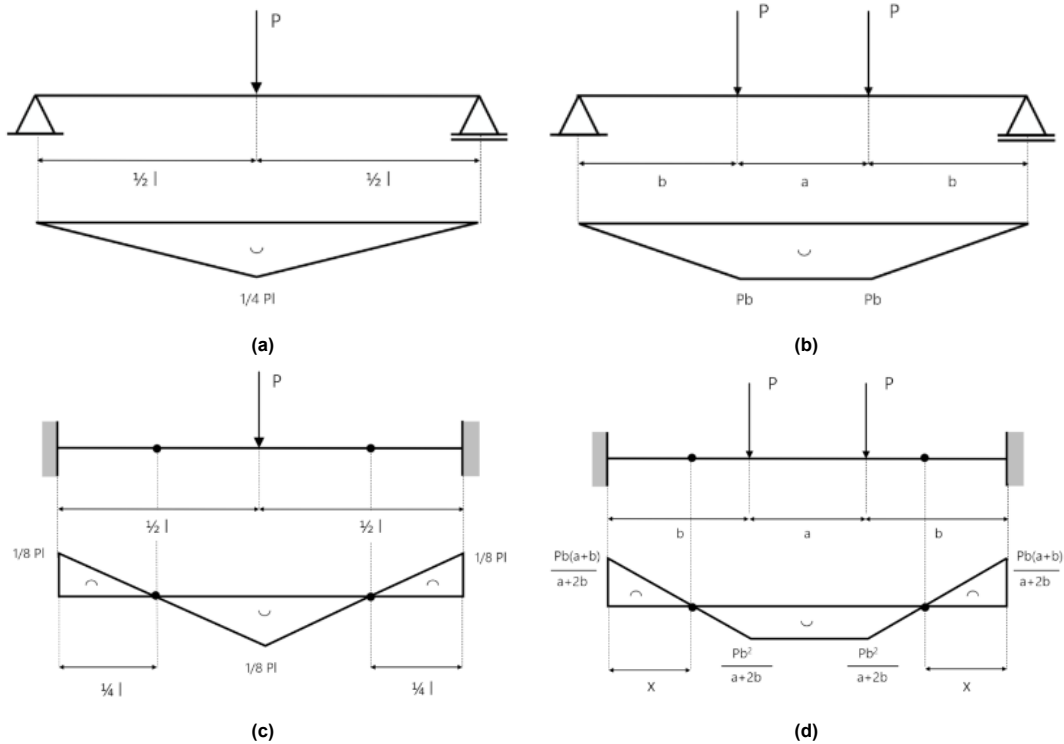


Figure 3.6: (a) Simply supported beam - single point load, (b) simply supported beam - double point load, (c) fixed beam - single point load and (d) fixed beam - double point load

3.3. Recapitulative conclusion

This chapter presents the behaviour of a conventional composite floor system to a demountable floor system which is analysed through a finite element software. The FE analysis indicated that a shift of the demountable connector further away from the supports leads to larger deflections. Altering the beam width has a slightly greater effect on the maximum deflection than changing the slab width. Furthermore, a shear model for the floor system is presented for optimised design. The model presented allows the incorporation of a shear connection in simply supported continuous floor systems. The demountable slab/slab-joint should be positioned at the positions that are considered to have a zero bending moment. Furthermore, a theoretical prediction of the load capacity for the conventional and demountable floor system is given. It is important to note that in practice, the connection should withstand a fraction of the bending moment that is active on the beam. This is due to the effect of various load combinations which are also prescribed by the Eurocode standard that need to be considered in the design. As a result of the various combinations, the maximum bending moment and position of zero bending moment slightly shift over the span which requires that the connection has some bending moment capacity.

4

Finite element model

In order to establish the behaviour and performance of a floor system that incorporate a deck-to-deck connection a preliminary numerical study is performed. Within this study a simple compact fragment of the slab/slab joint is modelled. The primary goal of this part is to establish the behaviour of the concrete-to-concrete slab connection and develop an incremental increasing level of complexity within the model, and avoid errors in the model as a result of convergence issues. The results obtained will be implemented within the application of the demountable floor system. The following sections provide details considering the test, geometric details, material properties including constitutive laws, element type, mesh, contact properties, and boundary and loading conditions. The models are developed through software package ABAQUS [92].

4.1. General and geometry

To determine the behavior of the deck-to-deck connection, a basic tensile test is conducted. The finite element model consists of two concrete blocks that are connected by a steel bearing plate at the top and bottom through bolts, where reinforcing steel diameter $\text{Ø}10$ is embedded within the concrete, following the configuration that is depicted in Figure 4.1. The behaviour of the connection is determined by pulling the concrete blocks horizontally in the opposite direction. The type of test results in the bolts being tested in its shear capacity through a (horizontal) displacement-controlled loading condition.

From the figure it can be observed that the reinforcement configuration employed within the model adheres to a design specifically for a tensile test, as opposed to the simulation of an extracted concrete slab that is cut from an existing structure where the reinforcing bars reach the concrete edges. The concrete segments that are being pulled in opposite directions present the possible occurrence of premature concrete break-out failure in between the bolts. In order to establish the performance of the bolts in this system, the reinforcement configuration employs a substantial anchorage, thereby providing enhanced resistance to possible premature concrete break-out failure [93, 94].

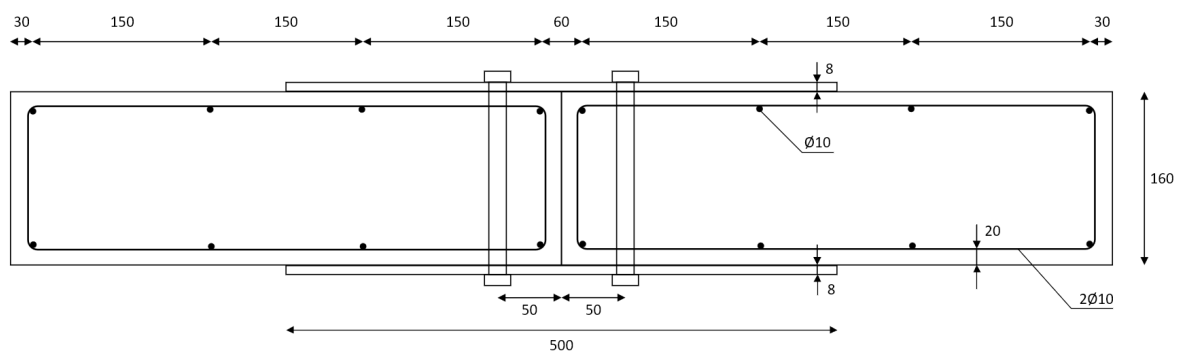


Figure 4.1: Geometry FEA model

For simplification purposes the bolt and nut are modelled as one individual element. The bolt model is simplified by neglecting the threaded shank of both the bolt and nut contact surface, and using instead of a hexagonal shape a circular one for the bolt head and nut. The finite element model is designed using nominal boltholes (18 mm) in both the concrete and steel sections to account for tolerances. The connection uses a pair of M16 bolts which consist of a 16 mm shank diameter and 24 mm head/nut diameter with identical height of 10 mm. The model equals in length, width and height to 1020, 140 and 160 mm, respectively.

Additionally, to reduce the complexity of the numerical model the implementation of a washer between the bolt-head/nut and the concrete section was not added to the model. This decreases the number of interactions, which subsequently benefits the efficiency and computational time of the model. The application of bolt hole cavities in the concrete and steel sections serves to facilitate the installation of bolts in all types of structural systems. In practice, nominal/oversized bolt hole cavities are used, which should provide sufficient certainty for the installation of steel members where no infill material is considered necessary [64]. In order to develop a model that serves to predict the behaviour of the connection, the model incorporates the application of nominal bolt holes that have a diameter larger than the bolt itself. However, ABAQUS requires bolt loads to converge in the case of bolt hole clearances. Therefore, the model that incorporates the effect of a bolt hole cavity is modelled by applying pretensioning of the bolts. As a result, the model developed consists of three steps including the initial step. The first step incorporates pretension of the bolts, where the second step accounts for the displacement. The displacement is activated on the extremes of the concrete blocks.

Preloaded bolted joints increase the friction between surfaces (see Section 2.4.1). This in turn affects the slip behaviour of the joint. Although nominal/oversized bolt hole cavities are useful in practice to account for tolerances, for theoretical insight the influence of bolt prestressing is evaluated by developing an additional finite element model where the concrete and steel element are in direct contact with the bolt shank, such as depicted in Figure 4.2. Note that the primary focus within this research context is on the application of a bolt hole cavity in both the concrete and steel section.

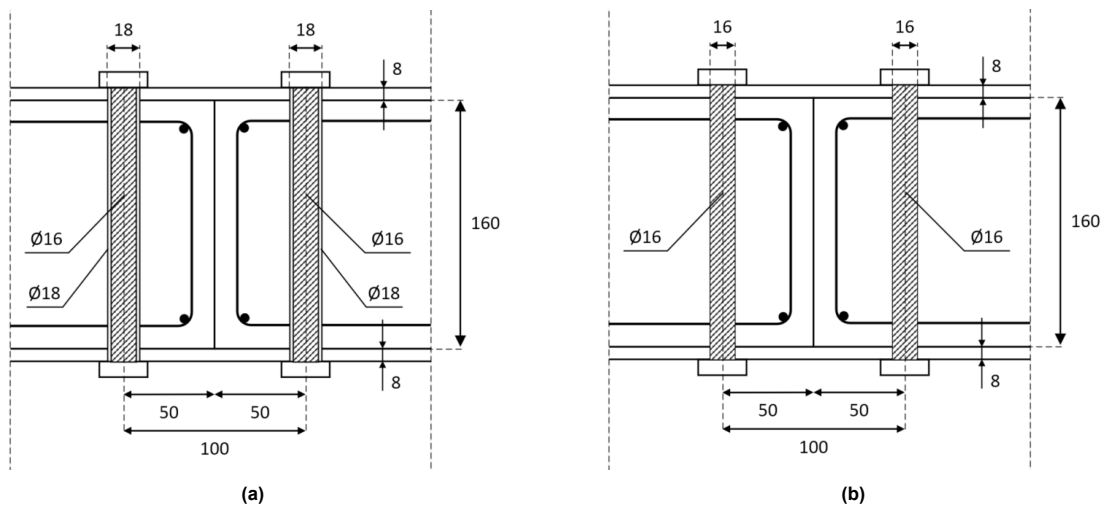


Figure 4.2: Application of (a) bolt hole cavity and pretensioned bolts and (b) direct contact and non-pretensioned bolts

4.2. Material models

Four different materials are defined for the components in the finite element model. This relates to the components that represent the concrete block and the deck-to-deck connection. Nominal material properties as provided in Eurocode are assigned to the elements.

4.2.1. Steel material constitution

In the numerical model three materials are defined for the steel elements. The materials relate to the steel plates, reinforcement and HSFGB including the nut. The elastic material properties are defined by the linear elastic material model assuming isotropic and homogeneous behaviour. The three materials are assumed to have identical elastic properties which include specified density of 7850 kg/m^3 , Young's

modulus of 210 GPa and Poisson's ratio of 0.3. The stress-strain relation of the different steel elements is defined using standardised material property data. The steel materials display initial elastic behaviour up to the corresponding yield points which are followed by further yielding or strain hardening before fracture. Linear curves are converted to represent the stress-strain relationships.

Tensile (coupon) tests allow to determine the stress-strain behaviour of steel samples. The stress-strain relationship is typically represented in an engineering stress and engineering strain diagram, where the strength is defined as the load divided by the cross-sectional area. The chosen cross-sectional area influences the stress-strain relationship. The engineering stress is determined as the load applied divided by the initial cross-sectional area of the material. The engineering stress increases to a maximum at the tensile strength, which relates to the engineering strain that is equal to uniform elongation. Hereafter, the engineering stress decreases while the engineering strain increases until fracture of the sample. The engineering stress and strain are considered nominal properties. However, ABAQUS accounts materials for a true stress-strain relationship where the applied load is divided by the cross-sectional area that changes over time due to deformation. The samples get stronger with deformation as a result of strain hardening. In true stress-true strain diagrams the stress does not drop after reaching maximum tensile strength. The true stress and true strain are obtained through Equation 4.1 and 4.2.

$$\sigma_{true} = \sigma(1 + \epsilon) \quad (4.1)$$

$$\epsilon_{true} = \ln(1 + \epsilon) \quad (4.2)$$

The steel plates are designed following the idealised trilinear constitutive stress-strain model that is proposed by Zou et al. [95] to describe the plastic behaviour. The initial stage relates to the elastic section where the linear slope represents the modulus of elasticity (E_s). The initial stage is followed by yielding until the yield strain reaches to $10\epsilon_y$. Then, the material follows with the strengthening section (strain hardening) that reaches to ultimate limit strain (ϵ_u). Figure 4.3a illustrates the stress-strain behaviour for the steel plates that is adopted in the FE model.

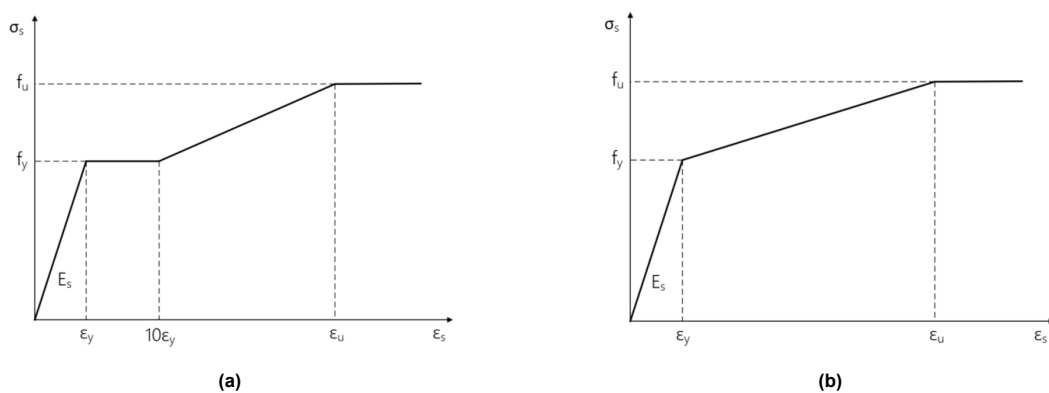


Figure 4.3: Material constitutions steel materials for (a) plates and (b) HSFGB

A bilinear stress-strain model is employed to describe the yielding and strain hardening behaviour of the bolt (see Figure 4.3b). In the initial stage, the modulus of elasticity is defined to characterise the linear behaviour before approximating the yield strength. The stress then increases up to the ultimate strength, after which it is held constant. The response of the HSFGB is constrained by an ultimate strain of 0.18 which, is in line with the study performed by Zhang et al. [96]. This relation is a simplification for the HSFGB that is assumed to deform linearly elastically at a specified point, where after the material deforms plastically. Compared to the stress-strain relation for the plates, the curve for the HSFGB does not include yielding from initial yield strain (ϵ_y) to ultimate yield strain ($10\epsilon_y$), as high strength bolts are utilised in the connecting elements. Preliminary analyses that performed push-out experiments showed that the reinforcement did not influence results in terms of ultimate load capacity. The experimental studies performed by An and Cederwall [97] and Spremić et al. [98] indicated that

reinforcing steel has no to little influence on local behaviour of shear studs. Therefore, the plastic behaviour of the reinforcing bars was not incorporated in the model.

Material	Yield stress		Ultimate stress	Elastic modulus	Ultimate strain
	f_y [MPa]	f_y [MPa]	f_u [MPa]	E_s [GPa]	ϵ_u [-]
HSFGB	10.9	900	1090	210	0.18
Plate	S355	355	510	210	0.20

Table 4.1: Plastic material input parameters steel - Reinforcement is neglected

4.2.2. Concrete material constitution

The concrete beam component uses concrete strength class C20/25. The compressive and tensile strength properties for these nominal classes are determined through the formulation specified by EN 1992-1-1 [74]. The Young's modulus for the concrete component considered are respectively 30 GPa with a Poisson's ratio of 0.2. The concrete uses a density of 2400 kg/m³.

Concrete Damage Plasticity (CDP) Model

The Concrete Damage Plasticity (CDP) material model is used to represent the concrete material in ABAQUS which is a modification of the Drucker-Prager strength hypothesis. The CDP model is widely used to model not only concrete but also other brittle materials proposed by different authors [99–101]. The plasticity model considers the following three hypotheses: the initial yield surface determines when plastic deformation starts; the flow rule determines the direction of plastic deformation; and the softening/hardening rule defines how the surface evolves with plastic deformation [102]. The CDP model is dependent on parameters that present dilation angle (ψ), flow potential eccentricity (ϵ), ratio of initial biaxial to uniaxial compressive yield stress (σ_{bo}/σ_{co}), ratio of second stress invariant on the tensile meridian to compressive meridian (K_c) and viscosity parameter that relates to the relaxation (μ). The dilation angle is interpreted as the internal friction angle within the concrete. The values for the parameters including reference of the CDP model adopted in the FE model are reported in table 4.2. Default values prescribed by ABAQUS manual are primarily used in the model.

Parameter	Value			
ψ	35	[°]	For the dilation angle it is recommended to take an angle that ranges between 30° to 40°. The bearing capacity of the component slightly increases with an increase in dilatation angle.	[103]
ϵ	0.1	[-]	The CDP model recommends to use an eccentricity equal to 0.1. This means that the material maintains a consistent expansion angle across a wide range of confining stress values.	[92]
σ_{bo}/σ_{co}	1.16	[-]	Ratio to which the concrete undergoes failure under biaxial compression. The value is recommended for the CDP model and considered a default in ABAQUS user's manual.	[92]
K_c	2/3	[-]	The principle stress ratio of 2/3 is recommended in the CDP model and considered a fixed (standardised) value in ABAQUS user's manual	[92]
μ	0.001	[s ⁻¹]	Recommended value for the viscosity coefficient equals to 0 in ABAQUS user's manual. An increase of the viscosity coefficient tends to increase the stiffness. In case of convergence issues, the parameter should appropriately be increased.	[92]

Table 4.2: Concrete Damage Plasticity (CDP) model parameters including recommendation/argumentation

Uniaxial compressive and tensile behaviour of concrete

The CDP model requires defining damage parameters for concrete in uniaxial compression and tension to simulate the degradation of the concrete's stiffness. The concrete's uniaxial compressive (a) and tensile (b) behaviour is depicted in Figure 4.4.

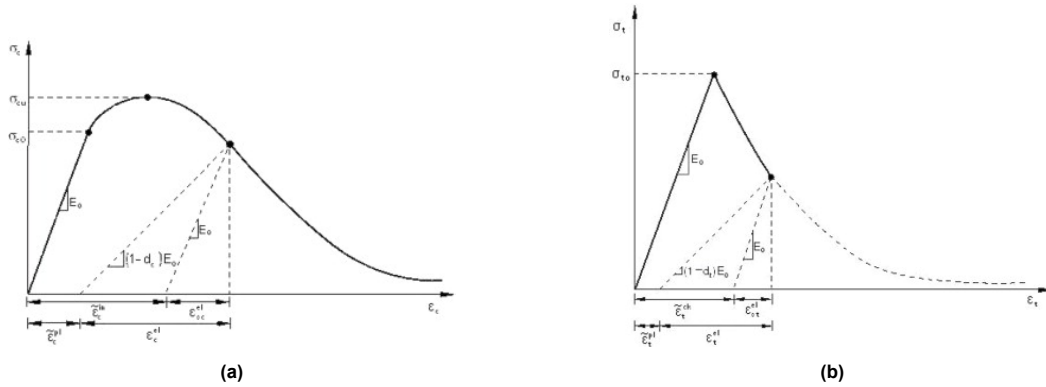


Figure 4.4: Uniaxial compression and tensile behaviour of concrete. (a) Stress-strain relation of plastic damage subjected to compression; (b) Stress-strain relation of plastic damage subjected to tension [104]

The compressive behaviour of the concrete is defined as the relation between the compressive stress and inelastic strain. The CDP model uses inelastic strains. The inelastic strains are determined by deducting the elastic part from the total strains (Eq. 4.4). The compressive uniaxial stress-strain behaviour according to EC2 [74] is defined only up to the nominal ultimate strain. The plasticity curve initiates with a linear ascending compressive stress up to $0.4 f_{cm}$ where the initial modulus of elasticity is specified to be secant in this range of $0-0.4 f_{cm}$. The curve increases non-linearly until ultimate compressive strength f_{cm} with nominal ultimate strain ϵ_{cu1} . The CDP model calculates the plastic strain through Eq. 4.5 after defining degradation parameter d_c .

$$\epsilon_{0c}^{el} = \frac{\sigma_{c0}}{E_0} \quad (4.3)$$

$$\epsilon_c^{in} = \epsilon_c - \epsilon_{0c}^{el} \quad (4.4)$$

$$\epsilon_c^{pl} = \epsilon_c^{in} - \frac{d_c}{(1-d_c)} \frac{\sigma_c}{E_0} \quad (4.5)$$

It is assumed that the plasticity curve of EC2 that considers nominal ultimate strain is sufficient. According to Pavlovic et al. [46], for conventional reinforced concrete structures the compressive strains in structural components are typically below nominal ultimate strain at maximum loads. Therefore, the sinusoidal - and linear extension part of the plasticity curve presented in Figure 4.4(a) are not considered for the uniaxial compressive behaviour of concrete. The compressive stress following EC2 is determined through Eq. 4.6, where $\eta \geq \epsilon_c / \epsilon_{c1}$ presents the nominal strain over the strain at f_{cm} and $k = 1.05 E_{cm} \epsilon_{c1} / f_{cm}$. The compressive damage parameter (d_c) is expressed by Eq. 4.7.

$$\sigma_c = f_{cm} \frac{k\eta - \eta^2}{1 + (k-2)\eta} \quad (4.6)$$

$$d_c = 1 - \frac{\sigma_c}{f_{cm}} \quad (4.7)$$

The uniaxial tensile behaviour of the concrete is defined by the relation between the tensile stress and cracking strain. The uniaxial stress-strain curve for concrete in tension consists of a linear-elastic region until ultimate tensile strength (f_{ctm}) and an abrupt softening branch that follows a sinusoidal shape as a result of concrete cracking. The strain at ultimate tensile strength is determined following Eq. 4.8, where E_0 denotes the initial elastic modulus of concrete. The cracking strain in tension ϵ_t^{ck} in the CDP model is obtained as shown in Eq. 4.9. The plastic strain for concrete in tension is determined identical to plastic strain in compression (Eq. 4.10).

$$\epsilon_{0t}^{el} = \frac{\sigma_{t0}}{E_0} \quad (4.8)$$

$$\epsilon_t^{ck} = \epsilon_t - \epsilon_{0t}^{el} \quad (4.9)$$

$$\epsilon_t^{pl} = \epsilon_t^{ck} - \frac{d_t}{(1-d_t)} \frac{\sigma_t}{E_0} \quad (4.10)$$

The tensile stress used for the determination of the tensile damage parameter is determined through the stress-strain relation defined by Wang and Hsu [105] (Eq. 4.11). The parameter n represents the weakening rate of the material, where the authors of [105] proposed the rate to be 0.4 for concrete. The tensile damage parameter (d_t) is determined through Eq. 4.12. Based on the material model for concrete the uniaxial stress-strain behaviour and damage parameters are obtained. The uniaxial compressive and tensile stress-strain relation and damage parameters for nominal concrete class C20/25 is adopted in the numerical model.

$$\sigma_t = \begin{cases} E_{cm} \epsilon_t & \text{for } \epsilon_t \leq \epsilon_{0t}^{el} \\ f_{ctm} \left(\frac{\epsilon_{0t}^{el}}{\epsilon_t} \right)^n & \text{for } \epsilon_t > \epsilon_{0t}^{el} \end{cases} \quad (4.11)$$

$$d_t = 1 - \frac{\sigma_t}{f_{ctm}} \quad (4.12)$$

Compressive behaviour		Tension recovery = 0		Tensile behaviour		Compression recovery = 0.5	
Stress	Inelastic strain	Damage par.	Inelastic strain	Stress	Cracking strain	Damage par.	Cracking strain
σ_c [MPa]	ϵ_c^{in} [-]	d_c [-]	ϵ_c^{in} [-]	σ_t [MPa]	ϵ_t^{ck} [-]	d_t [-]	ϵ_t^{ck} [-]
23.11430546	0	0	0	3	0	0	0
27.49671694	0.000167974	0.075913798	0.000167974	1	0.00025	0.080103616	1.77E-05
31.22714338	0.000264745	0.101025092	0.000264745			0.115607706	2.79E-05
34.24942766	0.000386806	0.128364910	0.000386806			0.264985738	7.05E-05
36.5007728	0.000536401	0.158288807	0.000536401			0.404418445	0.000116
37.91073064	0.000716045	0.191245167	0.000716045			0.5	0.000154624
38.4	0.000928571	0.227812657	0.000928571				
37.87899089	0.001177179	0.268760027	0.001177179				
36.24609991	0.001465496	0.315147438	0.001465496				
33.38562684	0.001797656	0.368511919	0.001797656				
29.1652419	0.002178384	0.431244198	0.002178384				
23.43288672	0.002613111	0.507479475	0.002613111				
		0.605785293	0.003108109				

Table 4.3: Plastic material input parameters CDP-model specimen C20/25

4.3. Element type and meshing

The finite element types and mesh size that are selected for the model highly depend on the type of simulation performed in the numerical analysis. For this study a stress/displacement simulation is executed. Multiple element types are available in ABAQUS element library, which are characterised through different parameters. Solid elements can be utilised for non-linear studies that involve contact interactions, plasticity and large deformations. The three-dimensional eight-node solid elements with reduced integration (C3D8R) are utilised for the connecting and beam elements in the model. The model is subjected to a stress/displacement simulation, which is why the degrees of freedom considers only three translations. Furthermore, first-order interpolation is applied on the elements which makes that there nodes on the corners of the hexahedral elements only. The result is an 8-node (linear) brick element. Using linear elements allow for a lower computational cost. The reinforcing bars are modelled

with the 2-node linear 3D truss elements (T3D2). The reinforcement bars are there to distribute ordinary forces. Therefore, it is suitable for the reinforcing bars to function as three-dimensional truss component. The T3D2 element considers three translations and three rotations per node.

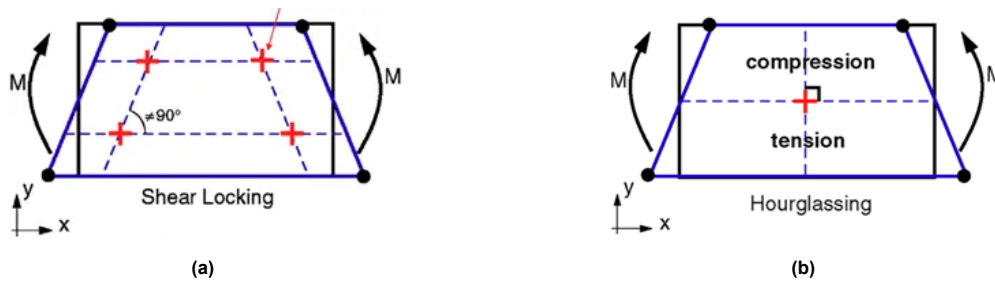


Figure 4.5: (a) Shear locking and (b) hourglassing

The C3D8R element is appropriate for non-linear analysis as it uses reduced integration that is active for all elements. Reduced integration may be less accurate for bending stresses when compared to full integration, but it prevents unexpected element shear locking (see Figure 4.5a). Shear locking is the phenomena that might occur in finite element methods if a part is similar to a slender beam, where the main deformation is a result of bending. Shear locking occurs if there is not a sufficient number of elements or the elements are distorted. The combination of first-order interpolation and reduced integration may lead to another phenomena that is known as hourglassing (Figure 4.5b). Hourglass deformation relates to elements in a model that deform where the strain energy is not computed. In such case the elements show a zig-zag formation (hour-glass shape). A relatively easy and effective solution to prevent the hourglass effect is to use fully integrated elements or using mesh refinement.

The mesh size of the parts is fundamental for the computation time and accuracy of the analysis. Therefore, an appropriate mesh should be chosen that enables to accurately describe the behaviour of the model where the computational cost is minimised. Hexahedral elements are generally preferred over tetrahedral elements, as it reduces the computational cost while achieving an equivalent accuracy. However, tetrahedral elements are preferred for the mesh generation of complex parts as they prevent highly distorted elements. Therefore, locations considered critical, the mesh is refined to overcome errors and minimise the number of distortions.

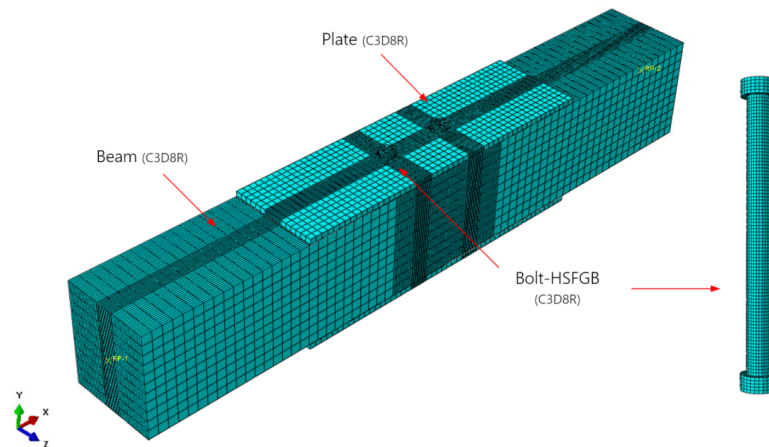


Figure 4.6: Finite element mesh of numerical model. Solid parts (beam, plate, bolt) are modelled using C3D8R elements, where truss parts (reinforcement) are modelled using T3D2 elements.

The beam and plate use a global element size of 15 mm. The mesh for both parts is refined at the locations that are expected to have high stress concentrations to 2 mm. This relates in particular to the area around the bolt and the area in the concrete that is expected to encounter high distortions as is depicted in Figure 4.6. The bolt uses an element size of 2 mm, where the reinforcing bars are modelled using an element size of 8 mm.

	C3D8R-element	T3D2-element
Part(s)	Bolt, beam, plate	Reinforcement
Family	Solid (continuum)	Truss
Degrees of freedom	3 translations	3 translations and 3 rotations
Interpolation	Linear 8-node	Linear 2-node
Integration	Reduced integration, hourglass control	-

Table 4.4: Finite element type and characteristics

4.4. Interaction and contact conditions

The contact pairs that affect the numerical results are taken into consideration within this numerical analysis. Defining interactions between different parts and materials is essential to properly model the behaviour of the connection. The interactions are defined through contact and constraint conditions.

Contact conditions

The contact between surfaces is defined by selecting a master and slave surface, where the master surface has the ability to penetrate the slave surface. The master surface of the part has as a general rule a higher stiffness and/or a coarser mesh size. In case a load is applied on one of two equal parts, the part that is burdened by the load should be considered the master surface. The master- and slave surface discretisation visualised in Figure 4.7. It is important to note that in some cases, the surface of a given part may become in contact with two or more surfaces simultaneously. This pertains to the surface of the bolt shank. To account for multiple interactions on a single surface, the bolt shank is partitioned using datum planes. The partition allows to assign a specific interaction onto the surface of the bolt shank.

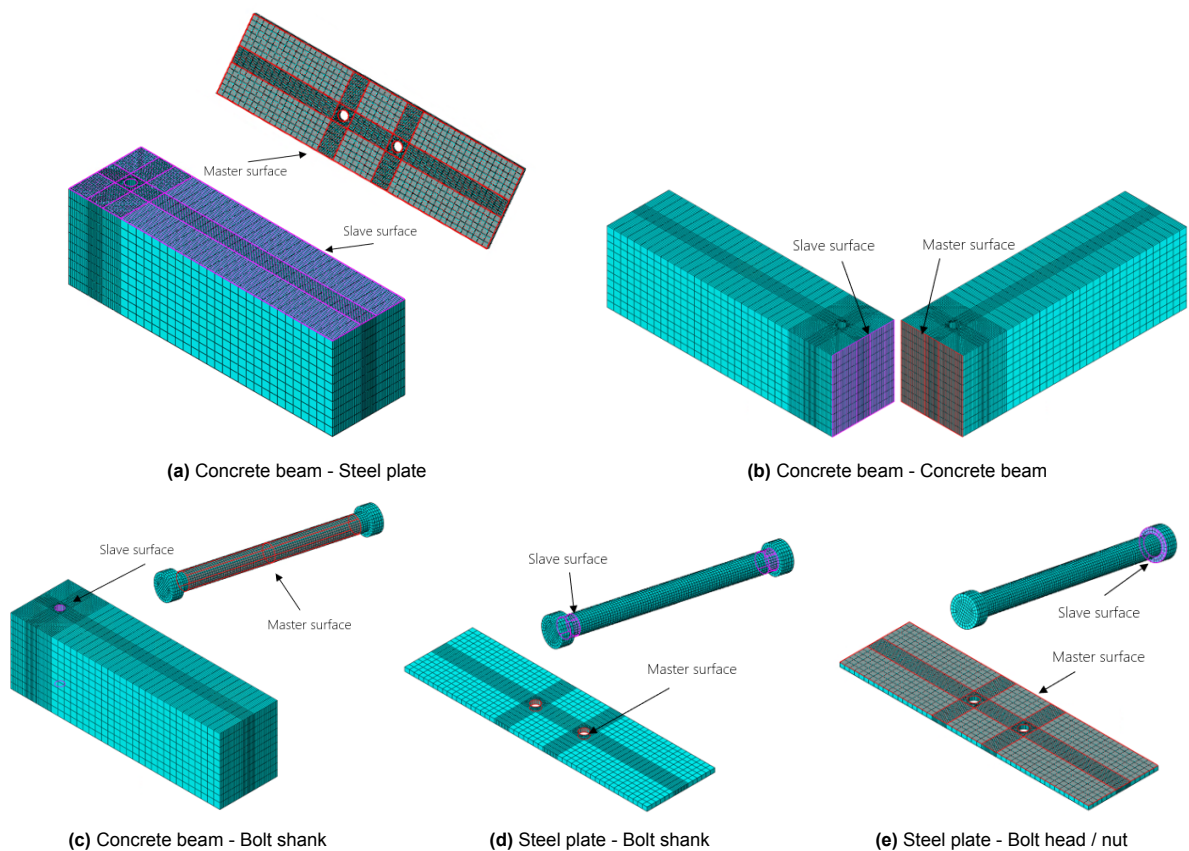


Figure 4.7: Master- and slave surface discretisation per contact pair

Furthermore, the discretisation of master and slave surfaces between concrete block parts is only active in the initial stage. For this unique contact, slave and master surface can be assigned interchangeably as symmetry conditions apply. It should be pointed out that in case of the application of a bolt hole cavity, the contact activation will vary as different steps are applied (see Table 4.5). This phenomenon relates to the contact between the bolt shank and the bolt hole in the concrete and steel member. The model that accounts for a bolthole cavity consist of three steps which include the initial, pretensioning of the bolt and the loading-step. With the application of direct contact and no bolthole cavity the step of pretensioning is not executed, meaning that the model only consists of the initial and loading-step. In case of the latter, contact activation is considered equal for all contact pairs in the initial step of the analysis.

Step - contact activation	Master surface	Slave surface	Contact pair
<i>Contact activation for no bolt hole cavity (direct contact) - No preloading force</i>			
Initial	Block	Block	Concrete to concrete
	Plate	Block	Steel to concrete
	Plate	Bolt head / nut	Steel to steel
	Bolt shank (Partition)*	Block	Steel to concrete
	Plate	Bolt shank (Partition)*	Steel to steel
Step 1: Loading step	-	-	-
<i>Contact activation for bolt hole cavity in both concrete- and steel section - Preloading force</i>			
Initial	Block	Block	Concrete to concrete
	Plate	Block	Steel to concrete
	Plate	Bolt head / nut	Steel to steel
Step 1: Preloading force	-	-	-
Step 2: Loading step	Plate	Bolt shank (Partition)*	Steel to steel
	Bolt shank (Partition)*	Block	Steel to concrete

* Relates to either the centre or top and bottom section of the bolt shank for contact with the concrete block or steel plate in step 1/2.

Table 4.5: Master- and slave surface discretisation including contact activation for block model(s)

To define the interaction between the parts, ABAQUS defines two particulate solutions that are considered suitable for this numerical model, one of which regards the general contact interaction. In case of general contact, ABAQUS assumes that all parts interact with one another with identical friction between each part. However, numerical models that incorporate bolt hole clearances in an implicit analysis are likely to lead to convergence issues as the algorithm does not allow to incorporate different frictions between various surfaces. Therefore, the surface-to-surface interaction is often considered a more suitable solution where multiple interaction properties can be defined between different surfaces, through partitioning the part into two or more sections.

Since both steel and concrete components are utilised in the model, three material interaction properties are considered. These include concrete-to-concrete, steel-to-concrete and steel-to-steel interaction. Therefore, the general contact algorithm that is by default surface-to-surface contact (automatically) is not used. Instead all contact conditions are manually defined using the finite sliding, surface-

to-surface contact interaction step also with accompanying normal and tangential properties through the master and slave surface discretisation. All contact constraints employed the default 'hard contact' in normal direction. This instance allows for the transmission of normal pressure and separation after contact. By default ABAQUS assumes that the contact between surfaces is frictionless. Therefore, the penalty formulation is used to describe the friction between the contact pairs. In general, surface-to-surface contact discretisation leads to higher accuracy and a better convergence within the model in comparison to node-to-surface contact discretisation. Table 4.6 reports the interaction and contact conditions.

Contact pair	Normal behaviour		Tangential behaviour	
	Pressure-Overclosure	Formulation	Friction coefficient (μ)	
Concrete to concrete	Hard contact	Penalty	0.60	
Steel to concrete	Hard contact	Penalty	0.35	
Steel to steel	Hard contact	Penalty	0.25	

Table 4.6: Interaction and contact conditions

Constraint conditions

Two types of constraint conditions are used for the numerical models. Adding constraints increases the complexity of the model and computation time, but has a significant influence on the accuracy. The constraint conditions relate to the coupling and embedded region constraint. The coupling constraint is used to assign a boundary condition of a surface through a single point. This point can be defined through a reference point (RP). The coupling constraints are applied through reference points of the supporting elements. The embedded region constraint is used to embed a region within a 'host' region. Therefore, to define the interaction between the reinforcing steel and enclosure of concrete the embedded region constraint is used. The bolt model is designed such that the nut is incorporated within the bolt section. In case the nut was designed separately from the bolt, tie constraints should be used to tie the contact of the nut to the bolt shank area. A tie constraint ties two surfaces that are separated together providing no movement between the surfaces. The tie allows to fuse two surfaces together that may have dissimilar meshes. However, to reduce complexity of the models it was decided to model the bolt and nut as a single functioning part.

4.5. Boundary and loading conditions

The boundary and loading conditions dictate to replicate a tensile test through displacement-controlled loading. The boundary conditions are applied to restrain surfaces- and or edges of the model that are subjected to forces, where loading conditions allow to simulate external forces onto parts of the model. Where the boundary conditions are considered independent of whether a bolt hole cavity is used or not, the loading conditions are only applied in case of bolt preloading (see Table 4.7). Therefore, the numerical model that incorporates a bolt hole cavity and preloaded bolts uses a time function consisting of three steps instead of only two steps. These include an initial step, pretensioning step and loading-step. The boundary and loading conditions are activated and either propagated or modified within one of these steps. The type of conditions and specifics are reported in Table 4.8.

Boundary conditions

Boundary conditions are applied at reference points (RP) which are centred at the extremes of the concrete blocks. The reference points are coupled to the element area of the block through the coupling constraint. The reference point not only allow to control the boundary conditions but also to easily retrieve reaction forces and displacements. The boundary conditions vary through the type of step within the time function. In the initial step the displacement/rotation condition is used for both reference point 1 and 2. Within the initial step, no displacements occur. Identically to the initial phase, no displacements are active in the pretensioning step, which is why the boundary conditions stated propagate. Finally,

in the loading-step the displacement condition is modified through a displacement in the U1 direction. The displacement set is equal to $U1 = -20 \text{ mm}$ in RP-1 and $U1 = 20 \text{ mm}$ in RP-2 direction (Figure 4.8a). For simplicity the modified boundary conditions use an amplitude that ramps linearly over step function.

Loading conditions

The model is designed using a bolthole diameter in both the concrete and steel plate part that is larger than the diameter of the bolt shank itself. ABAQUS requires bolt loads, in order to converge as a result of the bolthole clearance. Therefore, the loading condition option is used to simulate the effect of preloaded bolts. ABAQUS provides several loading conditions within its loading library, but one particular condition is suitable for preloaded bolts. This is the bolt load condition. In the initial step no loads are activated yet as the bolt load is considered an external applied load. Therefore, the bolt load is activated in step 1 of the time function, where the bolt is preloaded with a force of 50 kN. The pretension axis is identical to the symmetrical axis of the bolt, as visualised in Figure 4.8b. After the pretension stage the bolt is fixed at its current length. The model continuous with a displacement-controlled loading in both the negative and the positive direction of the X-axis which are assigned to reference points RP-1 and RP-2 (Figure 4.8c).

Condition type	Time function	
	Initial	Step 1: Loading step
Boundary condition	BC1	Displacement/rotation-RP1: $U1=U2=U3=UR1=UR2=UR3=0$ Modified: $U1=-20\text{mm}$
	BC2	Displacement/rotation-RP2: $U1=U2=U3=UR1=UR2=UR3=0$ Modified: $U1=20\text{mm}$

Table 4.7: Boundary conditions for model with no bolthole cavity - no preloading force

Condition type	Time function		
	Initial	Step 1: Preloading force	Step 2: Loading step
Loading condition	Bolt load	Apply force: 50 kN	Method: Fix at current length
Boundary condition	BC1	Displacement/rotation-RP1: $U1=U2=U3=UR1=UR2=UR3=0$ Propagated	Modified: $U1=-20\text{mm}$
	BC2	Displacement/rotation-RP2: $U1=U2=U3=UR1=UR2=UR3=0$ Propagated	Modified: $U1=20\text{mm}$

Table 4.8: Boundary- and loading conditions for model with bolthole cavity - preloading force

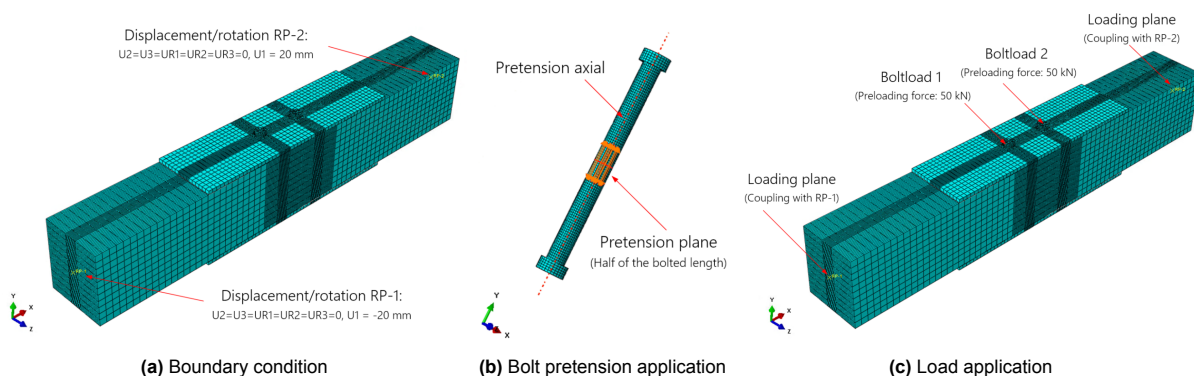


Figure 4.8: Boundary condition and loading application

4.6. Computational solver

Either the implicit or explicit method can be used to model the problem. For some problems, both implicit and explicit solvers can be used, but the type of analysis that is most appropriate in terms of efficiency differs for each analysis. Therefore, based on the modelling technique, the most efficient strategy is used for this numerical study. The numerical model is computed using the static general (implicit) solver provided by ABAQUS. The implicit solver is preferred to the explicit solver for slow contact problems. In addition, the Static, General (Implicit) solver allows the use of bolt loads. Since bolt loads are required in ABAQUS to include a bolt hole clearance, the static solver is suitable for this numerical model. The assigned time period is 1 when geometric non-linearity and automatic stabilisation are used. The incrementation is set to automatic where the increment size is set to be equal in each step. The solver uses the Full Newton solution technique. The method searches for dynamic equilibrium at each increment and simultaneously calculates the displacement. Table 4.9 reports the solver settings.

Static, General (Implicit)		
Time period	1	
NLGeom	On	
Automatic stabilisation	Dissipated energy fraction	0.0002
Incrementation	Automatic	
Increment size	Initial	0.01 mm
	Minimum	$1 \cdot 10^{-10}$ mm
	Maximum	0.1 mm
Solution technique	Full Newton	

Table 4.9: Computational solver Static, General (Implicit)- settings

5

Numerical model validation

The model developed simulates the effect of connecting concrete slabs on a small-scale where the bolts are being subjected to shear. The analysis performed functions as a preliminary study providing insight into the behaviour of a concrete slab/slab joint. The results from the model including the initial properties form the main framework for the follow-up model for application on a global scale. It is therefore of importance to establish the performance and verify whether the results are reliable. The failure mode including stress- and force distribution are used to validate the finite element model. This relates to load-displacement curve and the concrete compression and tension damage models. Verification of the FE model is mainly determined through an additional convergence study. To establish the influence of the bolt hole cavity, the difference in direct- and non-direct contact between the concrete's bolt hole and bolt shank is compared. However, note that the results presented are focused on the model that incorporates nominal bolt hole sizes in both the concrete and steel sections.

5.1. Failure mode

The numerical model employs a displacement-controlled load at the extremities of the concrete blocks. The blocks exhibit movement in the positive and negative X-directions. The bolts are subjected to shear, where the bolts are constrained by movement through the top- and bottom steel plate. As a consequence of the blocks being pulled, the concrete is compressed in the region at midspan, given that the block is constrained by the bolt. In the region where the concrete is not constrained by the bolt, tensile stresses are exhibited within the concrete. The reaction forces and displacement are obtained through reference points RP-1 and RP-2 (Section 4.5). A 20 mm displacement was applied to both concrete blocks, but it should be noted that failure was observed at an earlier stage of the model (see Figure 5.1).

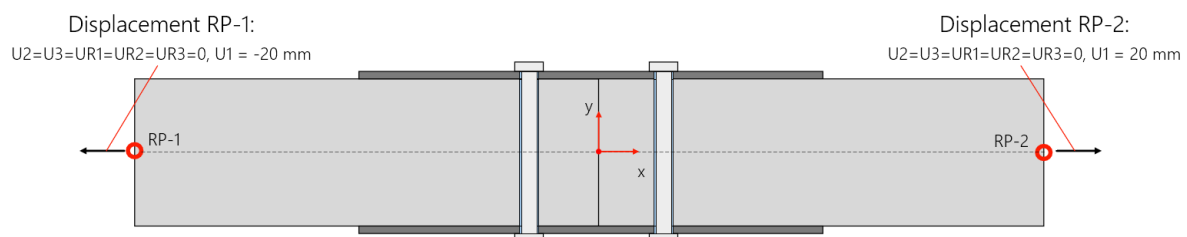


Figure 5.1: Displacement controlled load application

The type of failure observed within the model can be determined through the analysis of various indicators. One such indicator is the yield stress and plastic deformation of a part. If a part reaches its maximum yield stress, it indicates that the material is undergoing significant plastic deformation. It is evident that the material is unable to withstand any additional load without undergoing plastic strain. Moreover, a reduction in load following the attainment of yield stress in a particular component suggests

that this component has become a vulnerable point in the model. As the component deforms plastically, the overall stiffness and maximum load-bearing capacity may be reduced. While other components have not yet reached their maximum yield stress capacity, the component that has can exert a dominant influence on the overall response of the model. It is possible that the plastic deformation of this part may affect the load distribution, thereby leading to a redistribution of stresses which could potentially induce failure or deformation in other parts.

To confirm, the local stresses, strains and deformation patterns in the part(s) that reached ultimate stress levels are examined. The stress- and displacement distributions of the analyses that are obtained through the computational solver settings are typically presented through contour plots. The contour plots in the ABAQUS visualisation module are represented by an averaged value of 75% for the output parameter assigned over a specified region of the model. Within that region, the relative difference at a node is less than or equal to 75%. I.e. if this difference in output parameter at contiguous nodes is less than or equal to the assigned averaged value percentage, the values are replaced and displayed by a single averaged value. In case the difference is greater than the assigned percentage, the values are not averaged and kept separately.

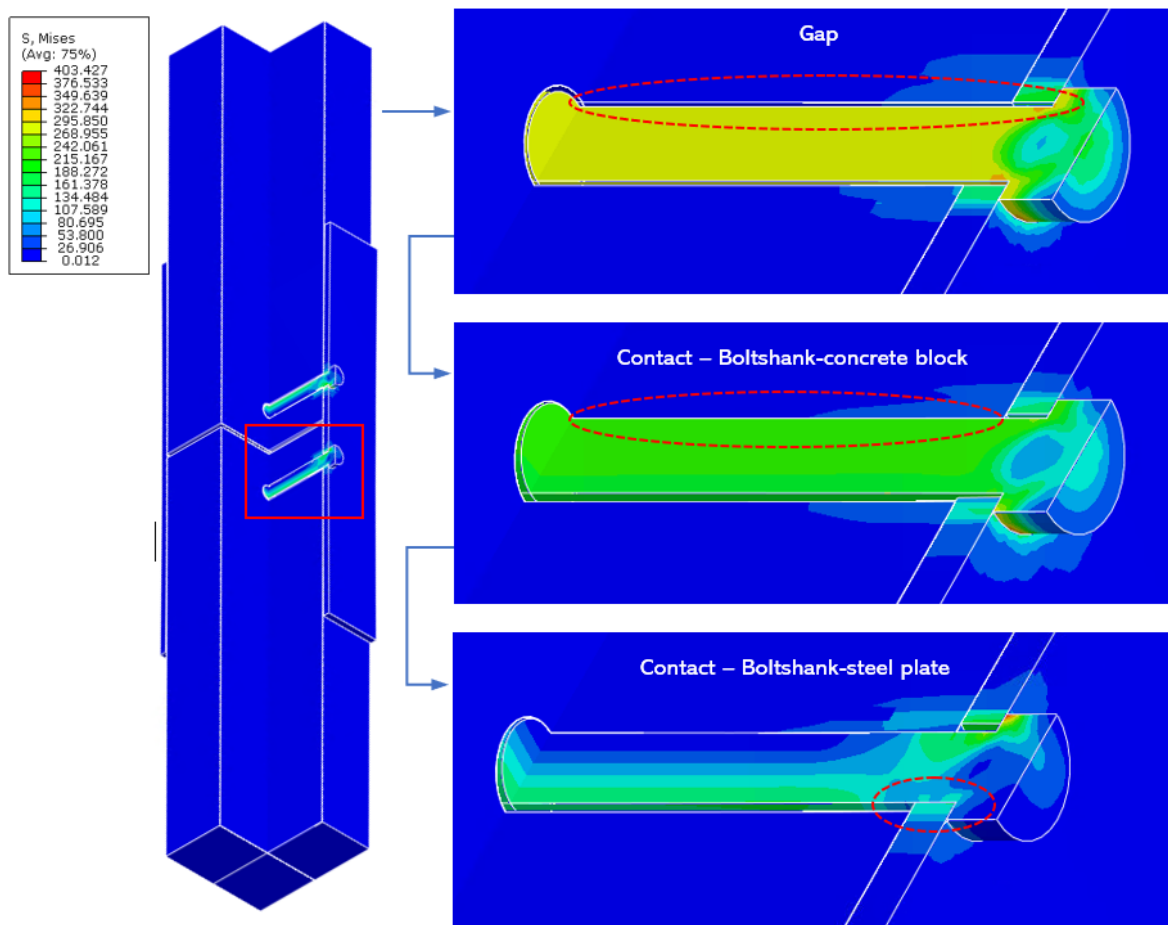


Figure 5.2: Bolt movement in finite element model with corresponding Von Mises stress distribution

Two type of failure modes are possible in the steel-concrete tensile model. These include cracking in the concrete and slipping of the bolt between the steel-concrete interface. The region(s) in the components that endure the highest stresses are compared through the maximum stress and corresponding timeframe. By comparing the ultimate stresses and the corresponding time frame it appears that the maximum stress concentration in the concrete is reached first, within the slipping phase, where at the end of that phase the bolt is in contact with both the concrete and steel plates. Where the Von Mises stress within the concrete drops after reaching its maximum stress level, the steel plate stabilises at its

plastic yield stress of 355 MPa. The highest stresses in the block and plates are concentrated in the rear of the deformed bolt holes. Moreover, the Von Mises stress distribution in the bolt section indicates that the maximum plastic yield stress has not been reached. At this point the bolt suddenly stops deforming plastically and the model shows no crack or tear in the bolt. As a consequence, the maximum reaction forces decreases drastically which is observed in the load-displacement graph. Therefore, based on the behaviour of the specific parts, the model is prone to fail through the concrete as a result of the relatively strong resistance of the bolt and plate.

5.1.1. Failure mechanism analysis - HSFGB shear connector

The internal stress distribution of the bolts during the displacement-controlled loading process are compared through their axial- and shear stress development at specific time frames. Figure 5.3 presents the axial stress over the length of the bolt for the top path (TP) and bottom path (BT) perpendicular to the loading direction. The stresses along the bolt length correspond to the axial stresses depicted by the red and blue lines. In order to assess the influence of bolt-pretensioning on the ultimate load carrying capacity pretension load levels of 5 kN, 25 kN and 50 kN are compared. Additionally, the shear stresses along the bolt length are obtained and presented through the centred path (CP), such as depicted in Figure 5.4. The stress distributions in the bolts that are presented in the figure consider the stages of fully applied preload and failure at the peak load.

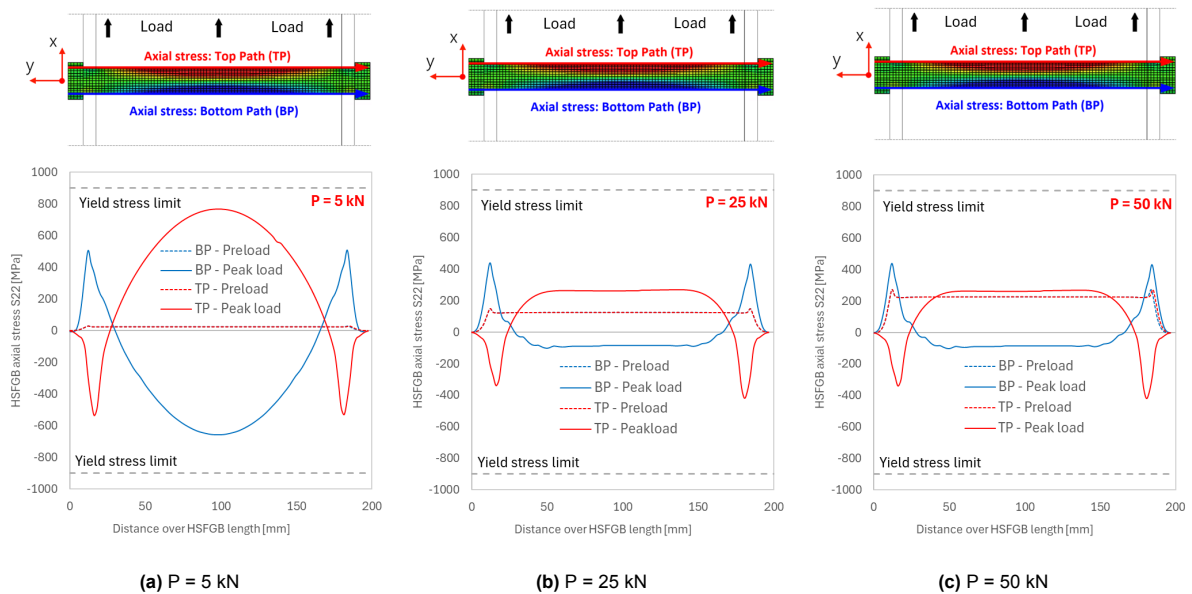


Figure 5.3: Axial stress (y-direction - S22) along top path and bottom path for bolt pretensioning

The displacement-controlled loading process performed on the model shows that the initial preload-ing phase leads to identical axial stress distributions at the bolt edges for the top- and bottom path for each distinct level of preloading. From the axial stress distribution in Figure 5.3 presented with the dashed line it has been established that as the preload level rises from 5 kN to 50 kN, the axial stress measured at the centre of the bolt exhibits a linear increase, with each increment of 5 kN resulting in an approximate rise of 25 MPa, under conditions where full bolt pretension is applied and displacement-controlled loading is not employed. The increase in axial stress at preload level is in accordance with expected results, since a higher level of preload causes a higher distribution of stresses.

With respect to the stress distribution at peak load, the stress distribution demonstrated that, in contrast, where the axial stress distribution at maximum preload increases with an increase in level of preload, at the peak load (failure) the axial stress reduces significantly. From the top- and bottom-path in the figure it is observed that the decreased stress distribution stabilizes in the bolt's centre when reaching the preload level of 25 kN, since the stress distribution in both the top- and bottom path remains constant with an increased preload of 50 kN.

The shear stress distribution presented in Figure 5.4 is significantly smaller than the axial stress distribution. The shear stress recorded at the preload level (dashed line) indicates the similar linear increase with increased level of preload. At the peak load, the highest stresses are observed in the bolt that uses the lowest level of preload. Both the axial- and shear stress distribution show the effect of the steel plates on stress distribution in the bolt. The application of the shear load causes the edge of the bolt's top part to be in tension, where the bottom edge is in compression. The maximum shear stresses were recorded between the bolt and steel plate contact region. The shear stress decreased abruptly close to the shear plane. According to [88], this phenomena is explained through the equivalent plastic strain (PEEQ) that occurs close to steel-plate and concrete-beam interface. ABAQUS describes this equivalent plastic strain as a scalar variable to represent the inelastic deformation of a material.

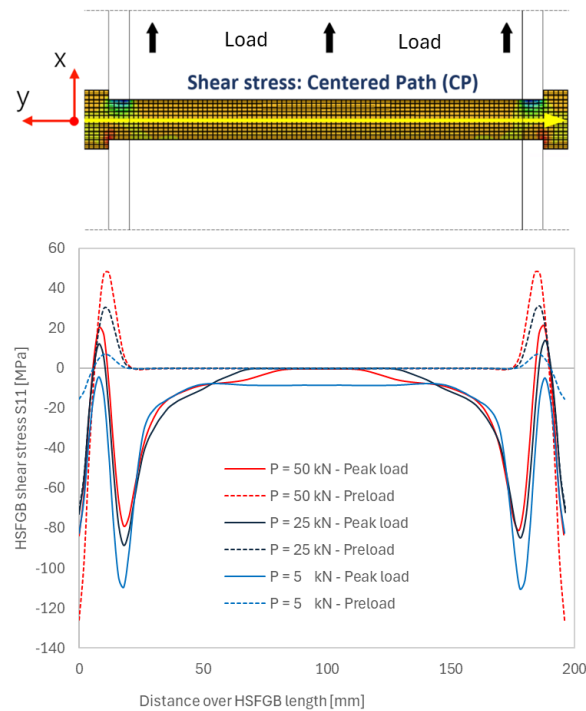


Figure 5.4: Shear stress (x-direction - S11) distribution along HSFGB

5.1.2. Failure mechanism analysis - Concrete block

The performance of the concrete block is analysed through the tensile and compressive damage models. A variation in concrete block height has been accounted for, to assess the influence of height on the performance. The height of the concrete block varies through 80-, 120- and 160mm models. The evolution and behaviour of the concrete damage models appears to be best described following the 160mm model. Figure 5.5 presents the evolution of the concrete damage models at centred cross-section in the z-plane for the distinct phases of a bolt subjected to shear as visualised in the theoretical load-slip curve presented in Section 2.8 (see Figure 2.23). The phases include bolt pretensioning, elasticity, slip, bolt bearing and failure.

From the figure it can be seen that in the first time step of the bolt pretensioning does not lead to any serious damage for both tensile and compressive models. The second time step, in which the displacement-controlled boundary condition is activated, appears to have a greater influence on the damage evolution within the concrete section, especially for the DAMAGET model. The elastic phase shows an highly distorted damage region that keeps on increasing until failure. Damage to the concrete in the initial stages for both tension and compression models is mainly observed in the concrete close to the steel plate and where the concrete is pulled towards the bolt. Appendix B presents the damage evolution for concrete block height of 80- and 120mm.

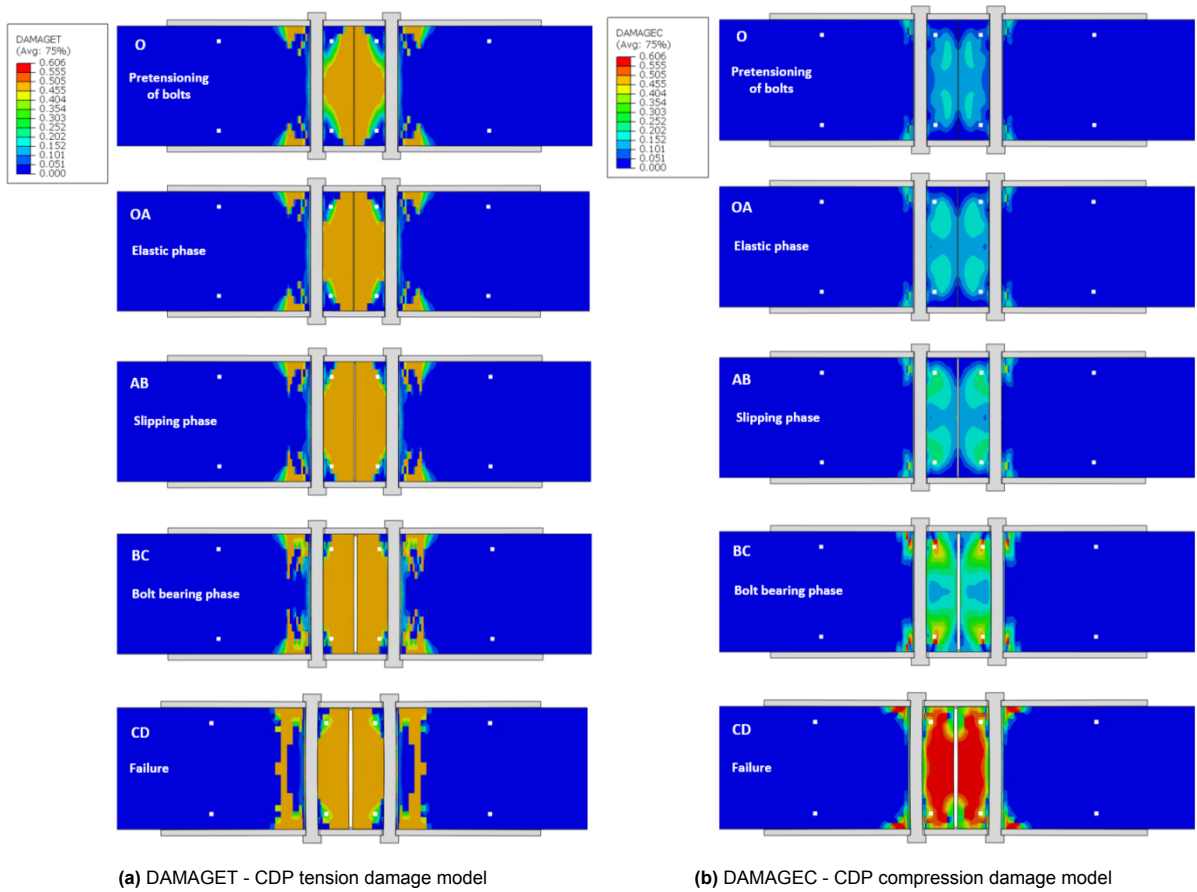


Figure 5.5: Evolution of concrete CDP damage models along the distinct phases of bolts subjected to shear until failure (cut in Z-direction) - Block height 160mm

As a result of the concrete segments being pulled, the concrete block can be divided into distinct regions to define the interaction between the concrete and steel bolt. The regions considered exhibit either tensile or a combination of shear and compressive stresses. The shear-compression region (blue) is located in front of the steel bolts where the concrete makes contact with the shank of the steel bolt. Within this region the shear force that is transferred through the bolts is balanced through the enclosing concrete. The shear-compression region is typically related to fracture of the bolt and local concrete crushing [88]. However, within this model the bolt deforms plastically in the bolt bearing phase until the concrete splits at level of the bolthole as a result of high tensile stresses. The tensile regions (red) are located at the top and bottom of the concrete, where the bolt's shank becomes in contact with the concrete (bolt hole) and in the rear of the bolts (see Figure 5.6). Local confinement in front of the shear connector is induced by a prying force. This initiates stresses in the concrete parallel to the shank of the bolt. The displacement-controlled boundary condition acts as a prying force within the tensile region causing bolt rotation [88]. Although the variations in the height of the concrete blocks indicated a different plastic deformation of the bolts, all models failed due to concrete failure.

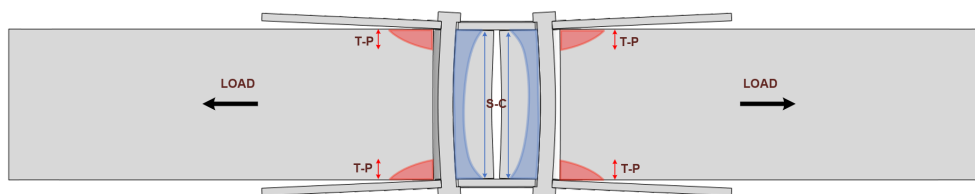


Figure 5.6: Schematic allocation of distinct regions - shear-compression (S-C) / tensile-prying (T-P)

5.2. Load-slip curve

5.2.1. Critical stages in load-slip curve

The load-slip curve for the model with preloaded bolts (50 kN) is visualised in Figure 5.7, where the tensile and compressive damage in concrete (160mm model) for the critical stages of the slipping phase is visualized in Figure 5.8. The step of pretensioning the bolts is followed by the second step, which simulates the displacement of the model, with the force gradually increasing over time as the displacement increases. From the graph it can be observed that the load-displacement curve can be divided into distinct phases, which correspond to the various stages of a push-out experiment that incorporates precast concrete elements (Section 2.8). The initial section of the graph illustrates a linear increasing load-slip line. This section is regarded the elastic phase (0-I) of the specimen, during which the load is insufficient to overcome the friction between the steel-concrete interface. It should be noted that within the elastic phase, the onset of slip engages that continuous until friction is overcome. The small slip in the stage occurs as a result of the high friction that is generated through pretensioning the bolt.

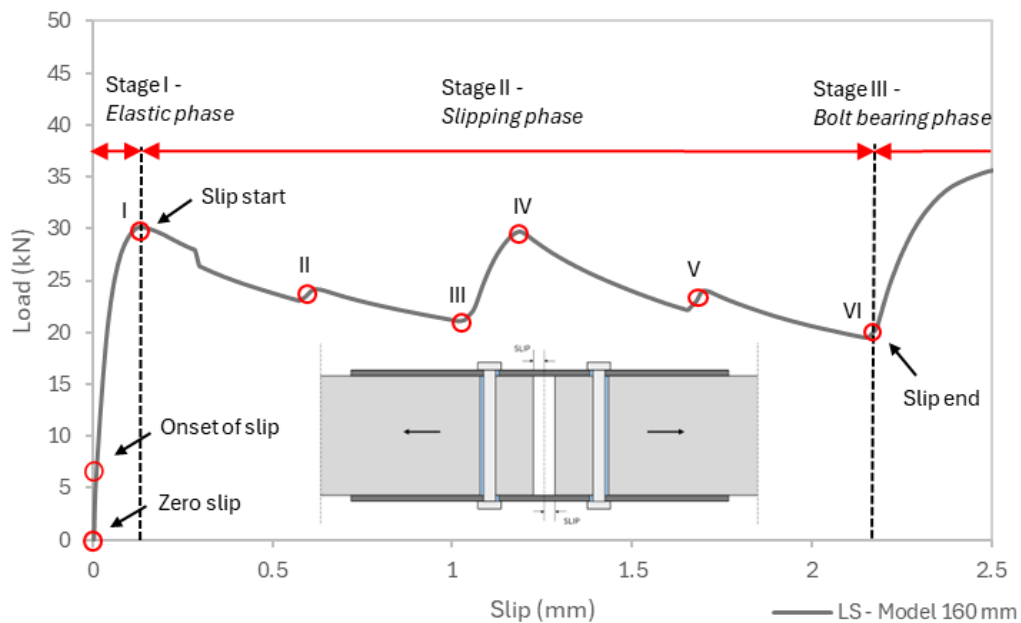


Figure 5.7: Load-slip curve for block model H = 160 mm - Preload = 50 kN - Distinct regions

After the linear elastic part the graph is followed by the slipping stage (I-VI), i.e. the bolt starts moving as a result of the clearance between the bolt and bolt holes in the concrete and steel section. From the Figure 5.7 it can be seen that within the slip phase the load-slip curves tend to be almost horizontal, indicating that the slip occurred suddenly in the load step and developed rapidly. Firstly, the maximum load decreases as the maximum interfacial static friction between the steel-plate and concrete-beam is overcome (I). This induces the concrete to translate horizontally through the tensile force, initiating bolt movement in the concrete hole (II). The graph reaches a minimum where the shank of the bolt is in contact with the concrete beam (III). The force increases again after this point where it reaches the maximum friction between the steel plate and the bolt head interface (IV). The maximum force generated by the interfacial friction between the steel parts is overcome (V), causing the bolt to start moving in the steel hole, where the force continues almost horizontally until the bolt shank contacts the hole in the steel plate (VI). As a result, the slip ends where it is smaller than 2.5 mm in this stage. This appears to be in line with a slip that is usually smaller than 3 mm as was suggested in the study performed by Guo et al. [106].

The sliding phase progressively passes into the bolt bearing phase. In this phase the bolt shank has come into contact with both the concrete and the steel, causing the bolt to be subjected to a combination of shear, tension and bending forces. The bolt exceeds the plastic yield stress and undergoes plastic deformation. The bolt bearing phase is followed by the bolt failure phase. For the application of high-

strength friction-grip bolts it is considered that stage I (elastic phase) is the service state that is allowed in design. Stage II (slip phase) and Stage III (bolt bearing phase) are only used to describe the bearing capacity of the bolt, which is used as an additional strength reserve.

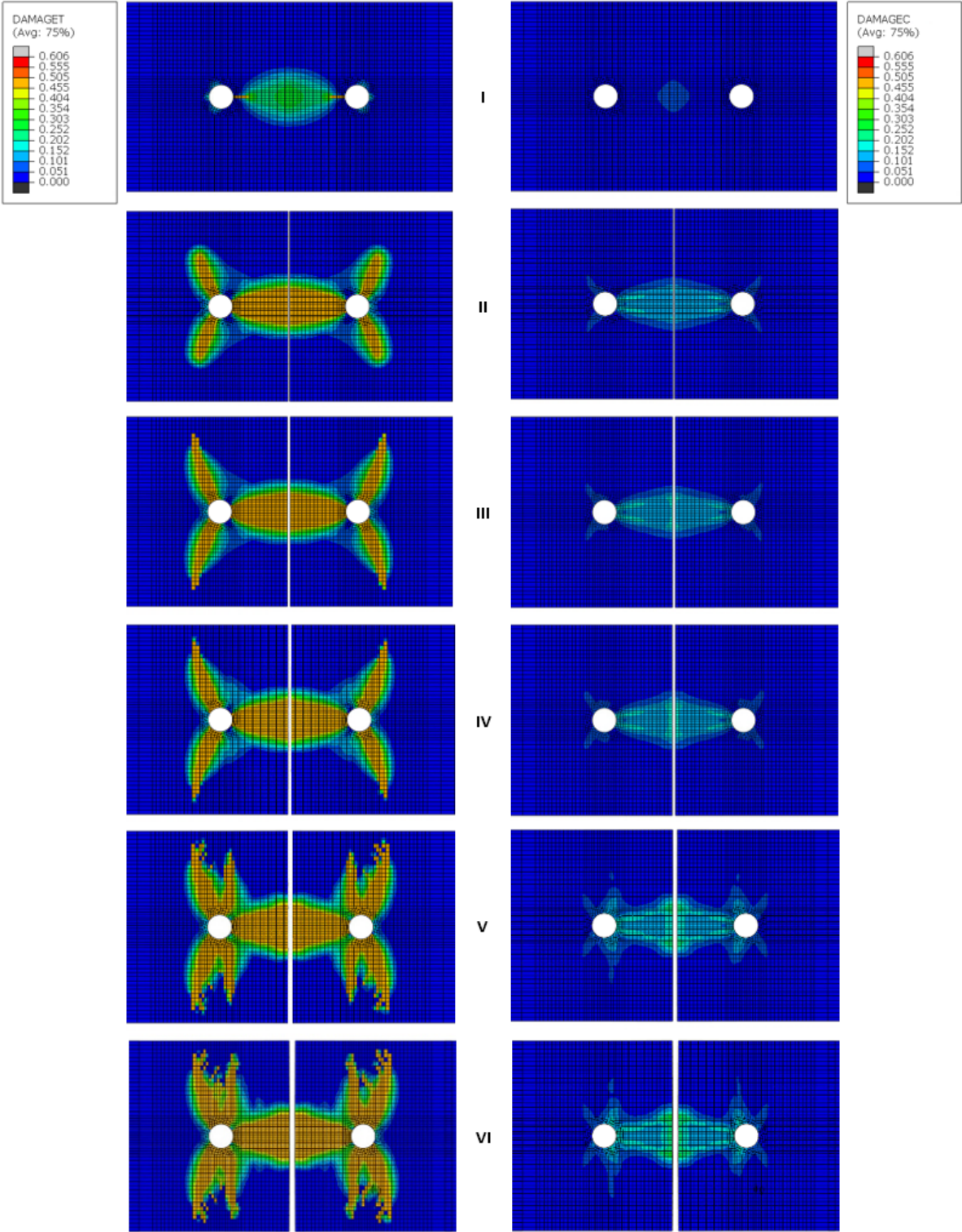


Figure 5.8: Crack pattern development in concrete following the DAMAGET (left) & DAMAGEC (right) models for particulate time frame, corresponding to load-slip graph (cut in Y-direction)

5.2.2. Evaluation of load-slip curve

In order to evaluate and compare variations in the load-slip curves the numerical results obtained are compared through their ultimate resistance P_u , ultimate slip δ_u and initial stiffness k_{ini} . The parameters are determined through the method presented in Figure 5.9, where the ultimate resistance and slip are related to the peak load. The initial stiffness is determined through the slope that is measured at half of the ultimate load carrying capacity of the model. It should be noted that the load-slip curves are presented using the total slip, rather than the relative slip. However, with respect to the determination of the initial stiffness the relative slip is used.

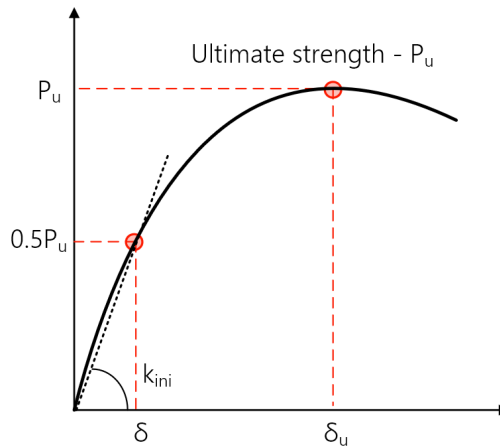


Figure 5.9: Determination principle for load-slip behaviour

5.2.3. Influence of concrete block height

To determine the effect of slab height, variation models were developed and modelled using slab heights of 80mm, 120mm and 160mm. The models use identical properties among which a pretension load of 50 kN. Reducing the thickness does not show significant differences in the elastic and sliding phases of the bolt (Figure 5.10). The load-slip behaviour indicates that the load after the linear elastic stage is slightly reduced. From the load-slip curves it appears that a decrease of 40 mm in concrete height shows an averaged decrease of 22% in load-carrying capacity. Where the load bearing capacity decreases as the slab height decreases, it appears that a smaller height does not have a significant effect on bolt slippage (4% reduction).

Moreover, a reduction in slab thickness indicates that there is less deformation of the bolt in the bearing phase, which reduces the ductility. The model using a concrete height of 80mm shows hardly bolt deformation, in contrast to the models with heights of 120mm and 160mm. As a result, the bolt becomes more susceptible to brittle failure. Additionally, the damage regions (S-C and T-P zone) for increased heights can relative easily be distinguished. However, for a reduced height in the concrete sections the regions overlap one another, resulting in a strength reduction (see Appendix B.1.4.).

The load-slip curves depicted in Figure 5.10, indicates that the ascending parts in the slipping phase show a relatively steep slope. Such slopes indicate a high stiffness of the model. Higher stiffnesses are generally attributed due to a small bolt to hole clearance, high pretension force and large bolt diameter. The parametric study carried out by Fang et al. [88] considered the effect of slab thickness, where the results indicated that increased thickness had a marginal effect on ultimate shear resistance, but showed steeper load-displacement curves, indicating that a greater stiffness is obtained with increased slab height. However, as aforementioned, the load-slip curves in these models indicate a contrasting averaged decrease of 22% in ultimate load carrying capacity with decreasing height of 25%. Furthermore, from the figure it appears that the height of the concrete slab has for these different models only a small impact on the slopes of the load-slip curves, since the initial stiffness reduces with only 3% through a decreased height from 160 to 120 mm. A stronger decrease is observed in the model that uses the height of 80 mm, which corresponds to a decrease of 20% when compared to the 160 mm model. The linear elastic phase presents the maximum friction resistance until the friction is overcome. The friction resistance that is generated through bolt pretensioning increases only slightly with an increasing concrete block height.

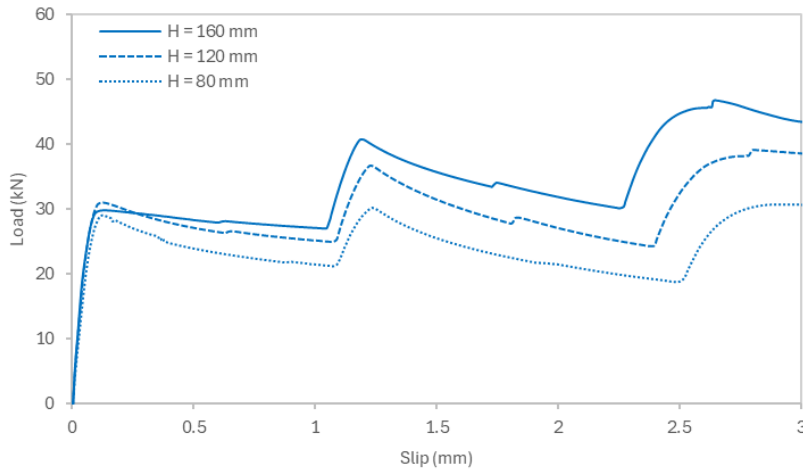


Figure 5.10: Load-slip curve for variant block height models

H [mm]	P_u [kN]	δ_u [mm]	k_{ini} [kN/mm]
160	46.6	2.6	423.6
120	39.0	2.8	412.0
80	30.7	2.9	352.3

Table 5.1: Results

5.2.4. Pretensioned vs. non-pretensioned bolts

The numerical model developed incorporates two distinct models which include the utilisation of a bolt hole cavity with bolt pretension and the absence of a bolt hole cavity with no bolt pretension in the concrete section (see Section 4.1). As aforementioned, the combination of a bolt hole cavity where no preloading of the bolts is applied leads to convergence issues when running the model. Therefore, it was decided to incorporate bolt pretensioning with the application of a gap (cavity) in between the bolt and bolt hole. To evaluate the influence of bolt pretensioning, three levels of pretension ($P = 5, 25$ and 50 kN) were applied to the model and compared to the non-pretensioned bolts.

In order to ascertain the distinction between preloaded and non-preloaded bolts within the model, the load-slip curves for the various models are compared. It is evident that the absence of a bolt hole cavity will result in a reduced slipping phase for the model, given that the bolt is constrained by the surrounding bolt holes in both the concrete and steel plate. As a result, the greater ultimate slip for preloaded bolts presented in the Table 5.2 is attributed to the presence of a bolt cavity of 2 mm. The load-slip curves demonstrate that with respect to relative slip (neglect the cavity of 2 mm), pretensioning of the bolts does not significantly impact the ultimate slip capacities. From the load-slip curves presented in Figure 5.11 it can be observed that in the elastic stage, the model with 50 kN bolt pretensioning exhibits the highest initial stiffness, as indicated by the steeper curve. It appears that bolt pretensioning shows an averaged increase of 40% in initial stiffness with an increase of 25 kN in preload.

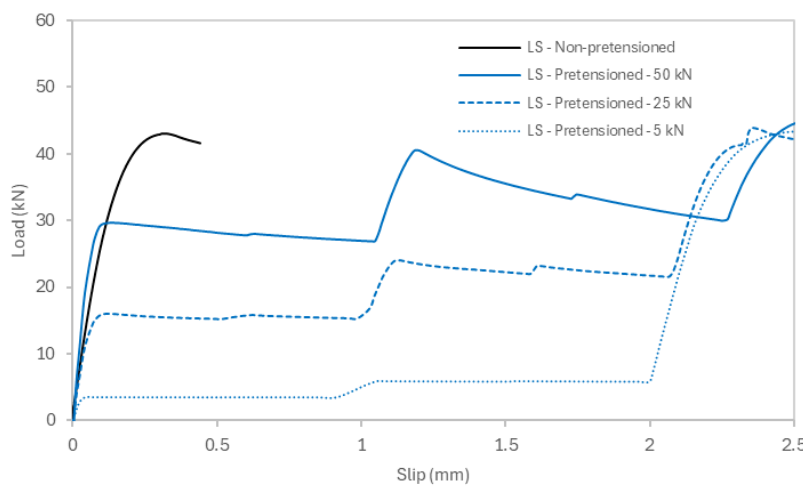


Figure 5.11: Load-slip curve for pretensioned vs. non-pretensioned bolts

P [kN]	P_u [kN]	δ_u [mm]	k_{ini} [kN/mm]
0	43.0	0.3	281.0
5	43.3	2.5	215.4
25	44.0	2.4	292.3
50	46.6	2.6	423.6

Table 5.2: Results

For the preloaded models with a bolt hole clearance of 2 mm, the initial stiffness is distorted due to bolt sliding. As a result, the non-preloaded bolt model showed a greater initial stiffness compared to the bolt preload of 5 kN. This observation was attributed to the direct contact of the bolt shank with the concrete in the non-preloaded model. Compared to the 25 kN and 50 kN preloaded models, the 5 kN preload appears to be too low, causing the bolt to slip almost immediately after the application of the horizontal displacement controlled load.

In order to verify whether the applied preload is in line with the assigned friction coefficient in the model, the maximum load after the initial elastic phase is compared to the friction resistance (see Table 5.3). The friction resistance P_μ is determined by multiplying the preload with the friction coefficient. The finite element model developed uses a combination of contact conditions, including steel-to-steel and concrete-to-steel, which use a coefficient of friction of 0.25 and 0.35 respectively. As a result, both contacts are taken into account, resulting in a summed frictional resistance between the two surfaces. The analytically derived frictional resistance appears to be close to that obtained by the FEM, showing good agreement.

Preload - P [kN]	Friction resistance - P_μ [kN]				
	Steel-steel (0.25)	Steel-concrete (0.35)	Analytical	FEM	Analytical / FEM
50	12.50	17.50	30.0	29.7	101%
25	6.25	8.75	15.0	16.1	93%
5	1.25	1.75	3.0	3.5	86%

Table 5.3: Verification of preload in FEM

In accordance with the maximum slip observed in Figure 5.11 the connector, whether preloaded or non-preloaded, is deemed non-ductile according to Eurocode 4 [32] as the characteristic slip capacity of 6 mm has not been reached. Based on the ultimate load capacities presented in Table 5.2 it can be concluded that bolt pretensioning does not have a significant effect on the ultimate load capacity of the block model.

5.3. Convergence study

The results obtained from the finite element model are highly dependent on certain input parameters that affect the type of analysis. Reducing the mesh size and increasing the order of elements typically increases the computational time of the analysis. It is therefore necessary to verify the accuracy whilst maintaining a reasonable level of efficiency. A convergence study is performed to determine if the results obtained from the finite element analysis are reliable. Convergence studies typically include the influence of mesh size and the influence of element type including the order of the elements used within the model.

5.3.1. Element order and mesh size

Finite elements consist of nodes and integration points. The nodes are positioned at the edges of an element, where the integration points are positioned in between the nodes. Finite element analyses are carried out by calculating displacements and forces at the nodes and then, based on the results obtained, interpolation allows mechanical properties to be determined at the position of the integration points in the finite element. Although increasing the number of nodes and integration points increases the complexity and computational time of the model, the accuracy is expected to increase as well. The numerical model includes a (linear) 8-node solid element. To assess the accuracy of the model, a higher order solid element (quadratic) including 20-nodes are used within the convergence study (see Figure 5.12). Note that the 2-node truss elements that are solely used to model the reinforcing bars are not modified in this study.

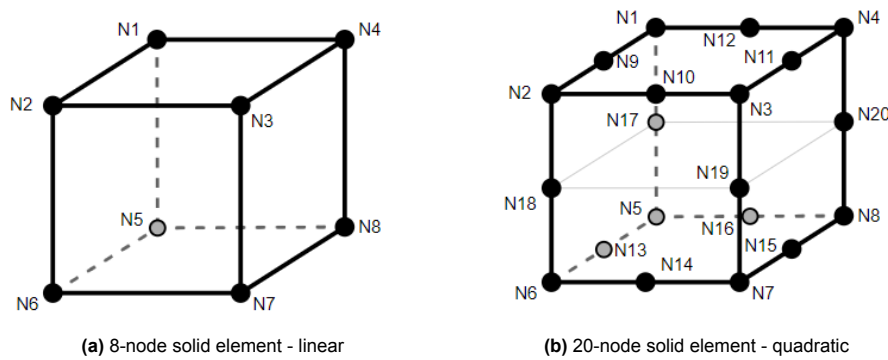


Figure 5.12: Linear vs. quadratic hexahedron solid element

A mesh sensitivity study is conducted to establish the accuracy of the analysis. Within the numerical model it was decided to apply mesh refinement in areas of the plate and block that were expected to have critical stress concentrations, such as described in Section 4.3. Therefore, the mesh sensitivity study particularly pertains to the element size within the critical region(s) of the finite element model. The accuracy of the model is verified through very-coarse/coarse/fine/very-fine mesh configurations. In addition, the alternation of decreasing mesh size in the FE model is performed in coherence with either linear or quadratic solid elements. A higher order element is expected to provide greater accuracy but at the cost of increased computational time. The analyses performed account for an identical decreasing mesh size regarding the plate and block within the refined mesh area. The bolt uses an incrementally decreasing element size in smaller increments, as elements that are too large for the bolt will result in large shape imperfections/errors. Table 5.4 reports the analysis type including mesh and type of element settings.

Analysis	Mesh	Element order	Element size (mm)		Nr. of elements	Comp. time (s)
			Plate / Block	Bolt		
A1-VC-L	Very coarse	Linear	15	5	11736	4701
A2-C-L	Coarse	Linear	8	4	32802	21466
A3-F-L	Fine	Linear	4	3	50332	48863
A4-VF-L	Very fine	Linear	2	2	94338	86331
A5-VC-Q	Very coarse	Quadratic	15	5	11736	30170
A6-C-Q	Coarse	Quadratic	8	4	32802	207223
A7-F-Q	Fine	Quadratic	4	3	50332	308686*
A8-VF-Q	Very fine	Quadratic	2	2	94338	Not executed**

*Analysis A7-F-Q was not completed and terminated upon reaching the ultimate load-carrying capacity

**Analysis A8-VF-Q was not executed for insufficient computational time reasons

Table 5.4: Mesh settings and element order - convergence study

5.3.2. Output

The analyses performed distinguish between the use of either linear or quadratic solid elements. This study analyses the convergence behaviour in order to ascertain whether it is consistent with the accuracy of the results while maintaining a high level of efficiency. Furthermore, it compares the influence of the mesh size and element order on the Von Mises stresses in the various parts of the model determined at the timeframe of maximum reaction force RF1. From the Table 5.4 it is observed that the analyses A7-F-Q and A8-VF-Q were terminated and/or not completed. The principal reason for this outcome is that the analyses were so computationally intensive that, prior to the generation of the result output, they were deemed to be inefficient. Although the A7-F-Q analysis was terminated due to its significant computational time, the results included the timeframe of maximum reaction force. Consequently, the output of the analysis is included in the final assessment, in contrast to the A8-VF-Q analysis. The results plotted in Figures 5.13 to 5.16.

Figure 5.13 depicts the displacement and maximum reaction force that is derived through the various analyses performed. The displacement and reaction force components from the analyses are obtained through the reference points (either RP-1 or RP-2), which are coupled to the surfaces through which the displacement controlled boundary condition is assigned to. It appears that the linear elements and quadratic elements converge in a very similar manner, as the results approach one another relatively close where decreasing the mesh size has only slightly effect on the convergency for both the displacement and maximum reaction force in the X-direction. Based on the deviation of results versus the number of elements that is depicted in Figure 5.13 it seems that the use of a mesh size that is considered 'very fine' can be altered to a size with a lower seed, since the results for these components exhibit minimal deviation.

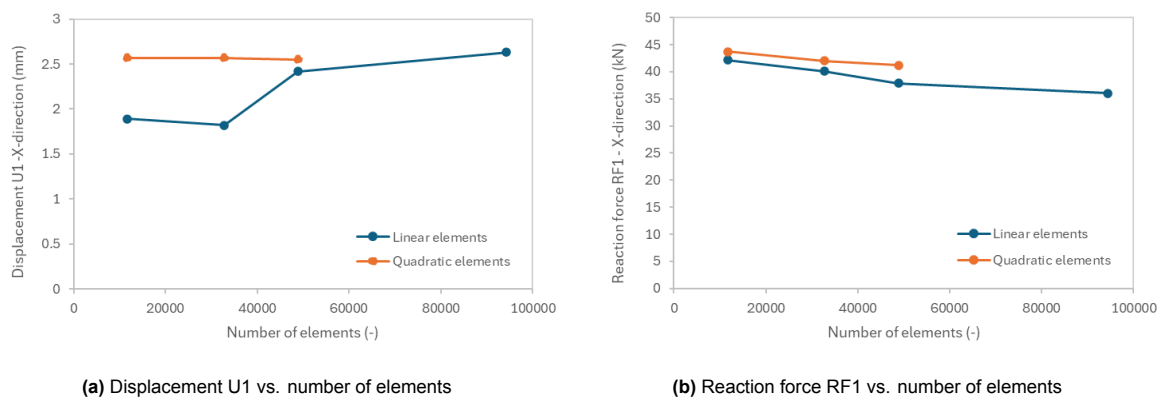


Figure 5.13: Comparison of displacement and reaction force in X-direction

The Von Mises stresses in the plate and bolt are determined through a region that is considered to encounter the highest stresses in the model. The regions per analysis consist of a variant number of nodes, since the number of nodes depend on the mesh size. For obvious reasons, a larger mesh size will lead to less nodes where a smaller mesh leads to an increase in the number of nodes in that specific region. In addition, the element order used per analysis may alter the number of nodes as well. For that reason, it is more likely for the analyses that have a larger mesh size to have a higher deviation and a lower accuracy in results. The main reason for selecting multiple nodes is to establish whether the stresses in the nodes are consistent. This strategy eliminates selecting any possible outliers that should be considered not reliable when comparing the different analyses. The nodes selected and compared to one another lie within the designated specified regions that is depicted in Figure 5.14. For the plate the critical region is considered where the bolt hole becomes in contact with the bolt shank, where for the bolt the critical region is positioned at the centre half that exhibits the highest (tensile) deformation. From the nodes selected in the specified regions, the results are compared from which the critical value is determined and plotted in the graphs in Figure 5.15.

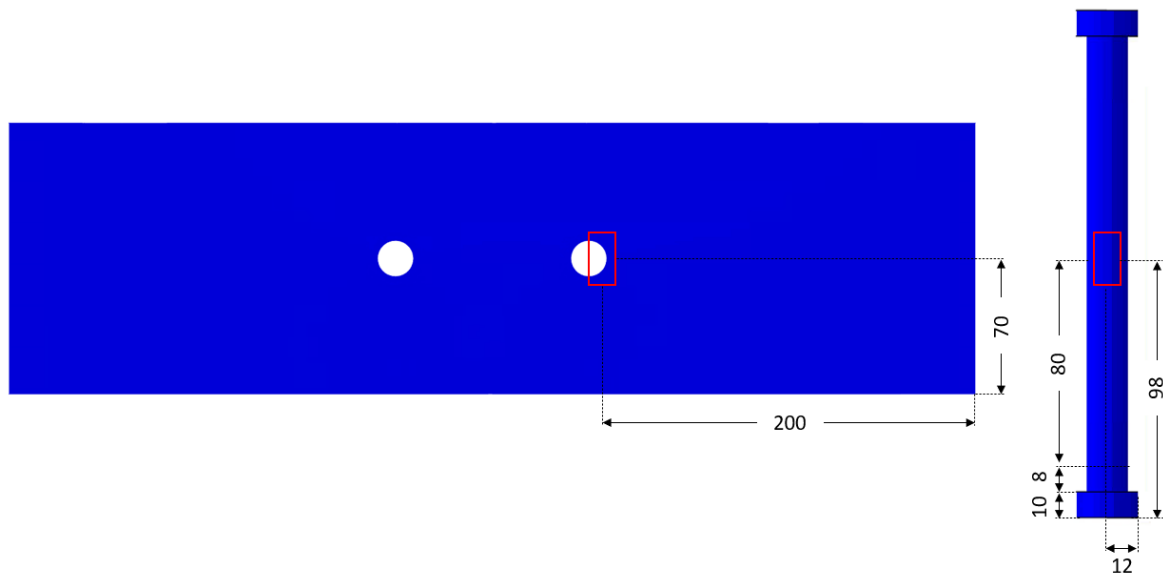


Figure 5.14: Selection and position of critical node-region in the plate (top-view) and the bolt (side-view) - not to scale

The Von Mises stresses for the plate and bolt demonstrate a contrasting behaviour when employing linear or quadratic elements. The plate utilises the stress measured at the nodes situated in the bolthole opening, with the nodes in the bolt derived from the centred section, where the bolt undergoes the greatest deformation. In the regions selected for the bolt and the plate in particular, the analyses employing linear elements exhibit a considerably lower Von Mises stress than those utilising quadratic elements. With respect to the Von Mises stress for the plate in Figure 5.15a it can be seen that the linear elements have a higher reliability than the quadratic elements when the assigned material properties are considered in relation to both elastic and plastic behaviour. Moreover, it can be observed that an increase in the mesh size for the linear elements results in a graph that remains constant, as the stresses in the plate are almost similar. The discrepancy in outcomes between the utilisation of quadratic and linear elements can be attributed to the augmented number of nodes when employing quadratic elements. A quadratic element consist of midside nodes, which are absent in linear elements. In the event of severe distortion, the displaced region of midside nodes may result in the formation of sharp corners or bends, which penetrate a face on the opposite side of the element. This phenomenon is known as mesh entanglement. Linear elements are less prone to this phenomenon due to the absence of midside nodes, which may contribute to excessive distortion. Consequently, linear elements are regarded as a more suitable option for the finite element model.

The von Mises stress in the bolt evinces a tendency to behave in a similar way to that observed in the linear and quadratic elements for the plate, with the quadratic elements predicting an overestimate where the linear elements underestimate the von Mises stress for the time frame considered. However, the stresses in both the linear and quadratic elements are within the specified elastic and plastic material properties. At the time of failure, which occurs at the beginning of the bolt bearing phase (see section 5.1), the bolt has undergone little plastic deformation. For similar reasons as described for the Von Mises stress in the plate, the results for the bolt using a linear analysis appear to be more reliable.

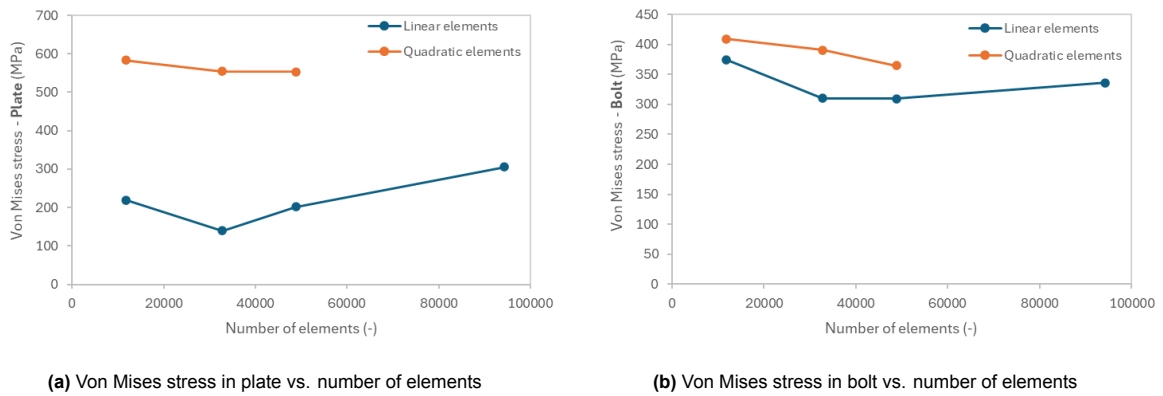


Figure 5.15: Comparison of Von Mises stresses in plate and bolt

The convergence study not only provides evidence of the reliability of the results, but also demonstrates the efficiency of the analytical procedures employed. The efficiency of a given method can be determined by measuring the amount of time required to calculate a model. Figure 5.16 presents the computational time required for each analysis. As aforementioned, due to the increased number of nodes, the quadratic analyses required an enormous computational time which is why the quadratic analyses that considered a 'fine' and 'very fine' mesh were terminated and not completed. Therefore, the corresponding computational time is not reported in the Figure 5.16. Although the computational time of analyses A7 and A8 are missing, it is evident that the linear analyses require less time than the quadratic analyses which are considerably more time-consuming. Therefore, based on the efficiency of the models it is highly preferred to use linear elements over quadratic elements in the finite element model.

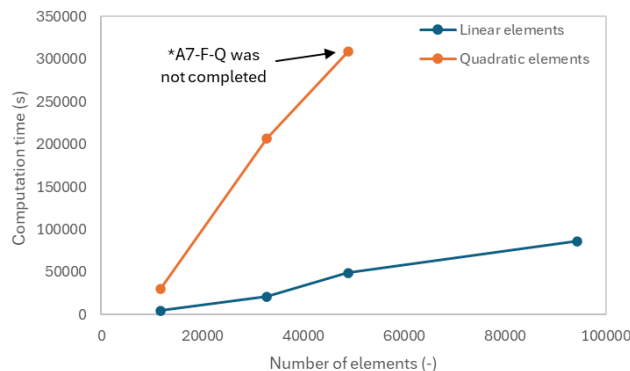


Figure 5.16: Computational time vs. number of elements

Optimal accuracy and efficiency

In order to ascertain the optimal balance between accuracy and efficiency, a mesh size should be used that is sufficiently small to ensure the desired level of accuracy while maintaining an acceptable time frame for the analysis. Based on the observed variations and consistency of the displacement and reaction force in the variant analyses it seems that the use of linear and quadratic elements are considered appropriate options. However, the consistency is not noticeable in the Von Mises stresses that were measured in the critical regions of the plate and bolt part. The use of quadratic elements appears to overestimate the stresses at the time frame of maximum reaction force. Moreover, the computational time of the analyses indicated that the use of linear elements is highly favourable over quadratic element. Therefore, based on the results of the various analyses, the use of linear elements is preferred over the use of quadratic elements, due to the reliability in results and the efficiency in terms of computational time. Furthermore, it was observed that the mesh size could be reduced for the analyses utilising linear elements, resulting in a fine mesh size. This enhances the efficiency of the analysis while ensuring the accuracy of the results.

6

Application of shear connector connection in beam model

To assess the performance of the finite element model on a large scale, the developed and validated connection model is deployed into a beam model to assess its behaviour and resistance compared to a conventional (non-demountable) floor system. Therefore, a conventional and demountable FE model are developed for structural analogy. The analysis aims to examine the demountability and reusability of the system, including its elastic and plastic behaviour. To achieve demountability and reusability, it is of importance to prevent plastic deformation when subjected to various load combinations.

6.1. Numerical model

The finite element models are tested on the bending capacity, to simulate the flexural stress-strain response. The demountable floor system that incorporates the effect of reused slabs follows the static scheme of a simply supported continuous beam, where the hinges present the applicability of the slab/slab joint (see Figure 6.1a). For simplification purposes the effect of a hogging bending moment is realised by using symmetry conditions on the concrete edges, i.e. at the position where the slab is supported. As a result, the finite element model modelled using a fragment of a continuous floor system and simulated following the static scheme of a fixed beam as depicted in Figure 6.1b. The demountable deck-to-deck connection is positioned at a distance $x = 1/4 l$ from the fixed supports, where the bending moment is considered zero following force equilibrium in a static beam. Theoretically, the distribution of forces in combination with positioning of the connection at zero bending moment location, the connection is subjected to pure shear forces. To reduce the computational time that is needed to complete the analysis, half of the beam is modelled where a second set of symmetry conditions is applied at mid-span section. Furthermore, as the beam model is a follow-on numerical model to the block model presented in Section 4, identical modelling settings are used within the beam model.

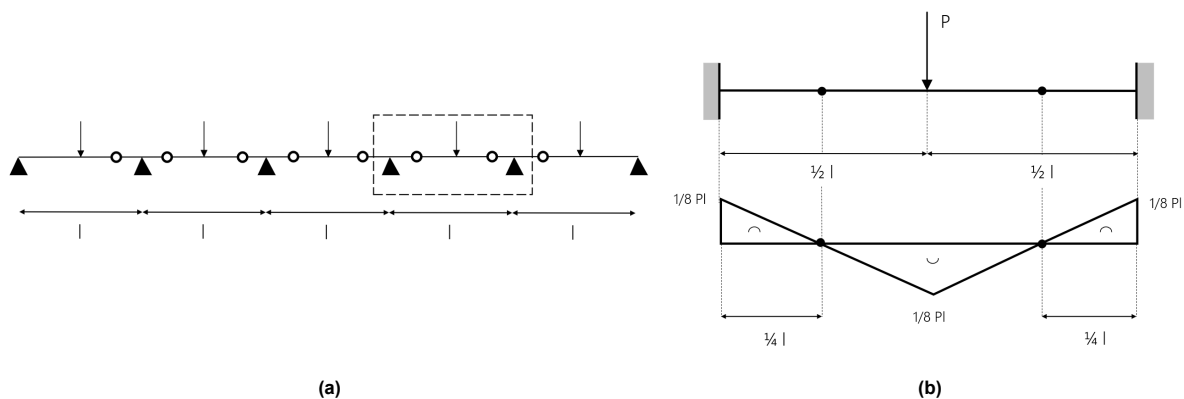
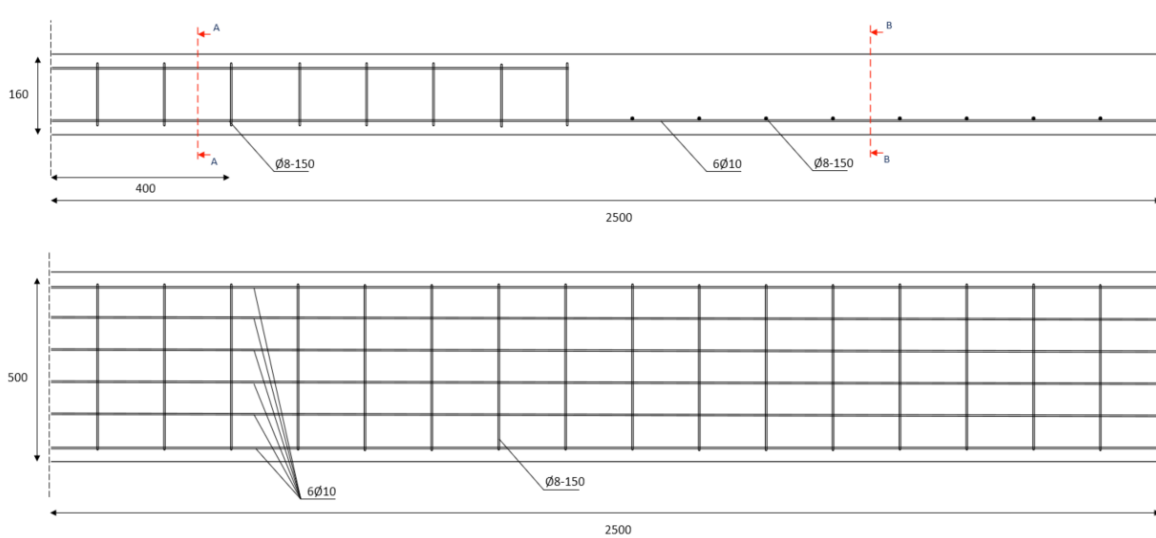


Figure 6.1: Application of shear connector connection in beam model - test setup

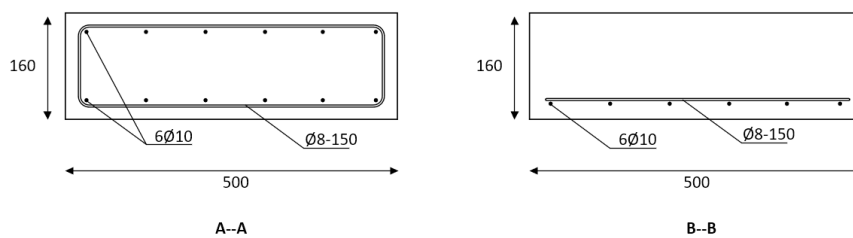
6.1.1. Geometry

The conventional and demountable beam models are designed using a span of 5000 mm. As aforementioned, for computational efficiency, the beam models are modelled using half of the beam length only, such as is depicted in Figure 6.2 and 6.3. The conventional beam model follows a similar reinforcement configuration that is established through the configuration used in the study on demountable slabs by Almahmood et al. [78]. Therefore, the models do not incorporate a layer of top reinforcement in the mid-span section.

The model is designed through a total of six 10 mm diameter longitudinal reinforcing bars with 8 mm diameter transverse reinforcing bars spaced 150 mm apart. To account for the shear force at the support that is generated through equilibrium of forces, stirrups diameter 8 mm are positioned at the edges of the beam. The beam is 160 mm in height and 500 mm in width. The beam models are tested on their structural performance through a vertical load that is positioned at midspan. In order to transfer the load onto the beam, a loading-support is incorporated in the model (not depicted). The surface of the loading-support is in length length and width equal to 100 mm and 500 mm, where a height of 50 mm is adopted.



(a) Conventional (non-demountable) beam model



(b) Cross-section A-A and B-B

Figure 6.2: Geometry and reinforcement configuration for conventional beam model for 5 meter span - Half of the beam models presented only as symmetry conditions are applied (Measurement in mm)

Unlike the conventional model, the demountable beam model consists of two separate beams with equal lengths of 1250 mm. The beam length considered is based on an equilibrium of forces where the position of the zero bending moment is considered according to the equilibrium of forces as shown in Figure 6.1. The beams are connected by the bolted shear connectors as developed in the preliminary finite element model with a spacing of 200 mm. However, for the beam model it was decided to use M20 instead of M16 bolts, where the bolt head/nut has a diameter of 30 mm and height of 12.5 mm. The plates used in the model consist of height of 8 mm. Figure 6.3 shows two types of demountable models, which differ in the reinforcement configuration in the centre beam (right beam-part). The demountable

beam model shown in Figure 6.3a represents the use of a newly cast beam where the reinforcement provides anchorage for the reinforcing steel, while the configuration shown in Figure 6.3b represents a concrete beam cut from an existing structure. In the latter, as a result of the cutting of the concrete, the longitudinal reinforcement is of the same length as the concrete beam in which the reinforcement is not anchored.

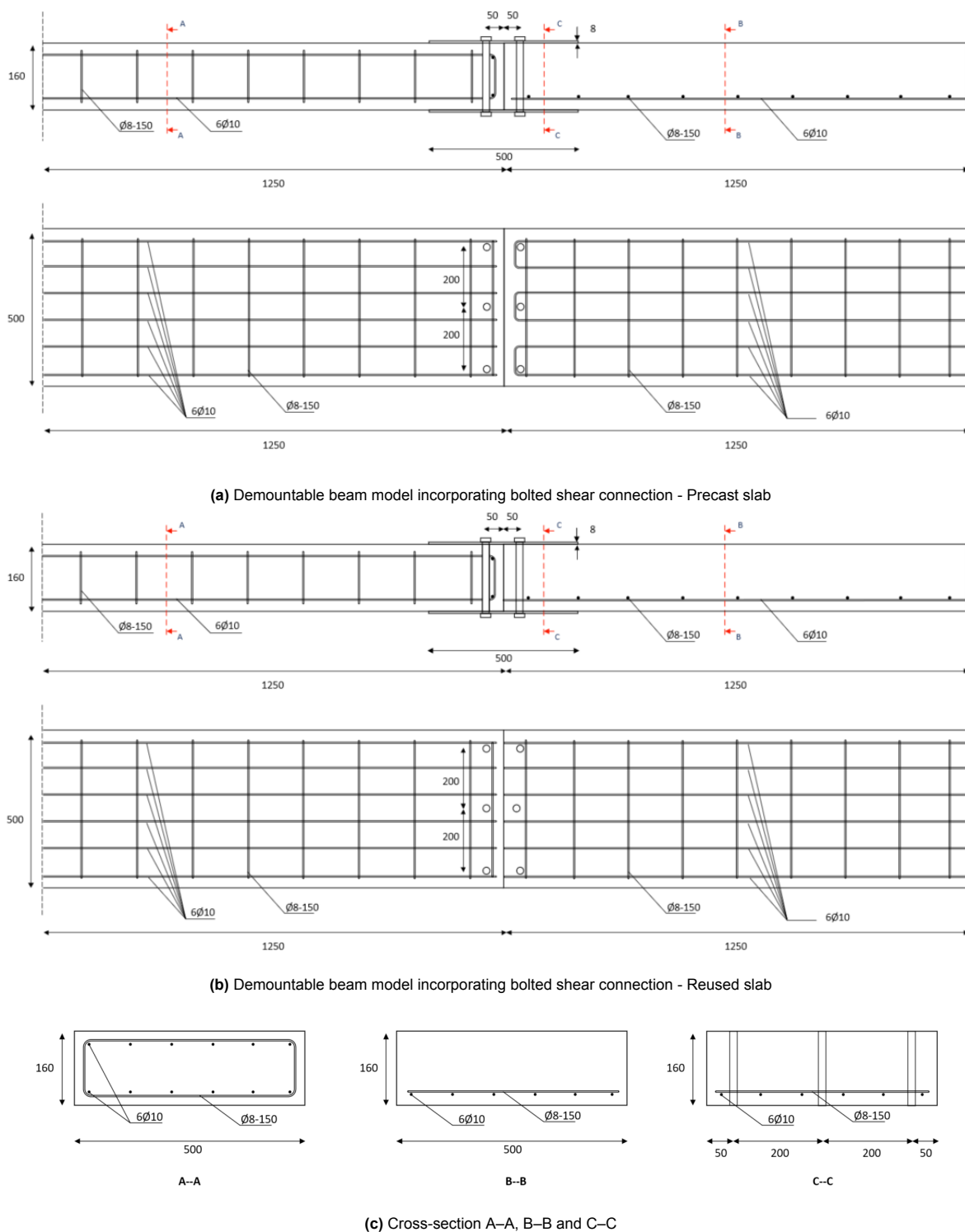


Figure 6.3: Geometry and reinforcement configuration for demountable beam models for 5 meter span - Half of the beam models presented only as symmetry conditions are applied (Measurement in mm)

6.1.2. Material models

The beam models are assigned to specified material models. For both conventional and demountable beam models, the identical materials defined in the preliminary block model are used throughout the analysis. However, as the ultimate load capacity of the demountable beam models is yet to be determined in order to establish their performance, the reinforcing steel is considered to be of significant importance. Therefore, in contrast to the simplified block model, the plastic properties for the steel reinforcement are considered within the model in order to incorporate the yielding of the reinforcement. The reinforcement is modelled through a bilinear stress strain curve such as depicted in Figure 6.4 and corresponding plastic properties in Table 6.1.

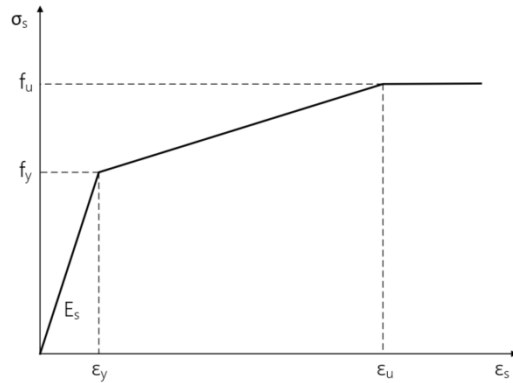


Figure 6.4: Bilinear material model - reinforcing steel

Reinforcing steel Ø8 - Ø10		
Yield stress	f_y [MPa]	400
Ultimate stress	f_u [MPa]	500
Ultimate strain	ϵ_u [-]	0.15

Table 6.1: Plastic properties reinforcing steel

To simulate a load through boundary conditions at the mid-span of the beam model, a load-bearing support is added to the model through which a load is uniformly distributed and transferred to the beam. In addition, the model is supported on its edges by an additional support. The supporting parts are considered to be a steel material, but with an infinite modulus of elasticity to increase stiffness and prevent any deformation of the part. The Table 6.2 summarises all materials used in the beam models. The plastic properties are only activated through the beam, bolt, plate and reinforcement element. The damage initiation model is solely used in the concrete section, through the CDP-model. Reusability was considered an important prerequisite which is why the damage initiation models regarding the steel elements are not included. For a detailed description of the material models including corresponding plastic properties (if applied) that are used in the beam model analyses, see Section 4.2.

Element	Property		Elasticity		Plasticity	
	Material	Strength class	Elastic modulus E (GPa)	Poisson ratio ν (-)	On/Off	Application
Beam	Concrete	C20/25	30	0.2	On	CDP
Bolt	Steel	10.9	210	0.3	On	Plastic
Plate	Steel	S355	210	0.3	On	Plastic
Support	Steel	-	∞	0.3	Off	-
Rebars	Steel	B500B	210	0.3	On	Plastic

Table 6.2: Material models for conventional - and demountable beam models

6.1.3. Element type and meshing

The beam models incorporate identical element types to the ones presented in the simplified block model. The reinforcing bars are modelled using the T3D2-elements, where all other parts use the C3D8R-element. In regards to the mesh size used, it should be pointed out that the beam-model is modelled using a larger mesh size than that is used in the block-model. The main reason for this pertains to an increased geometry, where for computational efficiency and time reduction a larger mesh

is more suitable. Moreover, as a result of the convergence study in Section 5.3, linear elements are used over quadratic elements for computational efficiency. To avoid computational errors in the more complex demountable beam model, the mesh is refined by applying local seeds in areas considered critical using datum planes (see Figure 6.5). These areas relate to interaction between the bolt, the concrete beam and the steel plate member. Table 6.3 reports the element type including the mesh size for each distinct part in the beam-models.

Part	Element	Element order	Mesh size (mm)	Conventional model		Demountable model	
				Global seeds	Local seeds	Global seeds	Local seeds
Beam	C3D8R	Linear	15	-	15	3	
Bolt	C3D8R	Linear	-	-	3	-	
Plate	C3D8R	Linear	-	-	15	3	
Support	C3D8R	Linear	15	-	15	-	
Reinforcement	T3D2	Linear	10	-	10	-	

Table 6.3: Element type and mesh size for conventional- and demountable beam model

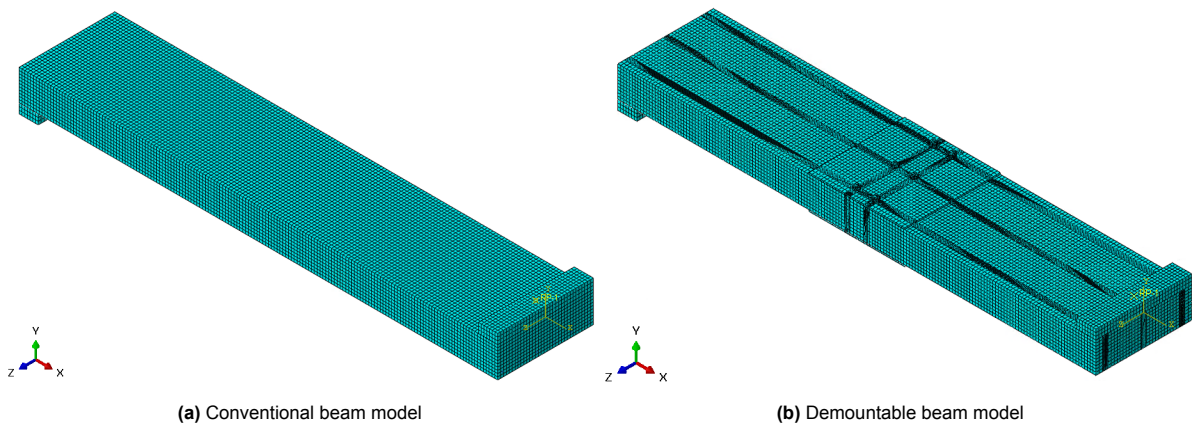


Figure 6.5: Meshing for beam models - Half beam model symmetry condition application

6.1.4. Interaction and contact conditions

The interaction and contact conditions used in the beam models strongly relate to the contact pairs established in the simplified block model. An additional contact pair is added to the beam model, which corresponds to the supporting parts and concrete beam. The additional contact pair is present in both the conventional and demountable beam models. However, the contact surfaces between support and concrete beam at the edge are tied to one another. The contact activation for the demountable beam model varies for some of the contact pairs. Table 6.4 and Table 6.5 present the contact activation per step if applicable and corresponding contact pairs for the conventional and demountable beam model.

Conventional beam model			
Step - contact activation	Master surface	Slave surface	Contact pair
Initial	Loading support	Beam	Support to concrete
Step 1: Loading step	-	-	-

Table 6.4: Master- and slave surface discretisation including contact activation for conventional beam model

Demountable beam model			
Step - contact activation	Master surface	Slave surface	Contact pair
Initial	Beam	Beam	Concrete to concrete
	Plate	Beam	Steel to concrete
	Plate	Bolt head / nut	Steel to steel
	Loading support	Beam	Support to concrete
Step 1: Preloading force	-	-	-
Step 2: Loading step	Plate	Bolt shank (Partition)*	Steel to steel
	Bolt shank (Partition)*	Beam	Steel to concrete

*Relates to either the centre or top and bottom section of the bolt shank for contact with the concrete block or steel plate in step 1/2.

Table 6.5: Master- and slave surface discretisation including contact activation for demountable beam model

The interaction and contact conditions regarding the concrete to concrete, steel to concrete and steel to steel contact remain identical with respect to the normal and tangential behaviour. The specific interaction conditions and settings are reported in Section 4.4. As a result of adding the beam to loading-support contact pair, another interaction property is incorporated within the model. The interaction property is defined through normal and tangential behaviour, using a friction penalty formulation with a coefficient equal to 0.25 for the latter. As aforementioned, an additional constraint is implemented in the model which relates to the tie-constraint. The support and beam on the edge where tied to ensure these parts performed as a single bond. Consequently, the beam models include three types of constraint conditions (tie-, embedded-region- and coupling-constraint). For the beam models only one reference point is coupled onto a specified surface, which pertains to a RP on the top surface of the loading support to assign a loading condition (see Figure 6.6 for coupling of RP-1).

6.1.5. Boundary and loading conditions

The boundary and loading conditions do not differ through the application of either a conventional or demountable beam model. To test the structural performance of both the conventional and demountable beam models, a displacement-controlled loading boundary condition at mid-span is employed. The models are supported on their edges through the supporting part, where the bottom surface of the support is fixed through the 'Encastre' boundary condition. Moreover, to enhance computational efficiency, only half of the beams are modelled, with symmetry conditions in the X-direction applied at the cross-sectional surfaces at mid-span and the edge. Note that the symmetry conditions in the X-direction are not coupled through a reference point, but to the complete edge surface that is displayed in red in Figure 6.6a. The loading conditions are only applied to the demountable beam model in order to simulate the effect of preloaded bolts (Figure 6.6b and c for the application of a bolthole cavity. Table 6.6 and 6.7 present the boundary- and loading conditions for the models.

Conventional beam model			
Condition type		Time function	
		Initial	Step 1: Loading step
Boundary condition	BC1	Symmetry /Antisymmetry/Encastre: XSYMM (U3=UR1=UR2=0)	Propagated
	BC2	Symmetry /Antisymmetry/Encastre: XSYMM (U3=UR1=UR2=0)	Propagated
	BC3	Displacement /rotation-RP1: U1=U2=U3=UR1=UR2=UR3=0	Modified: U2=-200mm
	BC4	Symmetry/Antisymmetry/ Encastre -Support: U1=U2=U3=UR1=UR2=UR3=0	Propagated

Table 6.6: Boundary and loading conditions numerical beam model - Conventional

Demountable beam model				
Condition type		Time function	Step 1: Preloading force	Step 2: Loading step
		Initial		
Loading condition	Bolt load		Apply force: 50 kN	Method: Fix at current length
Boundary condition	BC1	Symmetry /Antisymmetry/Encastre: XSYMM ($U_3=UR_1=UR_2=0$)	Propagated	Propagated
	BC2	Symmetry /Antisymmetry/Encastre- RP3: XSYMM ($U_3=UR_1=UR_2=0$)	Propagated	Propagated
	BC3	Displacement /rotation-RP1: $U_1=U_2=U_3=UR_1=UR_2=UR_3=0$	Propagated	Modified: $U_2=-200$ mm
	BC4	Symmetry/Antisymmetry/ Encastre - Support: $U_1=U_2=U_3=UR_1=UR_2=UR_3=0$	Propagated	Propagated

Table 6.7: Boundary and loading conditions numerical beam model - Demountable

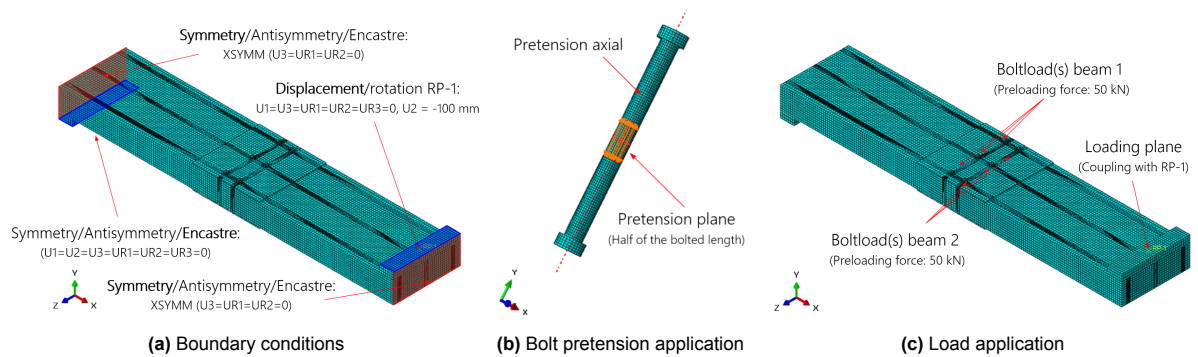


Figure 6.6: Boundary condition and loading application for demountable beam model - In case of the conventional beam model the boundary conditions visualised in (a) remain identical

6.1.6. Computational solver

In order to obtain the results for the beam models, the identical computational settings to those used for the block model are employed (see Table 4.9). The models are solved using the static, general (implicit) solver. The designated temporal interval is 1, wherein geometric non-linearity and automatic stabilisation are employed. The incrementation is set to automatic, with the increment size set equal in each step. The solver employs the full Newton solution technique. The method seeks to identify dynamic equilibrium at each increment, concurrently calculating the maximum resistance.

Static, General (Implicit)		
Time period	1	
NLGeom	On	
Automatic stabilisation	Dissipated energy fraction	0.0002
Incrementation	Automatic	
Increment size	Initial	0.01 mm
	Minimum	$1 \cdot 10^{-10}$ mm
	Maximum	0.1 mm
Solution technique	Full Newton	

Table 6.8: Computational solver Static, General (Implicit)- settings

6.2. Numerical results and discussion

The primary objective of this research is to establish the behaviour of the demountable floor system to a conventional one. In the demountable model, the failure shall occur either in the concrete or within the connection. To evaluate and compare the performance of the conventional and demountable beam models, the structural behaviour is assessed through the load capacity, maximum deflection and flexural stiffness of the beam models. Furthermore, with respect to the demountable beam model, the discrepancy of using either a precast slab or reused slab is established through the reinforcement configurations that are presented in Section 6.1.1.

6.2.1. Validation and evaluation of global beam behaviour

In order to establish the structural performance of the demountable beam concept to a conventional one, the global beam behaviour is assessed through the load-capacity and load-deflection response at midspan. From the analyses performed, the demountable model distinguishes between the applied reinforcement configuration. The total load capacities of the models are summarised in Table 6.11. The designations 'P' and 'R' in the table relate to the application of either a precast or reused reinforcement configuration simulation, respectively. The beam models developed adhere to the similar geometry and reinforcement detailing as that used in the study performed by Almahmood et al. [78] (see Section 2.5.2). I.e. the reinforcement configuration utilised in the aforementioned study serves as the basis for the design of the conventional and demountable models.

For purposes of comparison, the experimental study also included a conventional reference model that did not employ the use of any demountable connection. In order to evaluate the validity of the FEM the conventional reference model of the experimental study (REF-5m) is compared to the conventional model obtained through the numerical study (C1-5m). It should be noted when comparing the models, the experimental model differed in use of material properties as the concrete and reinforcement were designed using predominantly greater strength properties. Based on the variation in strength properties and slight adjustments of the geometry, the numerical model was expected to have a greater capacity (see Table 6.9 and 6.10).

	Experimental [78]		Numerical	
	f_y (MPa)	f_u (MPa)	f_y (MPa)	f_u (MPa)
Long.	574	784	400	500
Trans.	700	851	400	500

Note: f_y - yielding strength, f_u - ultimate strength

Table 6.9: Comparison reinforcing steel properties

	Experimental [78]		Numerical	
	f_c (MPa)	f_{ts} (MPa)	f_c (MPa)	f_{ts} (MPa)
Beam	37.2	1.96	32.6	3.0

Note: f_c - compressive strength, f_{ts} - tensile strength

Table 6.10: Comparison concrete properties

Furthermore, although the experiment evaluated the structural performance of the reference beam model through a four-point bending test with simply supported boundary beam conditions, the outcomes obtained for the conventional model in the experiment appear to be consistent with the maximum load levels observed in this numerical study. As anticipated, the deflection of the beam in the numerical study is considerably less than that observed in the experimental study, due to a discrepancy in material properties, the positioning of the connection at midspan and the utilisation of simply supported boundary conditions rather than fixed boundary conditions. In light of the validation of the small-scale finite element model (Section 4) in conjunction with the equivalent load levels and corresponding deflections between the numerical study and experiment performed by the authors of [78] it is considered that the FEM show a reasonable agreement for further evaluation.

Study - Exp. / num.	Model		Ultimate load - P_u (kN)
Experimental [78]	REF-5m	Conventional	85.80
Numerical	C1-5m	Conventional	93.72
Numerical	D1-5m-E50-S200-P	Demountable precast	91.27
Numerical	D1-5m-E50-S200-R	Demountable reused	91.17

Table 6.11: Comparison of results from numerical study to experimental study performed by Almahmood et al.[78]

Load-deflection relation

To ascertain the effect of the demountable beam model, the load-deflection relation is taken as the basis for analysis (see Table 6.11). The load-deflection curves are typically divided into three distinct stages. The first stage relates to the elastic range, where the load increases linearly with the deflection. The stage is followed by the elatic-plastic range where non-linearity is observed as a result of steel yielding and concrete damage, whereafter the hardening stage is initiated. Within the hardening stage the slowly increasing load coincide with a strongly increasing deflection as a result of steel hardening.

The load-deflection behaviour of the conventional and demountable precast/reused beams at the mid-span section is presented in Figure 6.7a. The total load capacities of the demountable models appear to be very close to that of the conventional model. It would appear that the application of multiple concrete slab components in combination with the geometrical measurements and material properties used allows for the demountable model to behave as a conventional continuous beam model. The connection provides a sufficient degree of rigidity for the demountable beam to cause failure as a result of an increased bending moment at either midspan or at the edges where the beam is fixated.

As stated, the load-deflection curves initially demonstrates the linear behaviour until the first flexural cracks emerge at midspan in the concrete section of all models and around the bolts in the demountable models. From the load-deflection curves, it can be observed that a slight kink is present when the model transitions from the linear to non-linear stage at a load level of approximately 25 kN for both the conventional and demountable models. Subsequent to the initial cracking, the conventional and demountable models exhibit a reduction in flexural stiffness as the load-deflection curves evolve towards the non-linear hardening behaviour. The curves demonstrate a gradual decline in capacity following the attainment of the ultimate level. It can therefore be concluded that the failure mode is more likely to be ductile than brittle.

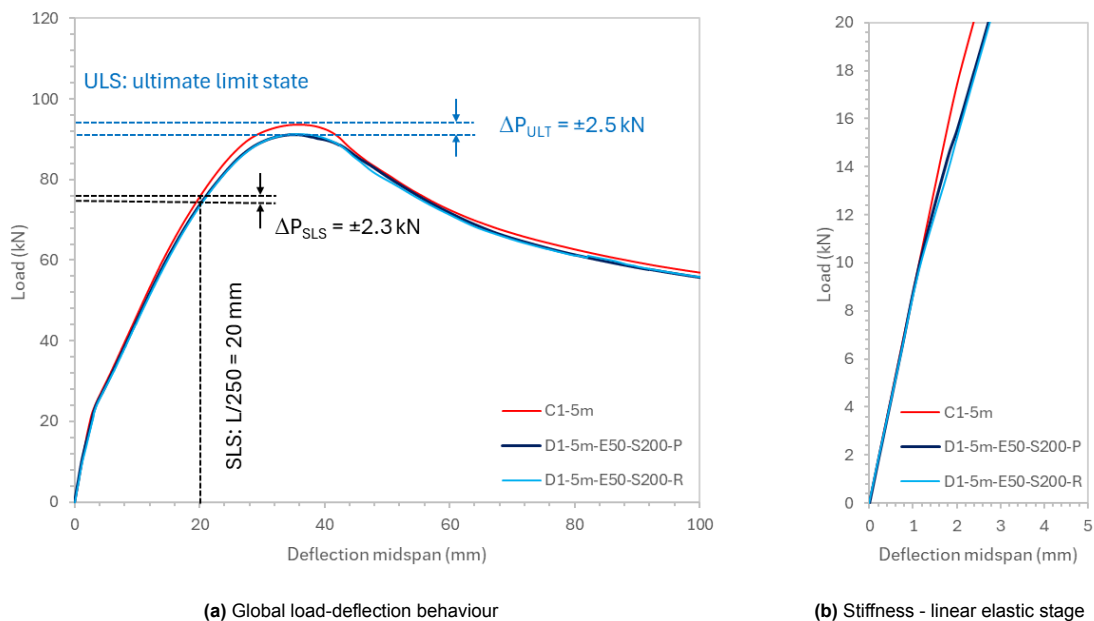


Figure 6.7: Load deflection behaviour at the beam mid-span section - conventional and demountable (precast/reused) model

The results indicate that the load-deflection curve of the conventional and demountable beam models reach closely to one another with an approximate discrepancy in ultimate load capacity of 2.7% (2.5 kN). Zooming in on the initial stiffness behaviour of the conventional and demountable models, the conventional model shows to have a slightly higher initial stiffness. The reduction in stiffness (3.3%) observed in the demountable models in Figure 6.7b, can be attributed to flexural crack development within the connection. The load capacities of all models read close to one another, which is also observed through the deflection measured at the maximum load capacity. The load-deflection response indicates that the effect of variant reinforcement configurations (precast/reused) has a negligible impact on the maximum load capacity and stiffness of the model, as the curves show almost identical behaviour to one another.

In accordance with the principles of structural design as set forth in Eurocode [107] regarding the serviceability limit state (SLS), the maximum permissible deflection is proportional to $L/250$. A span width of 5000 mm indicates that the maximum permissible deflection is 20 mm. Consequently, the maximum load capacity for the demountable beams in both the precast and reused models is approximately 3.0% (2.3 kN) lower than the conventional model, in accordance with the deflection limit of 20 mm for a span width of 5000 mm. Figure 6.8 demonstrates the deflection curve along the beam length (support-to-support), that is measured at a total of 90 kN. The deflection profile of the models indicate that there is no rotation at the edges of the beam as the beam uses fixed boundary conditions, where the demountable models exhibit an 11% (3.4 mm) higher deflection compared to the conventional model. However, although the demountable models show a good continuity, the deflection profile in Figure 6.8 reveals a slight kink at a distance of 1250 mm from the support, which coincides with the location of the connection. The kink in the deflection profile demonstrates a small vertical slipping movement which in turn affects the deflection of the demountable models at midspan.

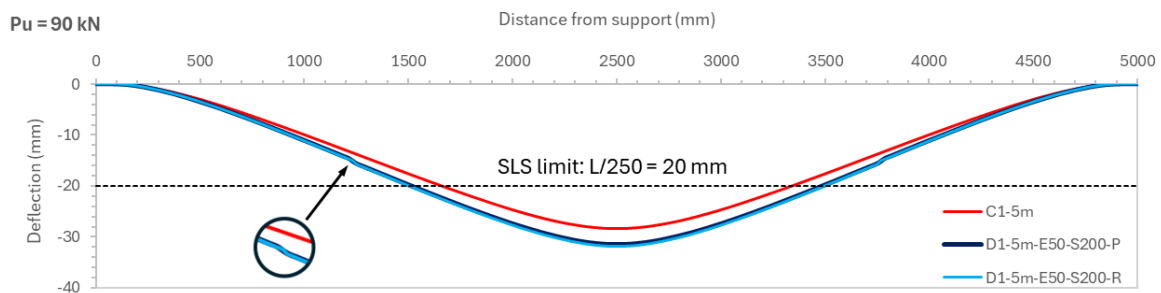


Figure 6.8: Deflection profile of beam models at 90 kN of the total load for 5000 mm model

Strain profile in beam section

The midspan strains at the full height of the beam for the conventional and (precast) demountable beam subjected to different levels of load application are visualised in Figure 6.9, to examine the effect of using external slabs in a floor system. It can be seen from the strain profiles that as the load increases, cracks start at the point of loading and gradually progress from the bottom of the beam towards the top. High tensile strains in reinforced concrete beams indicate that the beam has undergone a greater elongation in the tensile zone before failure or cracking. The neutral axis for both models appears to be at the same section height in the concrete. A load level of 15 kN (below the cracking load) indicates that the beams are not sustaining any tensile or compressive strains. As the load increases from 30 to 75 kN, a gradual increase in tensile strains is observed for both the conventional and demountable beam models. However, when the increasing tensile strain suddenly stops, both the conventional and the demountable model show strain lag. This sudden decrease in tensile strain occurs at concrete section height of 25 mm, which corresponds to the positioning of the longitudinal reinforcing steel. The strain lag initiation is already observable at a load level of 30 kN.

In reinforced concrete, strain lag refers to the strain in the concrete and reinforcing steel that does not develop uniformly despite the steel-concrete interaction and load transfer mechanism. The occurrence of strain lag observed in the reinforced concrete beams results from the combination of reinforcement yielding and concrete cracking. If the reinforcement starts to yield and the surrounding concrete does not take into account the redistribution of stresses, e.g. due to tensile stiffening, strain lag can develop in the concrete section. This redistribution of stress is influenced by cracking in the concrete section.

Under tensile stress, the concrete cracks and the strain in the steel reinforcement increases locally in the vicinity of the crack. As a result, strain variations occur along the length of the rebar between cracked and uncracked regions within the concrete.

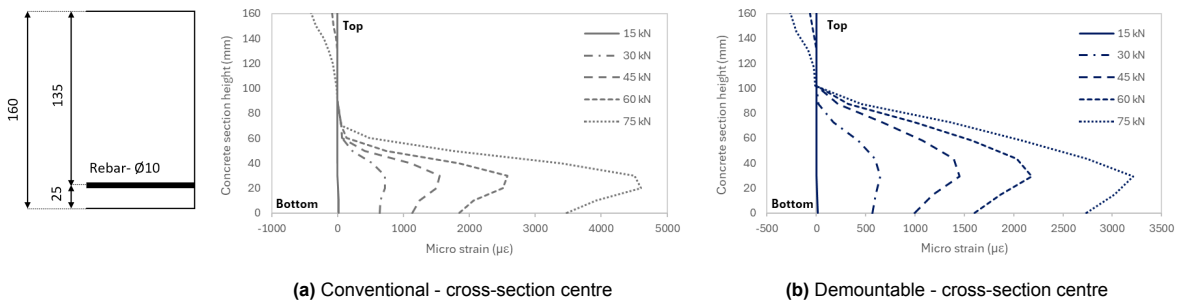


Figure 6.9: Average strain profile at midspan cross-section centre

Reinforced concrete structures can cause non-uniform stress distribution across the cross-section, resulting in strain variations [108]. Therefore, for the beam models, the mid-span strains are also measured at the edge of the cross-section, as the strain can vary for 'wide' concrete beams due to stress gradients (Figure 6.10). For both the conventional and demountable beam model, the strain measured at the centre is a fraction higher than the strain measured at the edge of the concrete. The strain profile, as measured at the edge of the concrete's midspan cross-section, indicates that the demountable model displays a reduced susceptibility to the yielding of the reinforcement, in accordance with the anticipated outcomes. However, where the demountable model demonstrates to be less affected by the occurrence of strain lag at the edge of the concrete, the conventional model exhibits a more pronounced strain lag across the entire cross-section surface at midspan. I.e. the conventional beam model demonstrates a more uniform stress distribution across the cross-section at midspan. The uneven strain distribution in the demountable model is an indicator for either a more poor ductility or overall reduction of the strength capacity due to premature reinforcement yielding and concrete crushing.

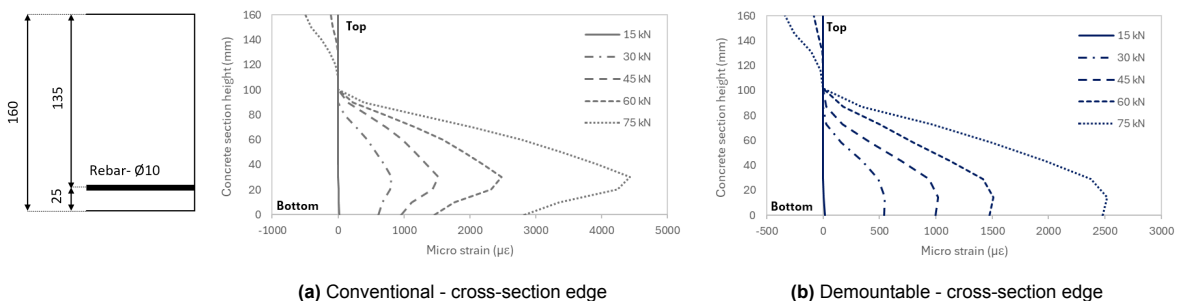


Figure 6.10: Average strain profile at midspan cross-section edge

Failure mode evaluation

The displacement-controlled loading boundary condition at the midspan, which is initiated in the loading phase following the preloading of the bolts, induces deformation in the beam at the point of testing its bending capacity. By positioning the connection at the zero bending moment locations in a strategic manner, the connection is subjected to shear forces to a significant extent. In contrast to the results observed in the block model, the beam analysis indicates that at the point at which the beam model reaches its ultimate strength capacity, the bolts within the connection have undergone no plastic deformation. The plates at the top and bottom of the beam deform only slightly at the peak load. The bolts and plate have undergone only elastic deformation as the components do not reach their plastic yield limit in accordance with the Von Mises stress distribution observed in the model. As per expectations, the highest Von Mises stresses in the reinforcing steel are observed within the bottom reinforcing steel at midspan and top reinforcement at the support section.

The failure process for the demountable model developed can be divided into three steps, which include pre-cracking of the concrete, cracking of the concrete and lastly steel yielding and failure. As the load is increased, minor cracks begin to emerge around the bolts in the concrete section. The reduction of net cross-section at the location of the bolts has been shown to cause a redistribution of stresses around the bolt holes. This, in turn, compromises the strength in this area. As a result of the bolt pretensioning, the friction generated between the components is not overcome when the load-displacement curve for the demountable model reaches its peak capacity. Damage on the concrete is primarily characterised by the cracks in bending-shear zones at the beam midspan and edge, such as depicted in Figure 6.11a.

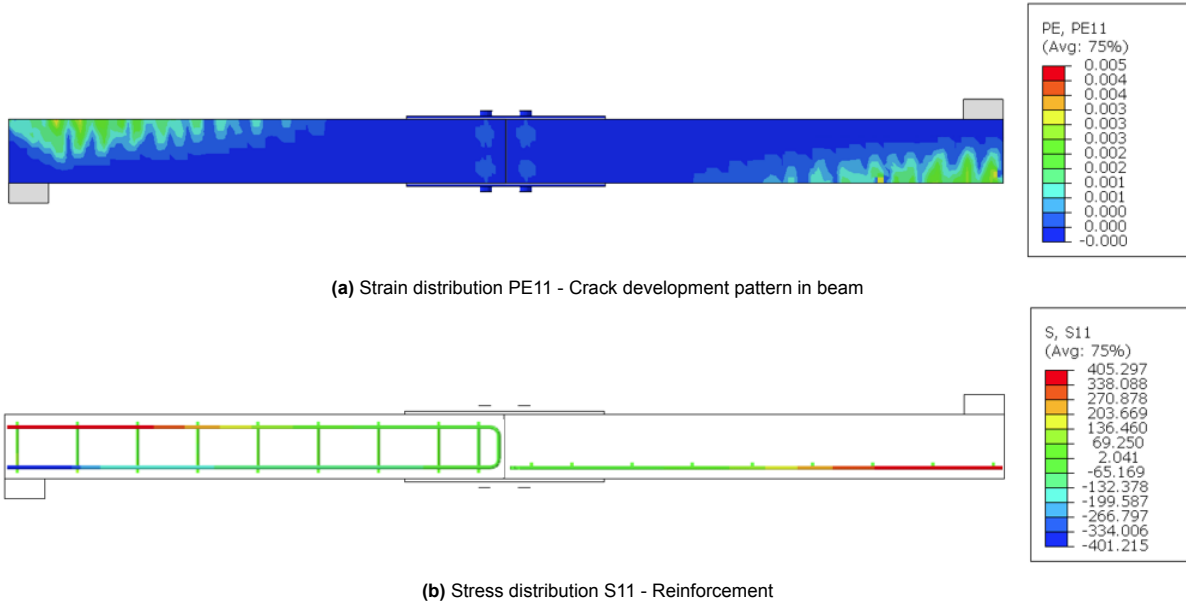


Figure 6.11: Failure mode evaluation

The distribution of stresses in the steel components within the connection, coupled with the development of cracks in the concrete, indicates that the peak capacity is a result of the increased damage at the edge of the beam, at midspan, and within the concrete surrounding the bolts which eventually induces failure of the beam model. Moreover, since the ultimate load capacities of the demountable beam models yield close results to that observed in the conventional model, failure of the models is not the result of premature failure within the connection. In addition, the maximum stress distribution in the steel reinforcement reveals that ultimate stress capacity has not been reached (see Figure 6.11b). Therefore, it is established that the overall failure of the model is attributed to concrete tensile splitting and compressive crushing, given the distribution of stress in the bolts and plates and the subsequent damage to the concrete at midspan and the edges of the beam. Based on the approximate reaction force of $P_u = 91$ kN obtained through the numerical model and equilibrium of forces the shear force capacity and bending moment capacity of the model are determined accordingly in Table 6.12.

	Midspan (1/2L)		Connection (1/4L)	
Shear force	P	$= 91.27$ kN	$\frac{1}{2}P$	$= 45.64$ kN
Bending moment	$\frac{1}{8}PL$	$= 57.04$ kNm	-	$= 0$ kNm

Table 6.12: Ultimate Shear force capacity and bending moment capacity of demountable beam model

6.2.2. Precast vs. reused slabs

The deflection profiles and load-deflection behaviour in respectively Figures 6.8 and 6.7 indicate that the simulation of a precast slab and a reused slab yield close results. Given the strategic positioning of the connection at zero bending moment locations, this appears to be a notable result. The purpose of the bottom reinforcing steel is to capture the bending moment at the bottom of the beam, where the anchoring of the reinforcement is typically required to transfer the force in the reinforcing steel to the surrounding concrete. However, as only a relatively small proportion of the bending moment is to be captured at the point of the connection, the reinforcing steel at the edges (near the connection) of the reused and precast concrete beam is not significantly affected by the load application at the midspan support. Consequently, the force in the reinforcing steel that is to be transferred to the surrounding concrete is deemed to be insignificant. Therefore, the impact of (not) anchoring the reinforcing steel results in minimalistic variations in the maximum capacity, deflection and stress distribution in the reinforcement of the precast and reused demountable beam model (see Figure 6.12).

Furthermore, the near-identical outcomes are also likely attributable to the modelling strategy employed, which pertains to the material properties of the 'reused slab' component. In this numerical model, the demountable beam incorporates identical material properties for the concrete and embedded reinforcement steel as those utilised in the model that considers a 'precast beam' component. The results obtained only differ through the reinforcement configuration such as depicted in Figure 6.3. In order to simulate the effect of a reused slab that shows a more distinct result between the precast and reused slab application, the material properties of the reused slab part should include weakening of the concrete and steel materials. Although weakening of the material properties is considered an important modelling setting in case of reusing concrete slabs, Küpfer et al. [109] demonstrated that the reuse of cut concrete slabs is a feasible solution by incorporating strength reduction through maximal span widths. The maximum allowable span for cut reinforced concrete pieces is determined through the following conditions:

- Total load level in receiver building (live loads and self-weight)
- Static system of the new structure
- Bending resistance of the cut reinforced concrete piece

In case a cut reinforced concrete slab meets the stipulated criteria and possesses the requisite capacity, the reused slab should be treated (in the case of modelling the material properties) in a manner that is consistent with that of a conventional slab in terms of its strength performance. It can therefore be assumed that the material properties of a precast and reused slab are treated equally, on the basis that the aforementioned prerequisites for the reuse of concrete slabs are complied with. This assumption indicates that the deflection profile for a demountable beam model using either precast or reused slabs, with geometrical settings comprising a span of 5000 mm, an edge distance of 50 mm and a spacing of 200 mm, closely approximates that of the conventional system.

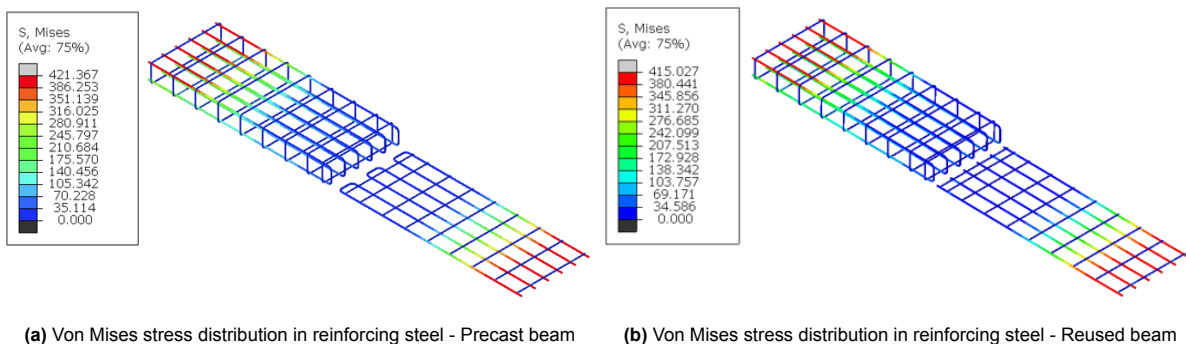


Figure 6.12: Effect of using various reinforcement configurations (half of the beam) - Maximum load capacity

6.2.3. Local connection behaviour

Upon closer examination of the concrete crack formation within the connection, it becomes clear that in accordance with the DAMAGET and DAMAGEC model for concrete, cracks (tensile damage) emerge gradually during the loading phase of the model. In contrast to the concrete tensile damage, the degree of compression damage sustained by the concrete slab is minimal. From Figure 6.13 it is evident that the compression damage model produces a significantly lesser outcome on the concrete slab in contrast to the tensile damage model. Although, the beam models are not purely tested on their tensile behaviour, the initiation and development of tensile and compressive damage within the connection follows similar patterns as to that observed in the damage models of the block model. The results demonstrate that the concrete is again significantly compromised at the edges of the concrete, in the region around the bolts. In particular, the areas in proximity to the bolt holes demonstrate a clear development of tensile damage (Figure 6.13a).

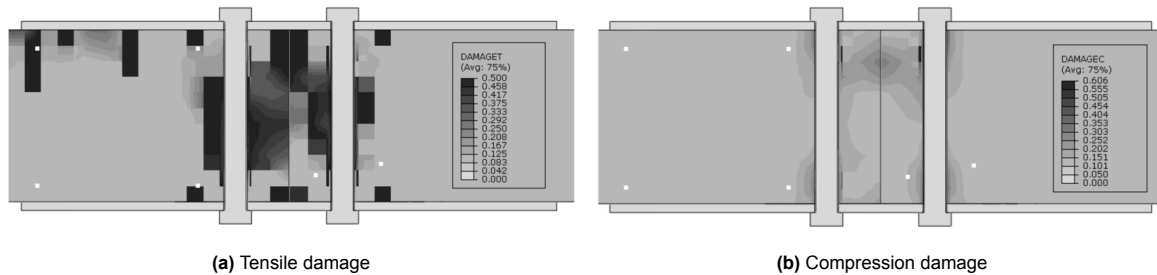
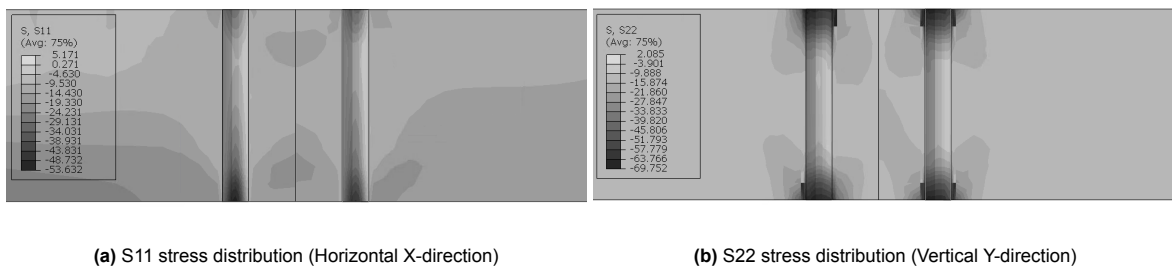


Figure 6.13: Local connection behaviour beam model - concrete damage models

Increased damage around the bolt holes is most commonly attributed to the reduction in net area at the bolt holes. The bolt holes cause a redistribution of stresses within this section, which subsequently can lead to a reduction in strength capacity. Furthermore, the stresses that originate at the upper part of the concrete beam, there where it is fixed on its edges, gradually redistribute towards the connection, affecting the distribution of stresses within the connection as well. Figure 6.14a demonstrates the increase in tensile stress at the top and compressive stress at the bottom of the concrete beam in S11 (horizontal) direction. The increased stresses in S22 (vertical) direction around the boltholes at the top and bottom part of the concrete beams result from bolt preloading (Figure 6.14b).



(a) S11 stress distribution (Horizontal X-direction)

(b) S22 stress distribution (Vertical Y-direction)

Figure 6.14: Stress distribution around the boltholes

6.3. Parametric study

6.3.1. Design variations, material models

In order to ascertain the impact of disparate geometrical configurations, a parametric study is conducted. The sensitivity of the beam models is evaluated in response to alterations in the geometry of the components. The variations include alterations to the span width of the beam, which are made in steps of 1000 mm, from 5000 to 8000 mm. Furthermore, the impact of the edge distance of the bolts in the concrete section is quantified through a stepwise increase in variation (50, 60, 80 and 100 mm). Additionally, the influence of the centre-to-centre distance on the structural behaviour is established through an investigation of the effect of the shear connector spacing (see Figure 6.15). Three connector spacings are considered: 100 mm (5d), 200 mm (10d) and 300 mm (15d).

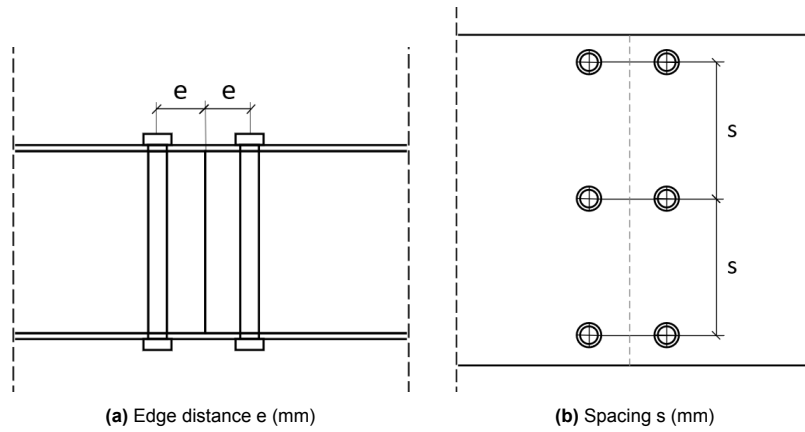


Figure 6.15: Parametric variation definition for edge distance and spacing application

It should be noted that the numerical models that have been developed and analysed in previous sections are considered a reference model. This involves a reference edge distance of 50 mm, span width of 5000 mm and bolt spacing of 200 mm. In case of the analyses that look into the influence of altering the spacing between the bolts, the width of the beam is kept constant. Therefore, the number of bolts incorporated in the model increases when the spacing is reduced, where the number of bolts decreases with an increased spacing. Since, the influence of using either precast slab - or reused slab components does not yield any significant differences, the parametric study is performed following the demountable model that pertains to the precast slab elements, where there is a reinforcement configuration that includes anchoring.

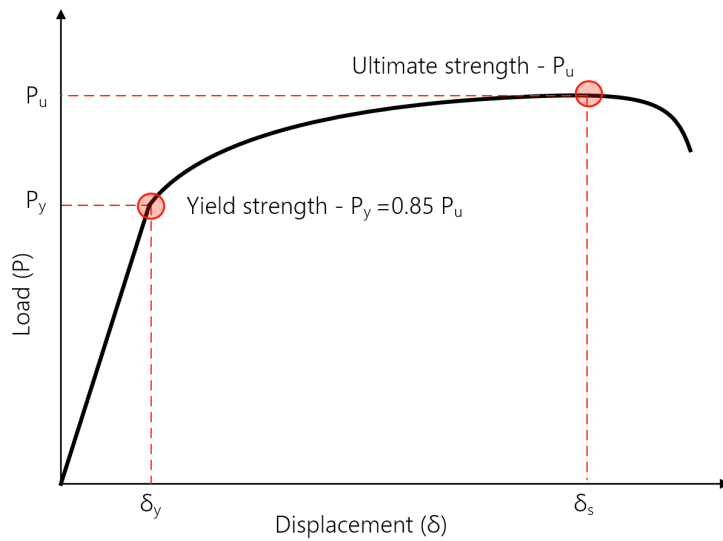
The material models for the concrete and steel components are based on the nominal stress-strain curves that were employed in the simplistic block model. The steel components are modelled without any damage initiation for reusability purposes, whereas the concrete is modelled using the concrete damage plasticity model. The material properties used throughout the parametric study within the damage model for concrete remain identical to those used for previous models (see Section 4.2).

6.3.2. Evaluation

In order to evaluate the numerical results obtained through geometrical variation, the models are compared based on the ultimate resistance P_u and the deflection in z-direction δ_z through the load-deflection curves. Furthermore, based on the load-deflection curves the behaviour of the geometrically varying beam models are evaluated through their flexural stiffness k_f and the displacement ductility D_δ . The (initial) flexural stiffness is determined before cracking of the concrete following Equation 6.1 [6], where ΔP is considered the force increment and $\Delta w_{L/2}$ the deflection increment at midspan of the beam. The parameters are evaluated at the linear-elastic stage which are based on the load-deflection diagrams. The linear elastic stage varies for all models as a result of geometric changes that affect the stiffness capacity of the models. The deflection used ranges between 0-5 mm.

$$k_f = \frac{\Delta P}{\Delta \delta_{L/2}} \quad (6.1)$$

The ductility of the beam models are predominantly determined through the (longitudinal) reinforcement configuration and the extent to which the reinforcement is burdened by the load application. The ductility factors of the beams are based on the load-deflection curves that were obtained through the FEM. The ductility of a beam is expressed based on the beam deflection by the displacement ductility D_δ . In general, high displacement ductility allows for the observation of visible warnings (large deformations) before failure occurs. Conversely, low displacement ductility presents the possibility of abrupt failure (brittle), which is why high displacement ductility is favourable. The ductility is determined through Equation 6.2, where δ_y and δ_u relate to the yielding deflection and ultimate deflection, respectively. The ultimate deflection δ_u is the deflection measured at the ultimate strength, where the yielding deflection is obtained at the yield strength ($P_y = 0.85P_u$) [110].



$$D_{\delta} = \frac{\delta_u}{\delta_y} \quad (6.2)$$

Figure 6.16: Displacement ductility

6.3.3. Results and discussion

The results of the parameter study in terms of the load-deflection behaviour, ductility and flexural stiffness is described in Figures 6.17 - 6.22. The results appear to provide insight into the effect of altering the geometry on the resistance of the reference model (D1-5m-E50-S200) to a conventional beam model (C1-5m). The findings observed in the models per geometrical variation are discussed in the following subsections. The load deflection curves and initial flexural stiffness in the linear-elastic phase for the variant beam models are visualised in appendix C. Table 6.13 reports the various models including geometrical settings. The reference models regarding the conventional-, precast- and reused beam model are assigned to the group R in the table.

Group	Analysis	Geometrical settings			Outcome			
		Span width L (m)	Edge distance e (mm)	Bolt spacing s (mm)	Load capacity P_u (kN)	Deflection (at P_u) δ_u (mm)	Flexural stiffness k_f (kN/mm)	Ductility D_{δ} (-)
R	C1-5m	5	-	-	93.72	35.46	7.17	1.63
	D1-5m-E50-S200-P	5	50	200	91.27	35.10	6.93	1.61
	D1-5m-E50-S200-R	5	50	200	91.17	35.40	6.83	1.61
M1	M1-5m-E60-S200	5	60	200	90.81	36.39	6.61	1.64
	M1-5m-E80-S200	5	80	200	90.29	36.90	6.13	1.63
	M1-5m-E100-S200	5	100	200	89.81	36.67	5.64	1.58
M2	M2-6m-E50-S200	6	50	200	67.20	28.70	4.51	1.16
	M2-7m-E50-S200	7	50	200	50.78	35.95	2.27	1.62
	M2-8m-E50-S200	8	50	200	40.11	43.86	2.08	1.57
M3	M3-5m-E50-S100	5	50	100	91.37	21.52	7.32	1.61
	M3-5m-E50-S300	5	50	300	90.95	22.26	6.49	1.61

Group R refers to reference models (conventional and demountable) from which the performance and numerical results are established in Section 6.2

Group M1, M2 and M3 refer to modifications in edge distance, span width and spacing, respectively

Table 6.13: Parametric models and geometrical settings

Effect of edge distance

The edge distance is considered an important geometrical aspect, with respect to concrete breakout failure. The edge distance should be such that the edge of the concrete does not influence the resistance of the bolts within the connection. Increasing the edge distance generally improves the load-carrying capacity, as the occurrence of concrete edge breakout or splitting failure is reduced. Furthermore, an increased edge distance allows for a greater area through which the stresses surrounding the bolts are distributed, which leads to a more ductile failure mode. This consequently may enhance the stiffness of the connection. Decreasing the edge distance increases the possibility for brittle type of failure modes, such as edge spalling or splitting of the concrete. This involves a more abrupt failure and which not only leads to a decreased load capacity, but lower ductility as well. However, it is important to note that the edge distance of bolts in a concrete section can also be considered to be too large. In such cases, the bolt is unable to effectively clamp the connecting components. This has the potential to compromise the rigidity of the connection under the prevailing loads. Furthermore, this may result in an uneven stress distribution, which can lead to a reduction in the overall strength of the model.

From Figure 6.17a it is observed that the effect of increasing the edge distance with the current employed geometry and material properties does not have any to no significant impact on the the ultimate load carrying capacity. The demountable models with an increasing edge distance demonstrate a behaviour that is similar to that of the conventional beam model, with only a little reduction in the ultimate load carrying capacity. This indicates that the connection is able to provide continuity in the concrete. Despite the stresses within the connection being redistributed as a result of the hole clearances, failure is observed not to occur within the connection. Therefore, based on the deformation that develops with increasing load, this is not considered to be a contradictory behaviour.

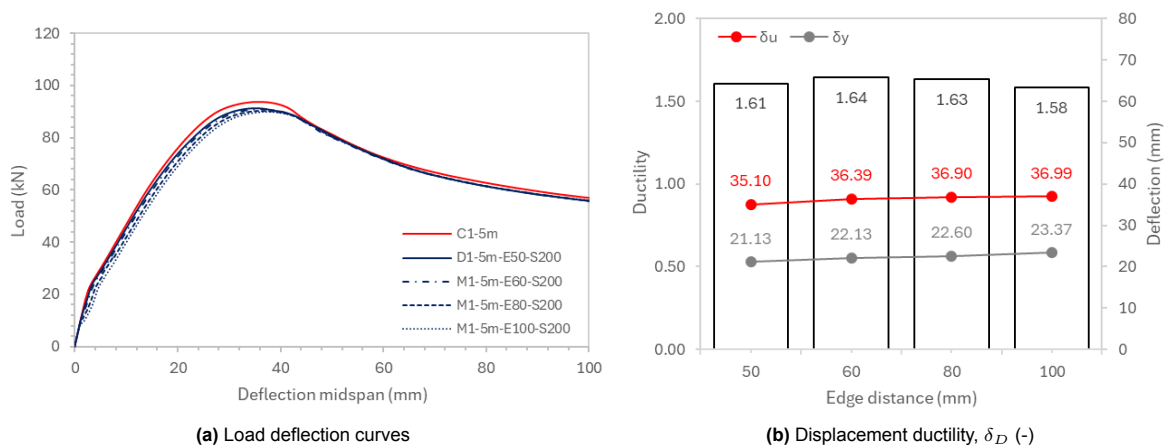


Figure 6.17: Effect of the change in edge distance

Furthermore, the displacement ductility is visualised in Figure 6.17b. The yield displacement δ_y and ultimate displacement δ_u of the models show a little increase in ultimate deflection with increasing edge distance. This in turn affects the displacement ductility. However the changes in the yield and ultimate displacement are so insignificant that the ductility is barely affected by an increasing edge distance. The figure demonstrates that the displacement ductility starts to increase with an increased edge distance from 50 mm to 80 mm. Nevertheless, the model that presents an edge distance of 100 mm exhibits a contradictory behaviour, as it was anticipated that an increased edge distance would enhance the ductility. Therefore, the edge distance of 100 mm may be considered too extensive for an optimal performance of the demountable model.

The resistance in terms of ultimate load capacity and initial flexural stiffness with variation in edge distance is visualised in Figure 6.18. A small increase in edge distance demonstrates to have a negligible effect on the ultimate load capacity, since an increasing of the edge distance by 20 mm decreases the load-carrying capacity of the connections only by 0.5%. Figure 6.18a reveals that the models reach close to the load carrying capacity of the conventional model. As illustrated in Figure 6.18b, the initial flexural stiffness exhibits a contrasting trend to that observed in the ultimate load capacity. An increase of 20 mm in edge distance results in a reduction of 6% in initial stiffness. This behaviour is visualised

in the linear elastic stage of the load deflection curve in Figure C.1b. The curve reveals a decrease in initial stiffness that is characterised by a kink. The kink in the load-deflection curve marks the end of this linear phase, which becomes more pronounced with an increased edge distance.

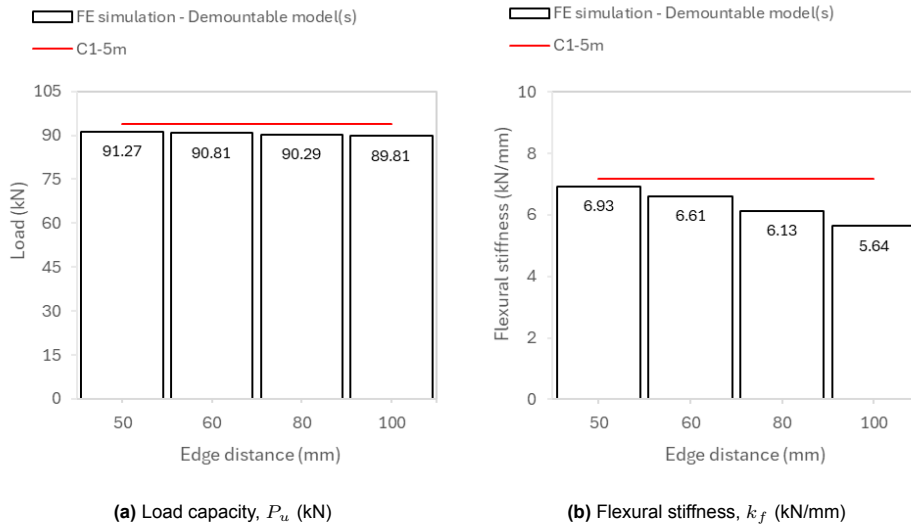


Figure 6.18: Resistance - Variation in edge distance

Effect of span width

The span width of the beam models was increased from 5000 mm (for the conventional and reference models) up to 6000, 7000 and 8000 mm spans. This increase in span provides insight into the maximum load capacity that the model, with its current settings, is able to withstand. The increase in span widths leads to a renewed bending moment distribution over the beam length. Consequently, the point of zero bending moment shifts along the length of the beam, situated at a distance $L/4$ from the supports under the prevailing boundary and loading conditions. The results indicate that increasing the span width by 1000 mm decreases the load capacity by 24% (see Figure 6.19a).

As illustrated in the load-deflection curves, an increase in span width results in a reduction in maximum load capacity at midspan. The graphs demonstrate that the maximum load capacity at midspan is significantly higher for beam models with a span width of 5000 mm and 6000 mm, with a distinct peak observed. In contrast, models with a span width of 7000 mm and 8000 mm exhibit a gradual increase in load capacity, with the peak becoming more distributed as the deflection at midspan increases. The ductility displacement in Figure 6.19b demonstrates that the ductility is not affected by the increasing span width. The yielding displacement δ_y and ultimate displacement δ_u show a linear response to an increased span width. The 1000 mm increase in span leads to an increased yielding an ultimate displacement of 20.7% and 20.1%, respectively.

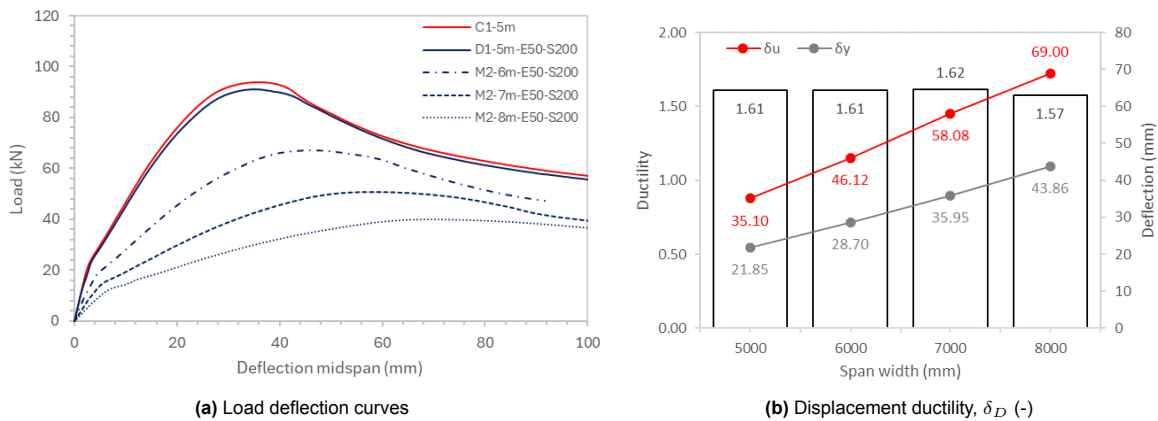


Figure 6.19: Effect of the change in span width

Furthermore, as per expectations, the effective bending stiffness of the beam model decreases with an increase in span width. As depicted in Figure 6.20, the diagram of the parametric study on span width, the stiffness exhibits a notable decline with an increase of 1000 mm in span width. However, beyond this point, the drop in stiffness becomes less pronounced with further increases in span width. An increasing of 1000 mm in the span width of the model indicated a reduction of 31% on average in initial flexural stiffness, without (significantly) compromising the ductility. The decrease in stiffness is also observed from the load-deflection curves in appendix C. From the perspective of validity, it is notable that the numerical results tend to demonstrate a higher stiffness than that observed in beams subjected to experimental testing. This is can be attributed to the bond between the concrete and the steel reinforcement. The numerical model assumes a bond that is considered perfect, which may influence the stiffness capacity in the non-linear behaviour of the beam model. It is therefore important to consider the possibility that the stiffness capacity may be slightly overestimated.

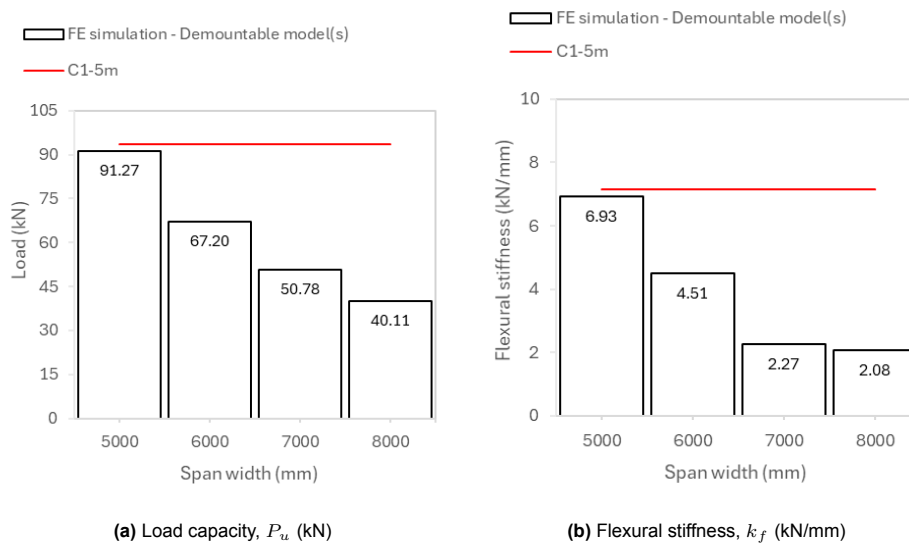


Figure 6.20: Resistance - Variation in span width

Effect of bolt spacing

The connector spacing reduced from 300 mm (15d) to 200 mm (10d) and 100 mm (5d), where the 200 mm model pertains to the reference design, which is elaborated on in previous Section 6.2. The reduction in spacing allows for an increase in the concentration of connectors within the beam section. In theory, an increased bolt spacing reduces the stress concentration around the bolts, which leads to a more uniform load transfer. Furthermore, greater spacing allow for the bolts to fail progressively following a more ductile behaviour. Decreasing the bolt spacing increases the overlapping area of stress concentrations around the bolts, which disturbs the stress distribution in the cross-section. Moreover, an increase in the number of connectors results in a reduction of the net cross-section, which in turn can compromise the concrete tensile strength in that specific area. A tight bolt spacing initiates crack formation within the concrete, which in turn may lead to premature failure and possible brittle failure.

Figure 6.21a compared the load-deflection curves under the influence of varying the bolt spacing. The curves follow the similar profile to that of the conventional (C1-5m) and reference demountable model (D1-5m-E50-S200). In particular, the linear and non-linear phase for each model is almost identical, indicating that the effect of bolt spacing has with current geometrical design settings no influence on the ultimate load carrying capacity. After reaching the ultimate capacity, all models gradually reduce in load capacity. Overall, either increasing or decreasing the bolt spacing did not show to have an influence on the loading capacities and initial stiffness on the models. The yielding and ultimate displacements δ_y and δ_u , regarding the ductility displacement are presented in Figure 6.21b. Overall, the similar behaviour as was established through the load-deflection curves is also found in the ductility of the beam behaviour. The ultimate and yielding displacement of the variant model do not show any contradicting behaviour. As a result the ductility factors of the beams are identical.

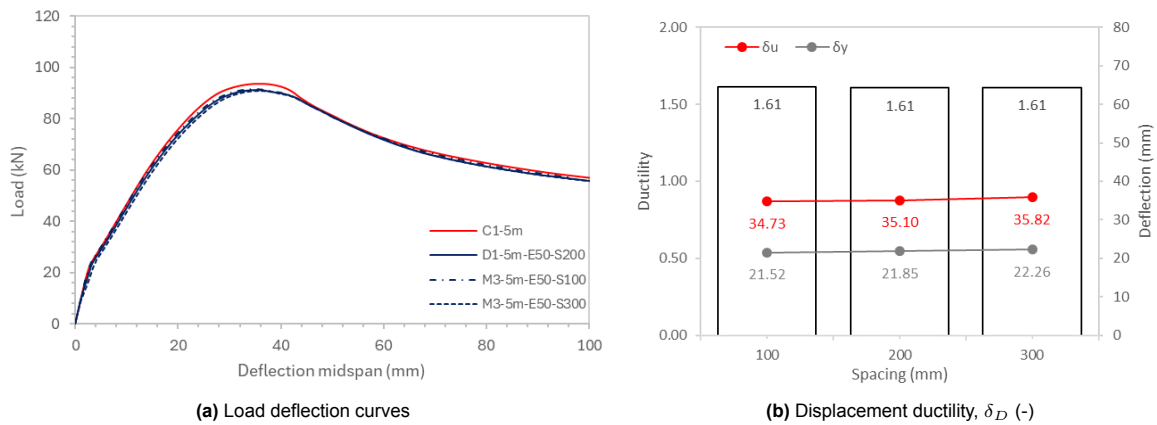


Figure 6.21: Effect of the change in spacing

The ultimate resistance of the variant models are presented in Figure 6.22, showing similar behaviour for all models. A slight gradual decrease of 6% in the initial flexural stiffness is observed with increasing bolt spacing. The discrepancies are very small that it has been established that, given the existing configuration and material characteristics, bolt spacing has little effect on both the ultimate load capacity and the initial stiffness. The analysis of the development of stresses in the bolts and plates indicates that all models (group M3) fail through concrete failure for the same reason as that certified in Section 6.2.1. The utilisation of a concrete grade that is of a higher quality than that currently employed in the models (C20/25) has the potential to delay the onset of the effects associated with a reduction in resistance.

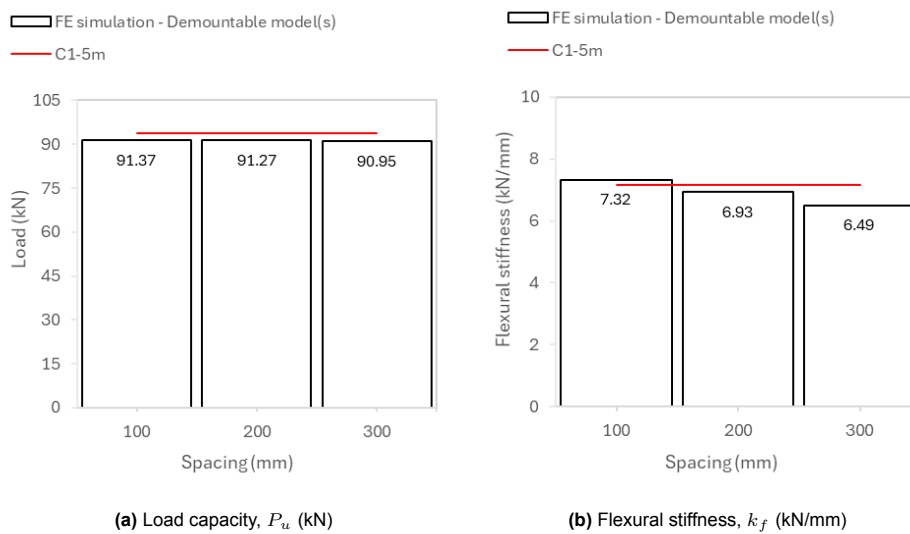


Figure 6.22: Resistance - Variation in spacing

7

Discussion

This section provides a review on the simplifications of the numerical results that are obtained through the analyses of the demountable reinforced concrete beam models and the limitations of the research. The results obtained through the finite element analysis in previous sections indicated that the ultimate load capacity of the demountable beam model shows a good agreement with the conventional model. Although the numerical results obtained provide a valuable insight and efficiency, their accuracy is influenced by assumptions, constraints and specific modelling choices. Identifying these simplifications and limitations is crucial in improving the reliability for future analyses.

7.1. Simplifications in numerical model

Although numerical results are a powerful tool for simulation and prediction, they often lack the validity and reliability of experimental results. This is due to the fact that the numerical models are based on a number of assumptions, idealisations, and simplifications that may not fully capture the true complexities of practical situations. The approximation of factors such as material behaviours, boundary conditions and interactions may result in discrepancies. Consequently, experiments serve as a more robust and reliable basis for validating theoretical models and designs.

In response to the uncertain validity when performing numerical analyses only, the material models that regard to the steel properties used throughout the numerical analyses rely on the assumption of an idealised trilinear or bilinear stress-strain behaviour. One of the risks on the reliability of the results is related to over-simplification of the material response. The complex plastic behaviour that is described through strain hardening, softening and non-linearities are not captured by the models. This may present the inaccurate predictions in especially near-yield or post-yield regions.

The numerical models were developed using idealised boundary conditions that represented a continuous simply supported floor system. Consequently, the boundary conditions at the edge of the model adhere to fixed conditions, thus allowing for the incorporation of a hogging bending moment at the supports. This approach permitted the investigation of the effect of zero bending moment location in the bending moment distribution, thereby allowing a connection at that position subjected to shear only. However, this simplification limits the effect of using a composite beam that comprises welded shear studs such as described in Section 2.8.

The connection was simplified through the utilisation of bolts that directly incorporate the nut, where washers were omitted. The bolt shank was modelled using circular head and a uniform diameter without a thread through which the circular nut is connected. This simplification avoided a complex mesh configuration and permitted the neglect of the interaction between the bolt and washer, as well as the bolt and nut. As a result the necessity for additional interactions and tie constraint are avoided which was beneficial in terms of computational efficiency. The simplification limits the effect of bolt tightening, which in turn may lead to a higher capacity of the bolts, leading to over-predictions of the actual results [111]. Nevertheless, the findings from the beam models demonstrated that there was no evidence of plastic deformation in the connecting elements. Therefore, although the bolt design is regarded as a potential limitation, the results appear to be unaffected by this simplification.

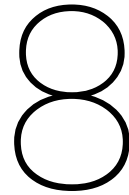
The implementation of the connection in a global system resulted in optimisation through the positioning of the deck-to-deck connector at the point of zero bending moment ($1/4L$), in accordance with the theoretical distribution of bending moments following a beam that is fixed on its edges. For the sake of simplicity, it was assumed that positioning the connector at this point would result in it being subjected to true shear forces. In practice, however, the connector is subjected to a combination of both shear and bending moment, as the distribution is dependent upon the reinforcement configuration and the extent to which the reinforced concrete is fixated on its edges.

The process of reusing concrete slabs has been simplified to a certain extent. In the research it is assumed that the reused slab uses identical strength properties regarding the concrete and steel reinforcement, where the effect of cutting a slab for reuse purposes is primarily simulated through the reinforcement configuration in the slab. The potential for strength reduction in the slab has not been accounted for, which may result in the numerical model overestimating the actual behaviour. Furthermore, The interaction between the surface of the reused slab, which has been cut from an existing structure, and the non-cut slab is of primary importance. This interaction prevails under the assumption that there is a perfect cut where the surface is not compromised by an uneven brittle surface. Consequently, a higher friction between the concrete slab surfaces is assumed than is actually the case. Moreover, the material properties that are used to describe the behaviour of the concrete slab use similar properties to those used in the connecting (non-reused) slabs. With respect to long-term behaviour of the concrete slab, the effect strength reduction due to creep, relaxation and shrinkage have not been accounted for in this analysis.

7.2. Limitations

While this study provides valuable insights into the behaviour of demountable floor systems, certain limitations should be acknowledged to contextualize the findings and guide future research efforts. The most significant limitation of the research is the absence of an experimental review. The lack of an experimental review precludes verification of the numerical models, thereby introducing uncertainty regarding the results obtained. Given the complexity of the finite element model, some constraints were considered necessary during the course of this study to improve computational efficiency. The accuracy that is described through the element order and mesh size employed in the model, presented limitations with respect to the computational time that was required to complete a model.

With respect to the parametric study conducted, the sole variable under consideration in this study relate to the edge distance and bolt spacing, which were varied in accordance with the research objectives. The influence of the parameters that relate to the geometrical aspects of the connection such as the bolt size, bolt hole diameter and plate thickness have not been examined in the present study. Moreover, the impact of a variation in material properties of the connecting elements and concrete has not been explored. Furthermore, the analyses were limited to the utilisation of preloaded bolts, with an identical level of preload employed throughout. In particular, the decision was taken to utilise preloaded bolts throughout the course of the study as a consequence of encountering convergence errors. The impact of utilising disparate load levels in preloaded bolts, as well as the deployment of non-preloaded bolts in demountable models, has not been subjected to evaluation within this research.



Conclusions and perspectives for future work

8.1. Conclusions

The research conducted contributes to the advancement of an innovative design strategy for steel-concrete composite floor systems, supporting the transition toward a more sustainable construction industry. The study numerically investigated the behaviour of a demountable concrete deck-to-deck connector utilising reused concrete slabs extracted from existing structures. The main goal of this research was to establish the performance of a system that incorporates such connection and how that performance compares to that of a conventional system. A preliminary three-dimensional finite element of the connection on a small scale was developed first and tested through a tensile test setup. The results of the model were evaluated and validated through an in depth result analysis and subsequent convergence study. Afterwards, the developed FE model was implemented in a beam model, to evaluate its performance on a global scale. The FEM was used to establish the behaviour of the connection in global beam system and compared to a conventional system. Lastly, the FEM was used to investigate the influence of geometrical alternations through a parametric study. The geometrical study included variation in the edge distance, span width and bolt spacing. Based on the results obtained through the numerical analyses the following conclusions can be drawn:

- The adoption of a bolted connection into a demountable beam system has demonstrated the capacity to withstand loads that are close to that of a conventional beam system. The ultimate load capacity and initial flexural stiffness of the demountable model exhibited a reduction of only 2.7% and 3.3% respectively compared to that of a conventional model. Consequently, the incorporation of a connection within the concrete section was found to provide an adequate level of continuity.
- The load-deflection curves indicated a ductile mode of failure in both the conventional and demountable beam model, where failure occurred in the concrete section as a result of tensile splitting and compressive crushing in the bending-shear zones. The serviceability load capacity of the demountable model is only 3% lower when compared to a conventional system.
- The non-uniform strain distribution across the cross-section of the demountable beam models has the potential to compromise the ductile behaviour, leading to an overall reduction in strength due to reinforcement yielding and concrete cracking. Although the demountable beam models were able to replicate the behaviour of the conventional model, the uneven strain distribution demonstrates the impact of an inadequate reinforcement configuration in beams and floors with a considerable width.
- The connecting elements (bolts and plates) within the demountable beam model demonstrated that upon reaching the ultimate load-carrying capacity no bolt slipping was observed. As a result, the bolts and plates were not subjected to plastic deformation, thus offering the possibility of reuse. The positioning of the connection at the zero bending moment locations represents a significant strategy for the avoidance of plastic deformation.

- An increased concrete height increases the load-carrying capacity of the deck-to-deck connection with an averaged of 22%, as a result of a more uniformly distribution and none overlapping distinct stress regions. A higher concrete slab height (increase of 40 mm) leads to an increase in the initial stiffness with an average of 12.5%. The slip capacity of the bolts appeared to be unaffected by modifications to the concrete height.
- Bolt pretensioning has shown an averaged increase of 40% in the initial stiffness of the connection while being subjected to tensile loading conditions. The level of preload does not appear to exert an influence on either the ultimate load-bearing capacity or the relative slip capacity.
- The application of a greater edge distance in the concrete section indicated to have a negligible impact on the ultimate load capacity and the ultimate deflection, with a more pronounced effect observed on the initial stiffness of the demountable models. An increase of 20 mm in edge distance reduces the initial stiffness by 6%.
- An increase of 1000 mm in span width has been observed to result in an approximate gradual reduction of 24% in ultimate load-carrying capacity. The yielding deflection and ultimate deflection increased by 20.7% and 20.1% respectively with an increase in span width. As a result, the ductility of the beam models did not appear to be affected by an increased span width.
- It was demonstrated that alterations to the bolt spacing in the connection had no impact on the ultimate load capacity of the demountable beam. Thus, alterations to the spacing had no impact on the ductility of the demountable beam. However, the development of tensile and compressive damage around the boltholes within the concrete section in the FEM (block- and beam-model), demonstrated a significant strength reduction in the concrete section due to a smaller net cross-section. The initial stiffness decreased by 6% with an increase of 100 mm in bolt spacing.

In conclusion, the implementation of a deck-to-deck connector to connect concrete slabs has demonstrated that it provides an ultimate load-carrying capacity that is near identical to that of a conventional system, where plastic deformation of the connecting components was not observed. The results obtained present a promising strategy for sustainable structural design that reduces the production of greenhouse gas emissions through the use of demountable structures and the reuse of materials. It is important to note that the results presented in this study are obtained through numerical analysis only. Consequently, a true validation of the results through comparison with experimental tests was not conducted within this research. It is considered vital to conduct experimental validation in order to establish the certainty of the results obtained. Nevertheless, the behaviour of the demountable models have shown their potential to contribute to a sustainable built environment.

8.2. Perspectives for future work

The research presented in this thesis provided insight into the behaviour of a demountable and reusable concrete floor system. The study of a modularised floor system incorporating concrete deck-to-deck connectors represents a novel design strategy in sustainable structural design. In order for this strategy to be implemented in design codes and employed in practice, additional research into the structural behaviour is required. This involves further improvement of the connection to understand and predict the behaviour on connector level and on composite floor system level. Based on the aforementioned conclusions and the discussion of results, the following perspectives for future work are put forth for consideration:

Connector level

- With respect to the research on connector level, the objective of the numerical study at the connector level was twofold: firstly, to determine local connection behaviour and secondly, to develop a reliable model that could be incorporated into a larger-scale finite element model. In order to enhance the reliability and applicability of the connection, experimental tests should be conducted. This allows to validate the results obtained through the numerical analysis, ensuring that the assumptions, boundary and interaction conditions can accurately represent the physical behaviour. Particularly the slip behaviour of the bolts in predrilled concrete bolt holes should be investigated, to determine the extent to which the model shows acceptable ductility and load carrying capacity.
- In order to evaluate the impact of specific material properties or geometrical design parameters, it is recommended to conduct a parametric study at the connector level. This parametric study

should involve modifications that adhere to the strength properties and geometry of the bolt and plate, respectively. This not only offers a more comprehensive understanding of the subject matter, but also establishes a framework for subsequent research in this field.

- It would be advantageous to investigate the possibility of optimising the design of the connector with respect to environmental exposure class conditions for concrete and potential corrosion deterioration for steel elements. This highlights the importance of investigating the behaviour of the environmental concrete exposure classes and the current design using stainless steel or galvanised steel elements regarding the bolts and the plates.

Composite floor system level

- The investigation of the behaviour of a demountable floor system in comparison to a conventional floor system is conducted exclusively through numerical analysis. In light of the aforementioned considerations regarding the analysis at the connector level, it is similarly important to conduct experimental tests at the floor system level in order to ascertain the reliability and validate the numerical results.
- The numerical study was conducted with certain simplifications in regard to the boundary conditions employed. The study did not consider the influence of welded shear studs in a composite beam that is connected to an external (reused) slab through the developed deck-to-deck connector. It would be relevant to ascertain the load-bearing capacity of the demountable beam models, taking into account the influence of the steel-concrete composite beam with welded shear studs in experimental/numerical analyses.
- The mode of failure in the demountable models concerned failure of the concrete at position where the bending moment is considered most critical (mid-span and supports). In order to investigate the failure mode and weaknesses of the connection, the connection should be translated to the location that is considered critical.
- The parametric study conducted on the demountable beam models in this research exclusively entailed geometrical variations. It would be beneficial to investigate the impact of material properties on the behaviour of the connection when implemented on true floor level, to understand the material behaviour, assess the sensitivity and optimise the design. Such a study should encompass variations in the properties of the bolt and plate, the concrete, and the reinforcing steel. This is particularly recommended given that no evidence of plastic deformation was observed in the demountable beam models.
- In order to accommodate for tolerances, the numerical model developed employed bolt hole cavities that are greater than the dimensions of the bolt itself. Consequently, in view of the convergence errors during the course of the study (that occurred as a result of using a greater bolthole cavity than the bolt itself), it was resolved by applying bolt pretensioning. A future research could investigate the impact of bolt pretensioning on the global beam behaviour on a greater extent, using different load levels of bolt pretensioning.
- It would be relevant to investigate the complications and limitations in regards to reusing a concrete slab that is extracted from an existing structure. The extraction of a concrete slab from an existing structure inevitably results in the exposure of the reinforcing steel, which subsequently undergoes gradual and detrimental deterioration. This should include research into the disassembly process of cutting the concrete decks. I.e. identify what specific challenges exist for concrete slabs that are extracted from existing structures and devise solutions enabling the integration of reused concrete slabs into steel-concrete composite structures.

References

- [1] Beresford's in-situ concrete specialists. *Precast Concrete Installation*. 2024. URL: <https://www.beresfordsflooring.co.uk/services/precast-concrete-installation/>.
- [2] European Commission. *Proposal for a regulation of the European Parliament and of the Council establishing the framework for achieving climate neutrality and amending Regulation EU 2018/1999*. (European Climate Law). 2018.
- [3] E. MacArthur. "Towards a circular economy: business rationale for an accelerated transition". In: *Greener Manag International* 20 (2015).
- [4] S. Mehra, M. Singh, G. Sharma, S. Kumar, Navishi, and P. Chadha. *Impact of construction material on environment*. 2021, pp. 427–442. DOI: 10.1007/978-3-030-76073-1_{ }22.
- [5] G. Brambilla, M. Lavagna, G. Vasdravellis, and C.A. Castiglioni. "Environmental benefits arising from demountable steel-concrete composite floor systems in buildings". In: *Resources, Conservation and Recycling* 141 (2019), pp. 133–142. DOI: 10.1016/j.resconrec.2018.10.014.
- [6] M. Nijgh. *A multi-scale approach towards reusable steel-concrete composite floor systems*. PhD dissertation. Delft University of Technology, 2021. ISBN: 978-94-6384-207-5.
- [7] I. Jakovljević, M. Spremić, and Z. Marković. "Demountable composite steel-concrete floors: A state-of-the-art review". In: *Građevinar* 73.03 (2021), pp. 249–263. DOI: 10.14256/jce.2932.2020.
- [8] R. Pimentel, R.F. Simões, and L.S. Da Silva. "Demountable Steel□Concrete composite floors for circular Economy: State of the art and design principles". In: *ce/papers* 5.2 (2022), pp. 172–183. DOI: 10.1002/cepa.1712.
- [9] F. Kavoura, Y. Zhang, and M. Veljković. "Structural performance of demountable hybrid floor systems under monotonic and cyclic loading". In: *ce/papers* 6.3-4 (2023), pp. 423–427. DOI: 10.1002/cepa.2755.
- [10] F. Kavoura and M. Veljković. *Design strategies for reusable structural components in the built environment*. 2023, pp. 799–806. DOI: 10.1201/9781003323020-97.
- [11] J. Kanters. "Design for deconstruction in the design process: state of the art". In: *Buildings* 8.11 (2018), p. 150. DOI: 10.3390/buildings8110150.
- [12] F.C. Rios, W.K. Chong, and D. Grau. "Design for Disassembly and Deconstruction - Challenges and opportunities". In: *Procedia Engineering* 118 (2015), pp. 1296–1304. DOI: 10.1016/j.proeng.2015.08.485.
- [13] S. Zhou and S. Smulders. "Closing the loop in a circular economy: Saving resources or suffocating innovations?" In: *European Economic Review* 139 (2021), p. 103857. DOI: 10.1016/j.euroecorev.2021.103857.
- [14] D.D. Tingley and B. Davison. "Design for deconstruction and material reuse". In: *Proceedings of the Institution of Civil Engineers* 164.4 (2011), pp. 195–204. DOI: 10.1680/ener.2011.164.4.195.
- [15] A. Kozma, J. Yang, A. Ahmad, and C. Odenbreit. "Demountable composite beams for a circular economy: Large□scale beam tests". In: *Steel Construction* 17.1 (2024), pp. 1–55. DOI: 10.1002/stco.202300017.
- [16] I.A. Gîrbacea, M. Nijgh, and M. Veljković. "Proof of concept of a demountable steel□concrete composite flooring system". In: *ce/papers* 3.3-4 (2019), pp. 571–576. DOI: 10.1002/cepa.1102.
- [17] *NTA 8713:2023 nl - Reuse of structural steel*. 2023. URL: <https://www.nen.nl/nta-8713-2023-nl-307691>.

- [18] A. Kanyilmaz, M. Birhane, R. Fishwick, and C. Castillo. "Reuse of steel in the construction industry: Challenges and opportunities". In: *International Journal of Steel Structures* 23.5 (2023), pp. 1399–1416. DOI: 10.1007/s13296-023-00778-4.
- [19] W. Salama. "Design of concrete buildings for disassembly: An explorative review". In: *International Journal of Sustainable Built Environment* 6.2 (2017), pp. 617–635. DOI: 10.1016/j.ijjsbe.2017.03.005.
- [20] C. Küpfer, M. Bastien-Masse, and C. Fivet. "Reuse of concrete components in new construction projects: Critical review of 77 circular precedents". In: *Journal of Cleaner Production* 383 (2023), p. 135235. DOI: 10.1016/j.jclepro.2022.135235.
- [21] C. Küpfer, M. Bastien-Masse, J. Devènes, and C. Fivet. "Environmental and economic analysis of new construction techniques reusing existing concrete elements: two case studies". In: *IOP Conference Series: Earth and Environmental Science* 1078.1 (2022), p. 012013. DOI: 10.1088/1755-1315/1078/1/012013.
- [22] A. Glias. *The "Donor Skelet": Designing with reused structural concrete elements*. Master thesis. Delft University of Technology, 2013.
- [23] N. Widmer. *Structural Design for Reuse of Sawn Cast-In-Place Reinforced Concrete Components, Case Study of a Residential Building Structure and Comparison to Conventional Construction Method*. Master Thesis. École Polytechnique Fédérale de Lausanne (EPFL), 2022.
- [24] N. Loqman, N.A. Safiee, N.A. Bakar, and N.A.M. Nasir. "Structural Behavior of Steel-Concrete Composite Beam using Bolted Shear Connectors: A Review". In: *International Conference on Civil, Offshore & Environmental Engineering (ICCOEE 2018)*. Vol. 203. Kuala Lumpur, Malaysia: EDP Sciences, 2018. DOI: 10.1051/mateconf/201820306010.
- [25] MasterSeries. *Calculating the shear connection of a composite beam to Eurocode 4*. Accessed: 2024-01-26. 2019. URL: <https://www.masterseries.com/blog/2019/calculating-the-shear-connection-of-a-composite-beam-to-eurocode-4>.
- [26] A.R.G. Azad, K. Kreitman, M.D. Engelhardt, T.A. Helwig, and E.B. Williamson. "A technique for strengthening existing continuous Non-Composite steel girder bridges using Post-Installed shear connectors and inelastic moment redistribution". In: *Report* (2017). DOI: 10.2749/vancouver.2017.1217.
- [27] R. Hällmark. *Composite Bridges : Innovative ways of achieving composite action*. PhD dissertation. Luleå University of Technology, 2018. ISBN: 978-91-7790-202-7.
- [28] V. Vigneri, C. Odenbreit, and A. Romero. "Numerical study on design rules for minimum degree of shear connection in propped steel–concrete composite beams". In: *Engineering Structures* 241 (2021), p. 112466. DOI: 10.1016/j.engstruct.2021.112466.
- [29] S.J. Hicks and R.M. Lawson. "Design of composite beams using precast concrete slabs". In: (2003). URL: https://steelconstruction.info/images/f/fc/SCI_P287.pdf (visited on 01/09/2024).
- [30] J. Sivamani and S. Kamaleshwar. "Review on Impact of Construction Waste Landfill on Environment and its Reutilization". In: *Ecological Engineering & Environmental Technology* 23.6 (2022), pp. 233–242. DOI: 10.12912/27197050/152918.
- [31] D. Lam, K.S. Elliott, and D.A. Nethercot. "Parametric study on composite steel beams with precast concrete hollow core floor slabs". In: *Journal of Constructional Steel Research* 54.2 (2000). DOI: 10.1016/S0143-974X(99)0049-8.
- [32] European Committee for Standardization. *EN 1994-1-1+C1:2011: Eurocode 4 - Design and calculation of steel-concrete structures - Part 1-1: General rules and rules for buildings*. Brussels, Belgium: CEN, 2011.
- [33] A.S.H. Suwaed. *Development of Novel Demountable Shear Connectors for Precast Steel-Concrete Composite Bridges*. Phd dissertation. University of Warwick, 2017.
- [34] I.M. Viest. "Investigation of stud shear connectors for composite concrete and steel T-Beams". In: *Journal of American Concrete Institute* 52.4 (1956). DOI: 10.14359/11655.

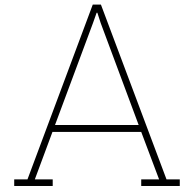
- [35] L. Pallarés and J.F. Hajjar. “Headed steel stud anchors in composite structures, Part I: Shear”. In: *Journal of Constructional Steel Research* 66.2 (2010), pp. 198–212. DOI: 10.1016/j.jcsr.2009.08.009.
- [36] G. Kwon, M.D. Engelhardt, and R.E. Klingner. “Behavior of post-installed shear connectors under static and fatigue loading”. In: *Journal of Constructional Steel Research* 66.4 (2010), pp. 532–541. DOI: 10.1016/j.jcsr.2009.09.012.
- [37] Y.-T. Chen, Y. Zhao, J.S. West, and S. Walbridge. “Behaviour of steel–precast composite girders with through-bolt shear connectors under static loading”. In: *Journal of Constructional Steel Research* 103 (2014), pp. 168–178. DOI: 10.1016/j.jcsr.2014.09.001.
- [38] X. Liu, M.A. Bradford, and M.S.S. Lee. “Behavior of High-Strength Friction-Grip bolted shear connectors in sustainable composite beams”. In: *Journal of Structural Engineering-asce* 141.6 (2015). DOI: 10.1061/(asce)st.1943-541x.0001090.
- [39] J. Chen, W. Wei, F. Ding, P. Xiang, Y. Yu, X. Liu, F. Xu, C. Yang, and L. Shu-Yao. “Behavior of an advanced bolted shear connector in prefabricated Steel-Concrete composite beams”. In: *Materials* 12.18 (2019), p. 2958. DOI: 10.3390/ma12182958.
- [40] A. Kozma, C. Odenbreit, M. Braun, M. Veljković, and M. Nijgh. “Push-out tests on demountable shear connectors of steel-concrete composite structures”. In: *Structures* 21 (2019), pp. 45–54. DOI: 10.1016/j.istruc.2019.05.011.
- [41] Y. Zhang, B. Chen, A. Liu, Y. Pi, Z. Jun-Ping, Y. Wang, and L. Zhong. “Experimental study on shear behavior of high strength bolt connection in prefabricated steel-concrete composite beam”. In: *Composites Part B: Engineering* 159 (2019), pp. 481–489. DOI: 10.1016/j.compositesb.2018.10.007.
- [42] A. Ataei. “Modelling of demountable steel-concrete composite connections: Validation of finite element model and parametric study”. In: *Journal of Constructional Steel Research* 198 (2022), p. 107585. DOI: 10.1016/j.jcsr.2022.107585.
- [43] N.U. Rehman, D. Lam, X. Dai, and A. Ashour. “Experimental study on demountable shear connectors in composite slabs with profiled decking”. In: *Journal of Constructional Steel Research* 122 (2016), pp. 178–189. DOI: 10.1016/j.jcsr.2016.03.021.
- [44] F. Yang, Y. Liu, Z. Jiang, and H. Xin. “Shear performance of a novel demountable steel-concrete bolted connector under static push-out tests”. In: *Engineering Structures* 160 (2018), pp. 133–146. DOI: 10.1016/j.engstruct.2018.01.005.
- [45] J. Wang, J. Guo, L. Jia, S. Chen, and Y. Dong. “Push-out tests of demountable headed stud shear connectors in steel-UHPC composite structures”. In: *Composite Structures* 170 (2017), pp. 69–79. DOI: 10.1016/j.compstruct.2017.03.004.
- [46] M. Pavlović, Z. Marković, M. Veljković, and D. Buđevac. “Bolted shear connectors vs. headed studs behaviour in push-out tests”. In: *Journal of Constructional Steel Research* 88 (2013), pp. 134–149. DOI: 10.1016/j.jcsr.2013.05.003.
- [47] X. Dai, D. Lam, T. Sheehan, J. Yang, and K. Zhou. “Use of bolted shear connectors in composite construction”. In: *Advances in Steel-Concrete Composite Structures* (2018). DOI: 10.4995/asccs2018.2018.7039.
- [48] A. Ataei, M. Zeynalian, and Y. Yazdi. “Cyclic behaviour of bolted shear connectors in steel-concrete composite beams”. In: *Engineering Structures* 198 (2019), p. 109455. DOI: 10.1016/j.engstruct.2019.109455.
- [49] A. Ataei, S.A. Mahmoudy, M. Zeynalian, A.A. Chiniforush, and T. Ngo. “Experimental study of innovative bolted shear connectors in demountable cold-formed steel–concrete composite beams”. In: *Thin-Walled Structures* 192 (2023), p. 111116. DOI: 10.1016/j.tws.2023.111116.
- [50] A.S.H. Suwaed and T.L. Karavasilis. “Novel demountable shear connector for accelerated disassembly, repair, or replacement of precast Steel-Concrete composite bridges”. In: *Journal of Bridge Engineering* 22.9 (2017). DOI: 10.1061/(asce)be.1943-5592.0001080.
- [51] A.S.H. Suwaed and T.L. Karavasilis. “Removable shear connector for steel-concrete composite bridges”. In: *Steel and Composite Structures* 29.1 (2018), pp. 107–123. DOI: 10.12989/scs.2018.29.1.107.

- [52] A.S.H. Suwaed and T.L. Karavasilis. "Demountable steel-concrete composite beam with full-interaction and low degree of shear connection". In: *Journal of Constructional Steel Research* 171 (2020), p. 106152. DOI: 10.1016/j.jcsr.2020.106152.
- [53] J. Yang, D. Lam, X. Dai, and T. Sheehan. "Experimental study on demountable shear connectors in profiled composite slabs". In: *Advances on Steel-Concrete Composite Structures* (2018). DOI: 10.4995/asccs2018.2018.6959.
- [54] M. Nijgh, A. Gîrbacea, and M. Veljković. "Elastic behaviour of a tapered steel-concrete composite beam optimized for reuse". In: *Engineering Structures* 183 (2019), pp. 366–374. DOI: 10.1016/j.engstruct.2019.01.022.
- [55] J. He, A.S.H. Suwaed, G. Vasdravellis, and S. Wang. "Behaviour and design of the 'lockbolt' demountable shear connector for sustainable steel-concrete composite structures". In: *Structures* 44 (2022), pp. 988–1010. DOI: 10.1016/j.istruc.2022.08.062.
- [56] S.W. Pathirana, B. Uy, O. Mirza, and X. Zhu. "Strengthening of existing composite steel-concrete beams utilising bolted shear connectors and welded studs". In: *Journal of Constructional Steel Research* 114 (2015), pp. 417–430. DOI: 10.1016/j.jcsr.2015.09.006.
- [57] S.W. Pathirana, B. Uy, O. Mirza, and X. Zhu. "Bolted and welded connectors for the rehabilitation of composite beams". In: *Journal of Constructional Steel Research* 125 (2016), pp. 61–73. DOI: 10.1016/j.jcsr.2016.06.003.
- [58] S.W. Pathirana, B. Uy, O. Mirza, and X. Zhu. "Flexural behaviour of composite steel–concrete beams utilising blind bolt shear connectors". In: *Engineering Structures* 114 (2016), pp. 181–194. DOI: 10.1016/j.engstruct.2016.01.057.
- [59] I. Henderson, B. Zhu X.and Uy, and O. Mirza. "Dynamic behaviour of steel–concrete composite beams with different types of shear connectors. Part I: Experimental study". In: *Engineering Structures* 103 (2015), pp. 298–307. DOI: 10.1016/j.engstruct.2015.08.035.
- [60] L. Wang, M.D. Webster, and J.F. Hajjar. "Pushout tests on deconstructable steel-concrete shear connections in sustainable composite beams". In: *Journal of Constructional Steel Research* 153 (2019), pp. 618–637. DOI: 10.1016/j.jcsr.2018.10.020.
- [61] E. Feidaki, G. Vasdravellis, J. He, and S. Wang. "Steel-Yielding Demountable Shear Connector for Composite Floors with Precast Hollow-Core Slab Units". In: *Journal of Structural Engineering-asce* 145.8 (2019). DOI: 10.1061/(asce)st.1943-541x.0002356.
- [62] M. Wintermans. *The application of reusable hollow core slab connections in steel frames: Investigating the behaviour of a newly proposed reusable connection with increased tolerances*. 2024. URL: <http://resolver.tudelft.nl/uuid:af82529b-1547-403c-9623-4cdb6226bb3f>.
- [63] European Committee for Standardization. *EN 1993-1-1:2006+A1: Eurocode 3 - Design and calculation of steel structures - Part 1-1: General rules and rules for buildings*. Brussels, Belgium: CEN, 2016.
- [64] M.P. Nijgh and M. Veljkovic. "Requirements for oversized holes for reusable steel-concrete composite floor systems". In: *Structures* 24 (2020), pp. 489–498. DOI: 10.1016/j.istruc.2020.01.021.
- [65] A.M. Gresnigt and J.W.B. Stark. *Design of bolted connections with injection bolts*. 1996, pp. 77–87. DOI: 10.1016/b978-008042821-5/50067-5.
- [66] B. Pedrosa, J. Correia, C. Rebelo, M. Veljković, and H. Gervásio. "Fatigue experimental characterization of preloaded injection bolts in a metallic bridge strengthening scenario". In: *Engineering Structures* 234 (2021), p. 112005. DOI: 10.1016/j.engstruct.2021.112005.
- [67] European Committee for Standardization. *EN 1090-2 Manufacture of steel and aluminium structures - Part 2: Technical requirements for steel structures*. Brussels, Belgium: CEN, 2018.
- [68] B. Pedrosa, L. Bücking, and M. Veljković. "Steel-reinforced resin for bolted shear connectors: Confined behaviour under quasi-static cyclic loading". In: *Engineering Structures* 256 (2022), p. 114023. DOI: 10.1016/j.engstruct.2022.114023.

- [69] B. Zafari, J. Qureshi, J. T. Mottram, and R. Rusev. "Static and fatigue performance of resin injected bolts for a slip and fatigue resistant connection in FRP bridge engineering". In: *Structures* 7 (2016), pp. 71–84. DOI: 10.1016/j.istruc.2016.05.004.
- [70] R. Asso, M. Domaneschi, G.C. Marano, F. Palmisano, and G Palombella. "Behavior of Half-Joints: Design and simulation of laboratory tests". In: *Infrastructures* 7.12 (2022), p. 160. DOI: 10.3390/infrastructures7120160.
- [71] P. Desnerck, J.M. Lees, and C.T. Morley. "Strut-and-tie models for deteriorated reinforced concrete half-joints". In: *Engineering structures/Engineering structures (Online)* 161 (2018), pp. 41–54. DOI: 10.1016/j.engstruct.2018.01.013.
- [72] P. Desnerck, C. Morley, and J. Lees. "Impact of Material Deterioration on the Strength of Reinforced Concrete Half Joint Structures". In: vol. 103. 2015. DOI: 10.2749/222137815815622753.
- [73] P. Desnerck, J.M. Lees, and C.T. Morley. "Impact of the reinforcement layout on the load capacity of reinforced concrete half-joints". In: *Engineering structures/Engineering structures (Online)* 127 (2016), pp. 227–239. DOI: 10.1016/j.engstruct.2016.08.061.
- [74] European Committee for Standardization. *EN 1992-1-1:2005+A1:2015+NB:2016+A1:2020 Eurocode 2 - Design and calculation of concrete structures - Part 1-1: General rules and rules for buildings*. Brussels, Belgium: CEN, 2020.
- [75] D. Figueira, A. Ashour, G. Yıldırım, A. Aldemir, and M. Şahmaran. "Demountable connections of reinforced concrete structures: Review and future developments". In: *Structures* 34 (2021), pp. 3028–3039. DOI: 10.1016/j.istruc.2021.09.053.
- [76] J. Xiao, T. Ding, and Q. Zhang. "Structural behavior of a new moment-resisting DfD concrete connection". In: *Engineering structures/Engineering structures (Online)* 132 (2017), pp. 1–13. DOI: 10.1016/j.engstruct.2016.11.019.
- [77] P.K. Aninthaneni and R.P. Dhakal. "Demountable precast RC frame building system for seismic regions". In: *International conference on earthquake engineering and seismology (IZIIS-50). Kiel, Germany*. 2015.
- [78] H. Almahmood, A. Ashour, D. Figueira, G. Yıldırım, A. Aldemir, and M. Şahmaran. "Tests of demountable reinforced concrete slabs". In: *Structures* 46 (2022), pp. 1084–1104. DOI: 10.1016/j.istruc.2022.10.097.
- [79] Hilti. *Hilti Corporation*. URL: <https://www.hilti.com>.
- [80] Allfasteners. *What is a Chemical Anchor?* 2022. URL: <https://www.allfasteners.com.au/news-articles/what-is-a-chemical-anchor>.
- [81] A.J. Aref, M. Chiewanichakorn, S.S. Chen, and I. Ahn. "Closure to "Effective Slab Width Definition for Negative Moment Regions of Composite Bridges" by Amjad J. Aref, Methee Chiewanichakorn, Stuart S. Chen, and Il-Sang Ahn". In: *Journal of Bridge Engineering* 13.4 (2008), pp. 426–427. DOI: 10.1061/(asce)1084-0702(2008)13:4(426).
- [82] R. Masoudnia. "State of the art of the effective flange width for composite T-beams". In: *Construction and Building Materials* 244 (2020), p. 118303. DOI: 10.1016/j.conbuildmat.2020.118303.
- [83] Y. Huang, J. Yang, Y. Chen, and J. Zeng. "Prediction for Effective Flange Width of Steel–Concrete Composite Beam with TALHG". In: *Arabian Journal for Science and Engineering* 47.4 (2022), pp. 5199–5218. DOI: 10.1007/s13369-021-06427-4.
- [84] C. Odenbreit, J. Yang, A. Romero, and A. Kozma. "A reusable structural system fit for geometrical standardisation and serial production". In: *ce/papers* 5.2 (2022), pp. 11–20. DOI: 10.1002/cepa.1693.
- [85] P. Smarzewski and A. Stolarski. "Properties and performance of concrete materials and structures". In: *Crystals* 12.9 (2022), p. 1193. DOI: 10.3390/cryst12091193.
- [86] F. Monney, Q. Yu, M.F. Ruiz, and A. Muttoni. "Anchorage of shear reinforcement in beams and slabs". In: *Engineering Structures* 265 (2022), p. 114340. DOI: 10.1016/j.engstruct.2022.114340.

- [87] Q. Xu, W. Sebastian, K. Lu, Y. Yao, and J. Wang. "Longitudinal shear performance of lightweight steel-UHPC composite connections based on large-diameter high strength friction-grip bolts". In: *Engineering Structures* 260 (2022), p. 114220. DOI: 10.1016/j.engstruct.2022.114220.
- [88] Z. Fang, L. Hu, H. Jiang, S. Fang, G. Zhao, and Y. Ma. "Shear performance of high-strength friction-grip bolted shear connector in prefabricated steel-UHPC composite beams: Finite element modelling and parametric study". In: *Case studies in construction materials* 18 (2023), e01860. DOI: 10.1016/j.cscm.2023.e01860.
- [89] A.M. Seyam and R. Nemes. "Age influence on compressive strength for concrete made with different types of aggregates after exposed to high temperatures". In: *Materials Today Proceedings* (2023). DOI: 10.1016/j.matpr.2023.06.403.
- [90] S. Barbhuiya, A. Jivkov, and B.B. Das. "A review of multi-scale modelling of concrete deterioration: Fundamentals, techniques and perspectives". In: *Construction and Building Materials* 406 (2023), p. 133472. DOI: 10.1016/j.conbuildmat.2023.133472.
- [91] *BASIC CONCEPT TRAINING SCIA Engineer 21*. English. Nemetschek Company - SCIA Engineer, 2021.
- [92] Michael Smith. *ABAQUS/Standard User's Manual, Version 6.9*. English. United States: Dassault Systèmes Simulia Corp, 2009.
- [93] V. Mahadik, A. Sharma, and J. Hofmann. "Cast-in and post-installed rebar anchorage systems in RC column foundation joints: System specific assessment and design". In: *Engineering Structures* 276 (2022), p. 115356. DOI: 10.1016/j.engstruct.2022.115356.
- [94] S. Cattaneo, V. Mahadik, G. Genesio, and J. Hofmann. "Influence of edge proximity on concrete breakout failure in post-installed RC columns foundation joints". In: *Materials and Structures* 56.7 (2023). DOI: 10.1617/s11527-023-02208-7.
- [95] Y. Zou, J. Di, J. Zhou, Z. Zhang, X. Li, H. Zhang, and F. Qin. "Shear behavior of perfobond connectors in the steel-concrete joints of hybrid bridges". In: *Journal of constructional steel research* 172 (2020), p. 106217. DOI: 10.1016/j.jcsr.2020.106217.
- [96] Y. Zhang, A. Liu, B. Chen, Z. Jun-Ping, Y. Pi, and M Bradford. "Experimental and numerical study of shear connection in composite beams of steel and steel-fibre reinforced concrete". In: *Engineering structures/Engineering structures (Online)* 215 (2020), p. 110707. DOI: 10.1016/j.engstruct.2020.110707.
- [97] L. An and K. Cederwall. "Push-out tests on studs in high strength and normal strength concrete". In: *Journal of Constructional Steel Research* 36.1 (1996), pp. 15–29. DOI: 10.1016/0143-974x(94)00036-h.
- [98] M. Spremic, Z. Markovic, M. Veljkovic, and D. Budjevac. *Push-out experiments of headed shear studs in group arrangements*. 2013, pp. 139–160. DOI: 10.18057/ijasc.2013.9.2.4.
- [99] A. Hillerborg, M. Modéer, and P.E. Petersson. "Analysis of crack formation and crack growth in concrete by means of fracture mechanics and finite elements". In: *Cement and Concrete Research* 6.6 (1976), pp. 773–781. DOI: 10.1016/0008-8846(76)90007-7.
- [100] J. Lubliner, J. Oliver, S. Oller, and E. Oñate. "A plastic-damage model for concrete". In: *International Journal of Solids and Structures* 25.3 (1989), pp. 299–326. DOI: 10.1016/0020-7683(89)90050-4.
- [101] J. Lee and G.L. Fenves. "Plastic-Damage model for cyclic loading of concrete structures". In: *Journal of Engineering Mechanics-asce* 124.8 (1998), pp. 892–900. DOI: 10.1061/(asce)0733-9399(1998)124:8(892).
- [102] T. Yu, J. Teng, Y.L. Wong, and S. Dong. "Finite element modeling of confined concrete-I: Drucker-Prager type plasticity model". In: *Engineering Structures* 32.3 (2010), pp. 665–679. DOI: 10.1016/j.engstruct.2009.11.014.
- [103] A. Earij, G. Alfano, K.A. Cashell, and X. Zhou. "Nonlinear three-dimensional finite-element modelling of reinforced-concrete beams: Computational challenges and experimental validation". In: *Engineering failure analysis* 82 (2017), pp. 92–115. DOI: 10.1016/j.engfailanal.2017.08.025.

- [104] P. Kmieciak and M. Kamiński. “Modelling of reinforced concrete structures and composite structures with concrete strength degradation taken into consideration”. In: *Archives of Civil and Mechanical Engineering* 11.3 (2011), pp. 623–636. DOI: 10.1016/s1644-9665(12)60105-8.
- [105] T. Wang and T.W. Hsu. “Nonlinear finite element analysis of concrete structures using new constitutive models”. In: *Computers & structures* 79.32 (2001), pp. 2781–2791. DOI: 10.1016/s0045-7949(01)00157-2.
- [106] Q. Guo, Q. Chen, Y. Xing, Y. Xu, and Y. Zhu. “Experimental Study of Friction Resistance between Steel and Concrete in Prefabricated Composite Beam with High-Strength Frictional Bolt”. In: *Advances in Materials Science and Engineering* 2020.1 (2020). DOI: 10.1155/2020/1292513.
- [107] European Committee for Standardization. *EN 1990-1-1:2002+A1: Eurocode 0 - Fundamentals of structural design*. Brussels, Belgium: CEN, 2019.
- [108] D.Y. Moon, J. Sim, and H. Oh. “Detailing considerations on RC beams strengthened with CFRP bars embedded in mortar overlay”. In: *Construction and Building Materials* 21.8 (2007), pp. 1636–1646. DOI: 10.1016/j.conbuildmat.2006.06.028.
- [109] C. K pfer, N. Bertola, and C. Fivet. “Reuse of cut concrete slabs in new buildings for circular ultra-low-carbon floor designs”. In: *Journal of Cleaner Production* 448 (2024), p. 141566. DOI: 10.1016/j.jclepro.2024.141566.
- [110] M. Rakhshanimehr, M.R. Esfahani, M.R. Kianoush, B.A. Mohammadzadeh, and S.R. Mousavi. “Flexural ductility of reinforced concrete beams with lap-spliced bars”. In: *Canadian Journal of Civil Engineering* 41.7 (2014), pp. 594–604. DOI: 10.1139/cjce-2013-0074.
- [111] Z. Wu, S. Zhang, and S.F. Jiang. “Simulation of tensile bolts in finite element modeling of semi-rigid beam-to-column connections”. In: *International Journal of Steel Structures* 12.3 (2012), pp. 339–350. DOI: 10.1007/s13296-012-3004-8.



Push-out test - Experimental programme EN 1994-1-1

A.1. Testing procedure

The structural behaviour of composite floor systems indicates that the ability for such system to be fully composite depends on the slip resistance of the shear connectors. The slip resistance of shear connectors is generally determined through experimental push-out tests. A push-out test for SCC is performed by attaching two concrete slabs on each side of a steel I-section. The specimen is then burdened by an axial load which causes the connectors on either side to be subjected to shear loading. In order to measure the displacements of the components within the specimen, multiple displacement transducers (LVDTs) are employed. The mechanical behaviour of the shear connector is determined based on a load-slip curve that is obtained through the experiment.

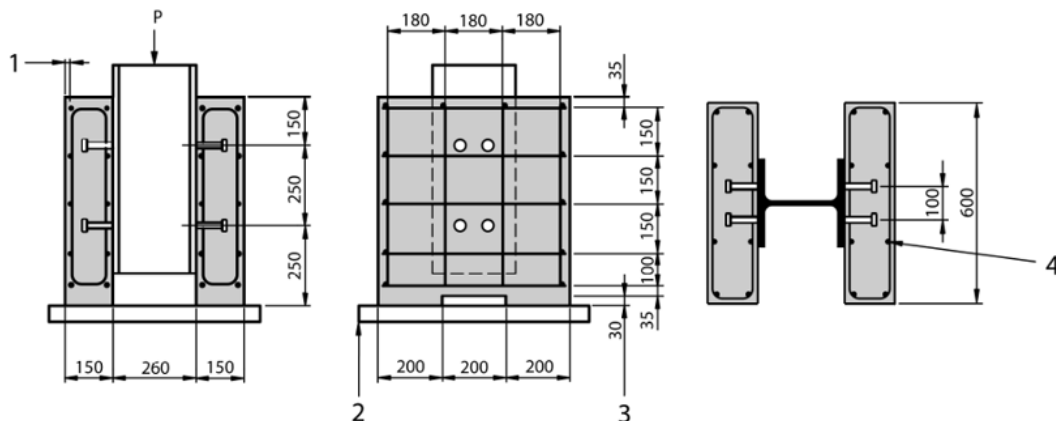


Figure A.1: Push-out test prescribed in EN 1994-1-1 [32]

1. Concrete cover 15 mm
2. Embedded in mortar or plaster
3. Cutout (optional)
4. Reinforcement: Ribbed bars $\varnothing 10$ mm with $450 \leq f_{sk} \leq 550 \text{ N/mm}^2$
Steel profile: HEB 260 or UC 254 x 254 x 89

A.2. Loading protocol and load-slip curve

The testing procedure for shear connectors can either be performed using monotonic or cyclic tests. A monotonic push-out test involves a steady increasing load until failure of the specimen occurs. Monotonic tests allow to determine the ultimate load-bearing capacity of the specimen. Monotonic tests are

in particular useful for understanding the strength and stiffness of a specific joint that is statically loaded. Cyclic push-out tests are performed by subjecting a specimen to repeated loading cycles. Cyclic test give insight in understanding the fatigue behaviour and response to a repeated stress. These tests are mainly useful in assessing the reliability and durability of a joint that is subjected to fluctuating loads, such as bridge constructions that endure cyclic loading of vehicles passing by. Steel-concrete composites follow the procedure prescribed by EN 1994 [32]. The cyclic test is executed by initially loading the specimen in reaching up to 40% of the predicted failure load. Then, the specimen should undergo 25 cycles of loading that fluctuates between 5-40% of the estimated maximum load capacity of the shear connectors. The cyclic test is followed by an imposed monotonic load. The monotonic load increases until failure of the joint or a load drop of 20% with respect to the ultimate load. Figure A.2a depicts the loading procedure on a (dismountable) shear connector. In order to fulfil Eurocode 4 requirements a slip capacity of at least 6 mm for the connector should be achieved.

The results of a push-out test on shear connectors are presented in the load slip-curve (see Figure A.2b). Depending on the loading procedure a monotonic and / or cyclic test is performed on specimens of a certain type of connector. In case of a monotonic push-out test the results on the load-slip curve are evident. The specimen is linearly loaded until failure or if a certain slip length is reached. The monotonic push-out test is generally used to retrieve the ultimate load capacity (P_u), initial stiffness (K_{ini}) and (ultimate) slip capacity (δ_{slip}). The cyclic push-out test results in load-slip hysteretic curves. The mechanical behaviour of the shear connector subjected to cyclic loading is characterised by the ductility (D), energy dissipation (E) and strength degradation (S). The parameters P_u , K_{ini} and δ_{slip} regarding the cyclic curves are determined through the load-slip envelope curve. This envelope curve defines the maximum load in a loading cycle and comprises the perimeter of all curves within the loading cycles.

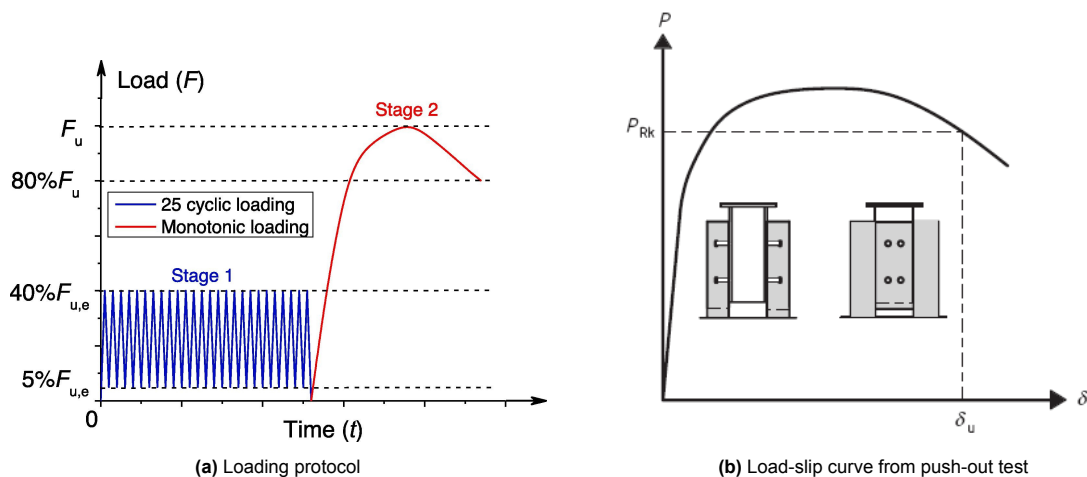


Figure A.2: Load-slip curve from push-out test prescribed by EN 1994-1-1 [32]

B

Failure mechanism validation FE block-model

B.1. Failure mechanism analysis - concrete block

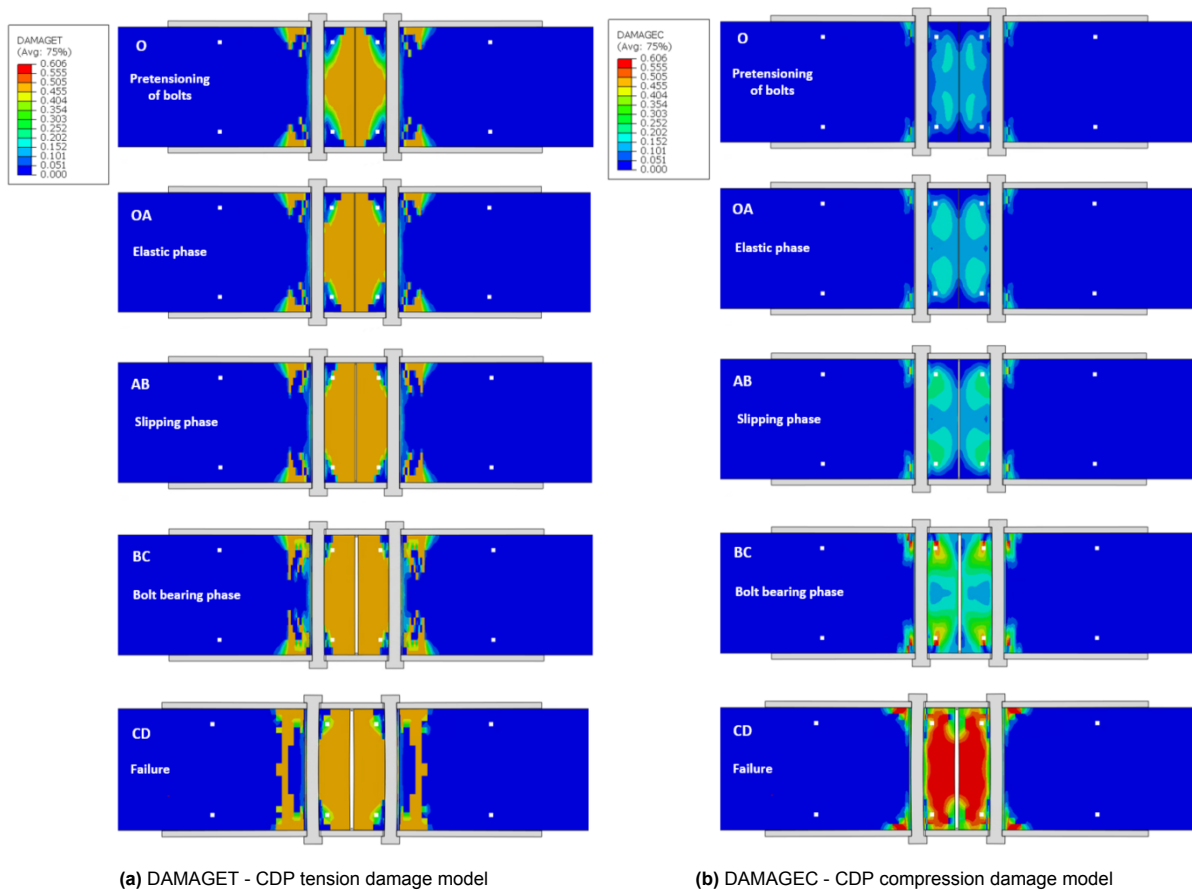


Figure B.1: Evolution of concrete CDP damage models along the distinct phases of bolts subjected to shear until failure - Block height 160mm (Bolt 10.9-16, Concrete C20/25)

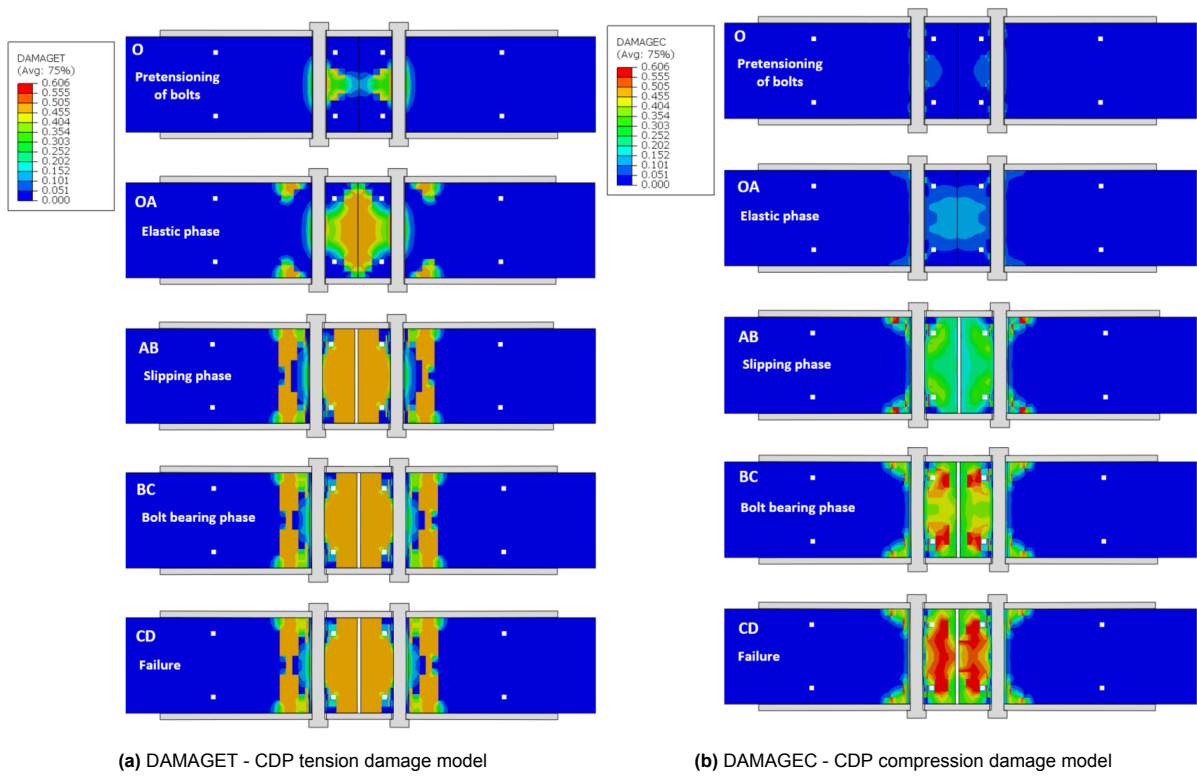


Figure B.2: Evolution of concrete CDP damage models along the distinct phases of bolts subjected to shear until failure - Block height 120mm (Bolt 10.9-16, Concrete C20/25)

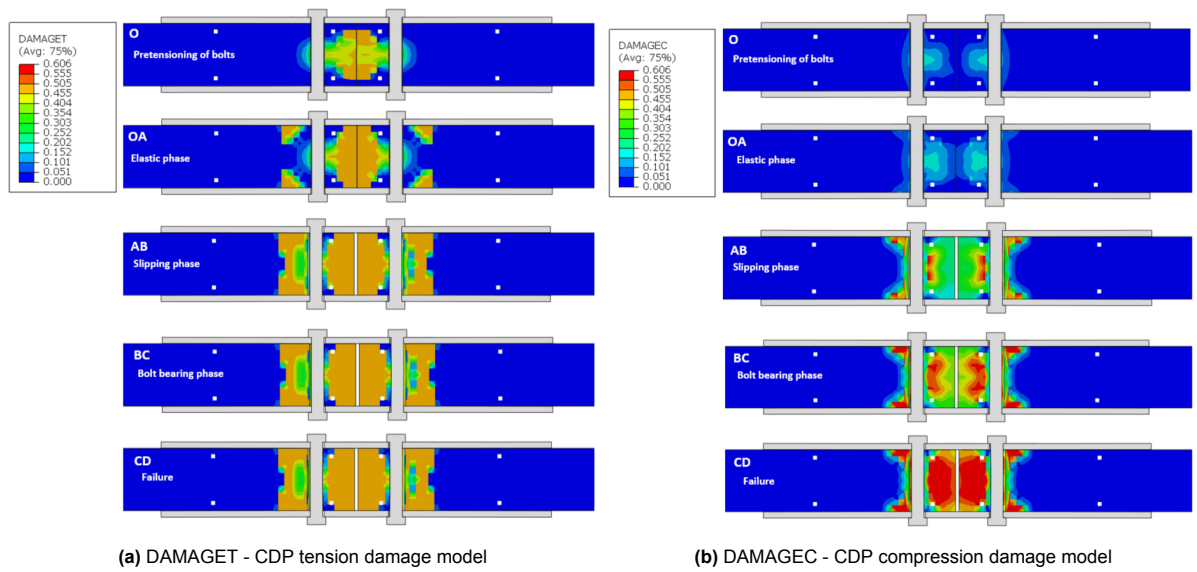


Figure B.3: Evolution of concrete CDP damage models along the distinct phases of bolts subjected to shear until failure - Block height 80mm (Bolt 10.9-16, Concrete C20/25)

B.2. Allocation and overlapping of distinct damage regions

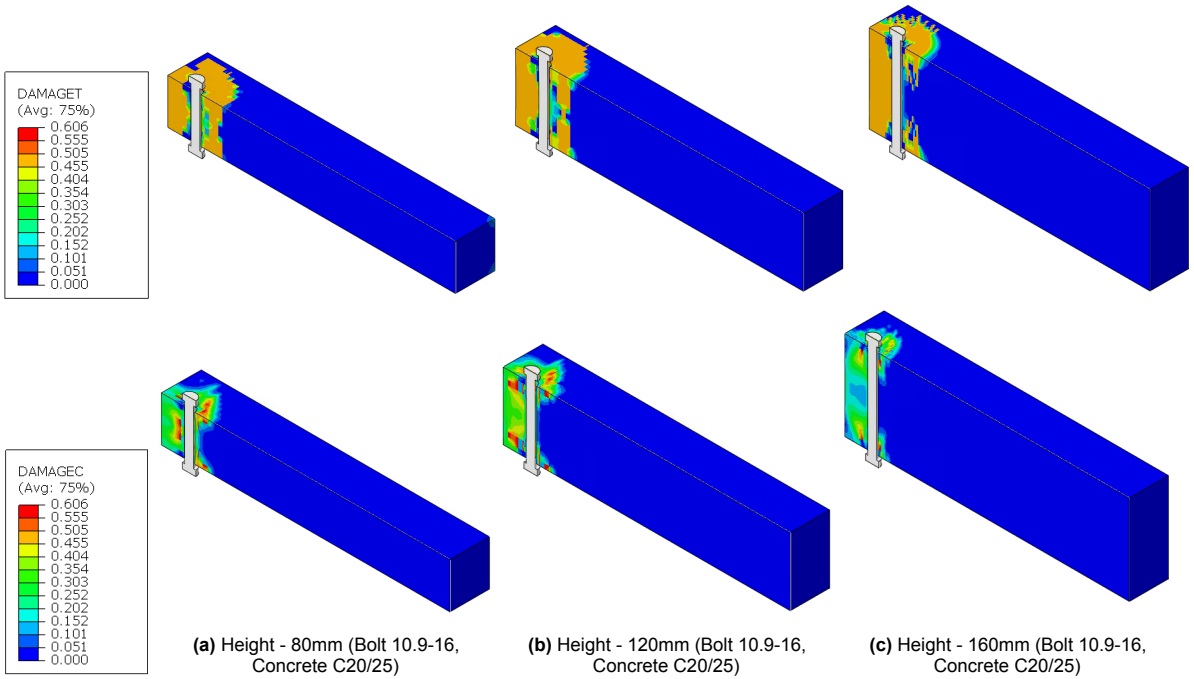
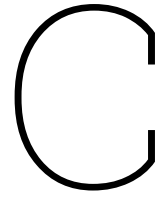


Figure B.4: Concrete failure mechanism for varying concrete block height (80, 120 & 160 mm) - Damage regions regarding shear-compression (S-C) zone and tensile-prying (T-P) zone



Parametric study - Load-deflection & initial flexural stiffness diagrams

This appendix contains the load-deflection curves for the parametric study, through which geometrical properties of the demountable connection in the beam model were varied with respect to the conventional and reference beam model. The details of the reference beam model are described in Section 6.1.1. Figure 1 illustrates the load-deflection curves for variations in edge distance, span width and spacing. The accompanying legend provides a detailed overview of the variants employed throughout the analysis. The first fragment of the legend indicates the group, the second fragment the span width (m), the third fragment the edge distance (mm) and the fourth and final fragment the spacing (mm). A summary of the results is provided in Section 6.3.3, in terms of the load capacity and effective bending stiffness.

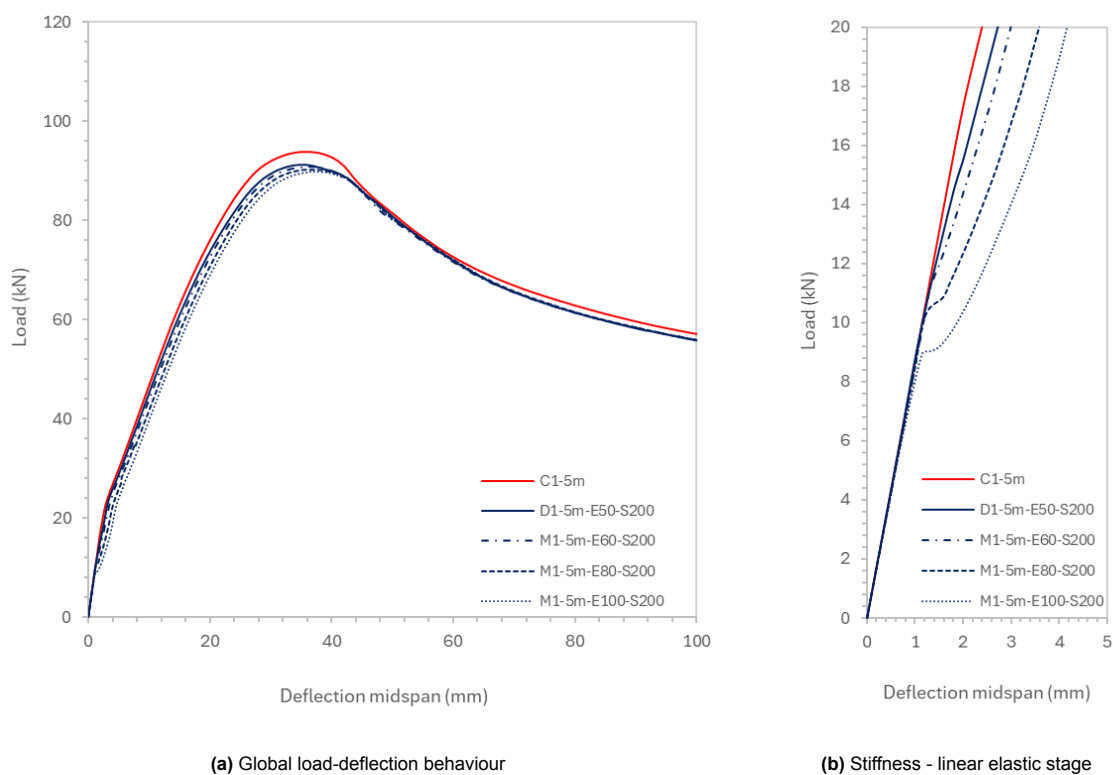


Figure C.1: Load deflection behaviour at the beam mid-span section - Edge distance

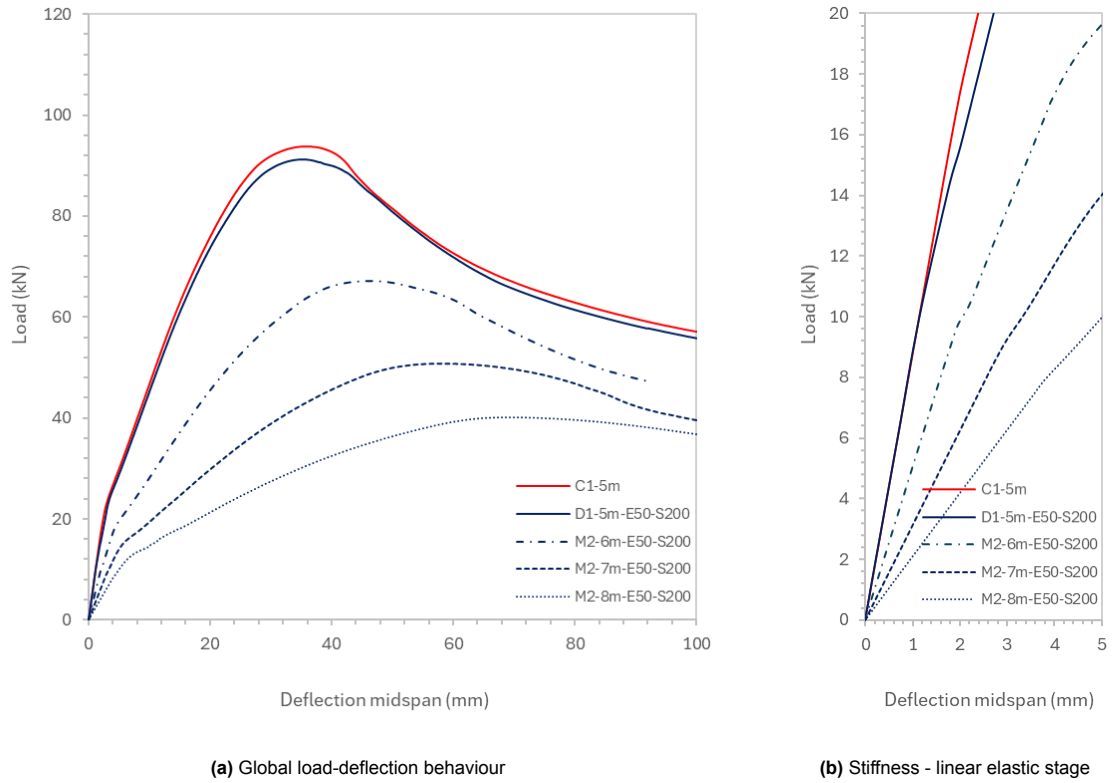


Figure C.2: Load deflection behaviour at the beam mid-span section - Span

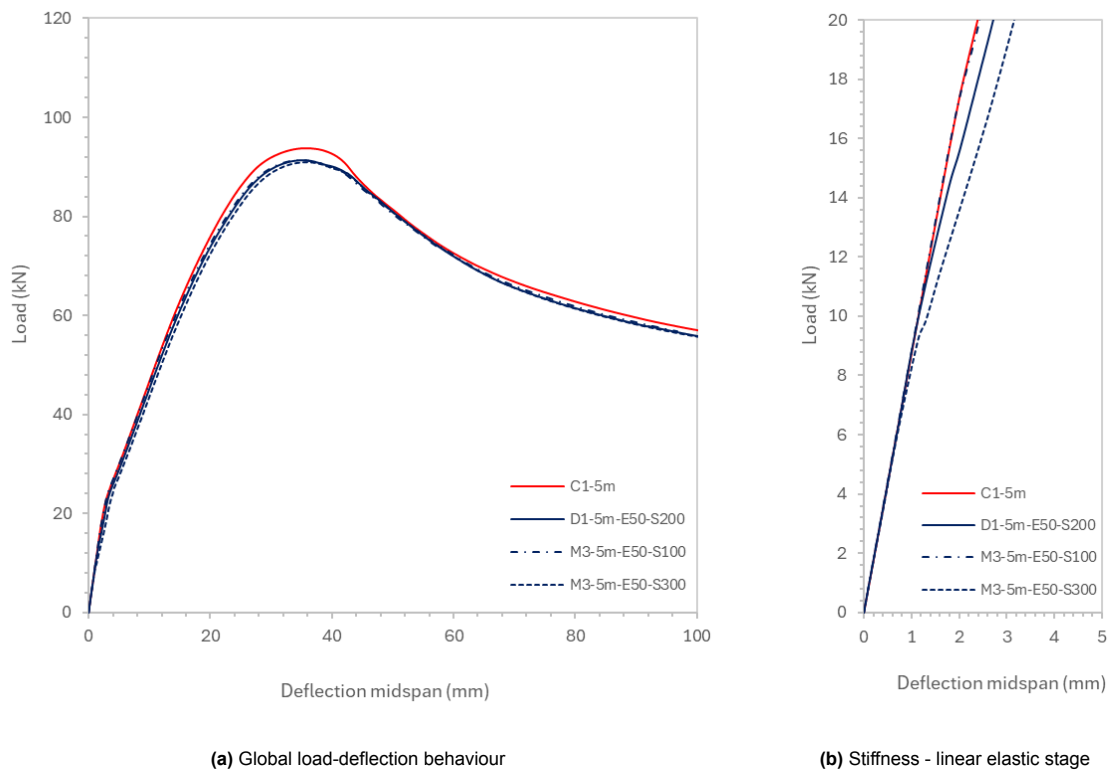


Figure C.3: Load deflection behaviour at the beam mid-span section - Spacing

